AD-A230 463

DTIC
ELECTE
JAN 07 1991
S B D

NONLINEAR ANALYSIS OF A SPINNING SYMMETRIC SATELLITE IN AN ELLIPTICAL ORBIT

THESIS

Michael Ulisse, Captain, USAF

AFIT/GA/ENY/90D-13

DEPARTMENT OF THE AIR FORCE
AIR UNIVERSITY
AIR FORCE INSTITUTE OF TECHNOLOGY

Wright-Patterson Air Force Base, Ohio

DISTRIBUTION STATEMENT A
Approved for public release;
Distribution Unlimited

91 1 3 083

AFIT/GA/ENY/90D-13

NONLINEAR ANALYSIS OF A SPINNING SYMMETRIC SATELLITE IN AN ELLIPTICAL ORBIT

THESIS

Michael Ulisse, Captain, USAF

AFIT/GA/ENY/90D-13

DTIC
ELECTE
JAN 07 1991
S D
B

Approved for public release; distribution unlimited

AFIT/GA/ENY/90D-13

NONLINEAR ANALYSIS OF A SPINNING SYMMETRIC SATELLITE IN AN ELLIPTICAL ORBIT

THESIS

Presented to the Faculty of the School of Engineering

of the Air Force Institute of Technology

Air University

In Partial Fulfillment of the

Requirements for the Degree of

Master of Science in Astronautical Engineering

Michael Ulisse, B.S.

Captain, USAF

December, 1990

Approved for public release; distribution unlimited

Preface

This work extends the knowledge base for nonlinear effects on the stability and control of a spinning symmetric satellite in an elliptical orbit. The full nonlinear controlled and uncontrolled equations of motion were evaluated using various nonlinear analysis techniques. The origin of an attractor in the global phase space found in Cole's work analyzing the modal coordinate Floquét control design was the incentive for this investigation. However, in order to attempt to trace the origin of this complex phase trajectory structure in a global sense, a simplified rate and position feedback controller was created and evaluated. The results of this thesis show that a global stability analysis yields results particular to a very specific set of conditions. One can only hope to characterize a small set of these conditions. But, there is still much to be learned about the linear and nonlinear stability characteristics for this problem.

I have to thank Dr. Wiesel for his advice and expertise on the computer programs I used for many parts of this study. Also, I must give special thanks to Dr. Calico for the precious time he took from his busy schedule to assist me with Cole's results. Most of all, I am indebted to my advisor, Captain Jim Planeaux, for his patience, insight, and guidance over the past year. Finally, I am especially grateful to my wife Patricia for her love and support that made this work possible.

Michael Ulisse

For
:I
d
ion
Distribution/
Availability Codes
Dist Avail and/or Special
A-1
QUALITY INSPECTED 4

Table of Contents

		Page
Preface		ii
Table of Contents		iii
List of Figures		v
List of Tables		x
Abstract		xi
I.	Introduction	1-1
II.	Theory	2-1
	2.1 Uncontrolled Equations of Motion	2-1
	2.2 Floquét Theory	2-4
	2.3 Controlled Equations of Motion	2-7
III.	Numerical Methods for Nonlinear Analysis	3-1
	3.1 Nonlinear Analysis and the Computer	3-1
	3.2 Bifurcation of Solutions	3-3
	3.3 Poincaré Maps	3-6
	3.4 Hamiltonian Systems	3-8
	3.5 Continuation	3-9
IV.	Results	4-1
	4.1 Floquét Analysis	4-2
	4.1.1 Uncontrolled Equations of Motion	4-2
	4.1.2 Floquét Controlled Equations of Motion	4-27
	4.1.3 Rate and Position Feedback Equations of Motion	4-29
	4.2 Poincaré Maps	4-34

4.2.1 Uncontrolled Equations of Motion 4-42

4.2.2 Floquét Controlled Equations of Motion 4-47

4.2.3 Rate and Position Feedback Equations of Motion 4-59

4.3 Continuation 4-65

4.3.1 Modified Orbit Equations of Motion for AUTO ... 4-70

4.3.2 Uncontrolled Equations of Motion 4-73

4.3.3 Floquét Controlled Equations of Motion 4-73

4.3.4 Rate and Position Feedback Equations of Motion 4-78

V. Conclusions and Recommendations 5-1

Appendix A: Equations of Motion A-1

A.1 Attitude Angular Velocities A-1

A.2 Kinetic Energy of the Satellite A-6

A.3 Potential Energy of the Satellite A-9

A.4 Lagranges Equations of Motion A-12

Bibliography BIB-1

Vita VITA-1

List of Figures

Figure		Page
3.1.	Types of Bifurcations	3-4
3.2.	Motion on a Torus	3-6
4.1.	Uncontrolled System Multipliers (0.0≤e≤0.7,s=1.0,K=0.7) ...	4-3
4.2.	Uncontrolled System Multipliers (0.38≤e≤0.41,s=1.0,K=0.7) .	4-5
4.3.	Uncontrolled System Multipliers (0.46≤e≤0.47,s=1.0,K=0.7) .	4-6
4.4.	Uncontrolled System Multipliers (0.6316≤e≤0.6317,s=1.0,K=0.7)	4-7
4.5.	Uncontrolled System Multipliers (0.63274217≤e≤0.63274218,s=1.0,K=0.7)	4-8
4.6.	Uncontrolled System Multipliers (0.0≤e≤0.7,s=1.5,K=0.7) ...	4-9
4.7.	Uncontrolled System Multipliers (0.0≤e≤0.7,s=2.0,K=0.7) ...	4-10
4.8.	Uncontrolled System Multipliers (0.0≤e≤0.7,s=2.5,K=0.7) ...	4-11
4.9.	Uncontrolled System Multipliers (0.0≤e≤0.7,s=3.0,K=0.7) ...	4-12
4.10.	Uncontrolled System Multipliers (0.0≤e≤0.7,s=0.0,K=0.7) ...	4-13
4.11.	Uncontrolled System Multipliers (0.0≤e≤0.7,s=-1.0,K=0.7) ..	4-14
4.12.	Uncontrolled System Multipliers (0.0≤e≤0.7,s=-2.0,K=0.7) ..	4-15
4.13.	Uncontrolled System Multipliers (0.0≤e≤0.7,s=-3.0,K=0.7) ..	4-16
4.14.	Uncontrolled System Multipliers (0.0≤e≤0.7,s=1.0,K=1.0) ...	4-19
4.15.	Uncontrolled System Multipliers (0.0≤e≤0.7,s=1.0,K=0.5) ...	4-20
4.16.	Uncontrolled System Multipliers (0.0≤e≤0.7,s=1.0,K=0.25) ..	4-21
4.17.	Uncontrolled System Multipliers (0.0≤e≤0.7,s=1.0,K=0.0) ...	4-22
4.18.	Uncontrolled System Multipliers (0.0≤e≤0.7,s=1.0,K=-0.25) .	4-23
4.19.	Uncontrolled System Multipliers (0.0≤e≤0.7,s=1.0,K=-0.5) ..	4-24

4.20. Uncontrolled System Multipliers ($0.0 \leq e \leq 0.7, s=1.0, K=-0.75$) . 4-25

4.21. Uncontrolled System Multipliers ($0.0 \leq e \leq 0.7, s=1.0, K=-1.0$) . 4-26

4.22. Floquét Controlled System Multipliers
($e=0.5, s=1.0, K=0.7, 0.0 \leq G_i \leq 1.0$) 4-28

4.23. Rate Feedback System Multipliers
($e=0.5, s=1.0, K=0.7, 0.0 \leq G_j \leq 1.0$) 4-30

4.24. Rate Feedback System Multipliers
($e=0.5, s=1.0, -1.0 \leq K \leq 1.0, G_j=0.85$) 4-32

4.25. Rate Feedback System Multipliers
($e=0.5, -3.0 \leq s \leq 3.0, K=0.7, G_j=0.85$) 4-33

4.26. Rate Feedback System Multipliers
($0.0 \leq e \leq 0.7, s=1.0, K=0.7, G_j=0.85$) 4-35

4.27. Rate and Position Feedback System Multipliers
($e=0.5, s=1.0, K=0.7, G_j=0.85, 0.0 \leq G_i \leq 1.0$) 4-36

4.28. Rate Feedback System Multipliers
($e=0.5, s=1.0, K=0.7, G_j=0.85, 0.0 \leq G_i \leq 1.0$) 4-37

4.29. Rate Feedback System Time Response for θ_1
($e=0.5, s=1.0, K=0.7, G_j=0.85$) 4-38

4.30. Rate Feedback System Time Response for θ_2
($e=0.5, s=1.0, K=0.7, G_j=0.85$) 4-39

4.31. Rate Feedback System Time Response for θ_1'
($e=0.5, s=1.0, K=0.7, G_j=0.85$) 4-40

4.32. Rate Feedback System Time Response for θ_2'
($e=0.5, s=1.0, K=0.7, G_j=0.85$) 4-41

4.33. Poincaré Map of θ_1 vs θ_2 for Uncontrolled System
(2500 Orbits Sampled at 2π, $e=0.15, s=1.0, K=0.7$) 4-43

4.34. Poincaré Map of θ_1' vs θ_2' for Uncontrolled System
(2500 Orbits Sampled at 2π, $e=0.15, s=1.0, K=0.7$) 4-44

4.35. Poincaré Map of θ_1 vs θ_2 for Uncontrolled System
(2500 Orbits Sampled at 2π, $e=0.5, s=1.0, K=0.7$) 4-45

4.36. Poincaré Map of θ_1' vs θ_2' for Uncontrolled System
(2500 Orbits Sampled at 2π, $e=0.5, s=1.0, K=0.7$) 4-46

4.37. Poincaré Map of η_1 vs η_2 for Floquét Controlled System

(400 Orbits Sampled at 4π,e=0.5,s=1.0,K=0.7,G_1=G_2=0.4) 4-48

4.38. Poincaré Map of η_3 vs η_4 for Floquét Controlled System
(400 Orbits Sampled at 4π,e=0.5,s=1.0,K=0.7,G_1=G_2=0.4) 4-49

4.39. Poincaré Map of η_1 vs η_2 for Floquét Controlled System
(2500 Orbits Sampled at 4π,e=0.5,s=1.0,K=0.7,G_1=G_2=0.4) ... 4-50

4.40. Poincaré Map of η_3 vs η_4 for Floquét Controlled System
(2500 Orbits Sampled at 4π,e=0.5,s=1.0,K=0.7,G_1=G_2=0.4) ... 4-51

4.41. Poincaré Map of θ_1 vs θ_1' for Floquét Controlled System
(2500 Orbits Sampled at 4π,e=0.5,s=1.0,K=0.7,G_1=G_2=0.4) ... 4-53

4.42. Poincaré Map of θ_2 vs θ_2' for Floquét Controlled System
(2500 Orbits Sampled at 4π,e=0.5,s=1.0,K=0.7,G_1=G_2=0.4) ... 4-54

4.43. Poincaré Map of θ_1 vs θ_1' for Floquét Controlled System
(2500 Orbits Sampled at 4π,e=0.5,s=1.0,K=0.7,G_1=G_2=0.4) ... 4-55

4.44. Poincaré Map of θ_2 vs θ_2' for Floquét Controlled System
(2500 Orbits Sampled at 4π,e=0.5,s=1.0,K=0.7,G_1=G_2=0.4) ... 4-56

4.45. Poincaré Map of θ_1 vs θ_1' for Floquét Controlled System
(5000 Orbits Sampled at 4π,e=0.5,s=1.0,K=0.7,G_1=G_2=0.4) ... 4-57

4.46. Poincaré Map of θ_2 vs θ_2' for Floquét Controlled System
(5000 Orbits Sampled at 4π,e=0.5,s=1.0,K=0.7,G_1=G_2=0.4) ... 4-58

4.47. Rate Feedback Gain Effect on Multipliers
($0.46 \le e \le 0.50$,s=1.0,K=0.7) 4-60

4.48. Poincaré Map of θ_1 vs θ_2 for Small Rate Feedback Gain
(500 Orbits Sampled at 4π,e=0.5,s=1.0,K=0.7,G_3=0.01) 4-61

4.49. Poincaré Map of θ_1' vs θ_2' for Small Rate Feedback Gain
(500 Orbits Sampled at 4π,e=0.5,s=1.0,K=0.7,G_3=0.01) 4-62

4.50. Poincaré Map of θ_1 vs θ_2 for Small Rate Feedback Gain
(500 Orbits Sampled at 2π,e=0.5,s=1.0,K=0.7,G_3=0.01) 4-63

4.51. Poincaré Map of θ_1' vs θ_2' for Small Rate Feedback Gain
(500 Orbits Sampled at 2π,e=0.5,s=1.0,K=0.7,G_3=0.01) 4-64

4.52. Poincaré Map of θ_1 vs θ_2 for Small Rate Feedback Gain
(10000 Orbits Sampled at 2π,e=0.5,s=1.0,K=0.7,G_3=0.01) 4-66

4.53. Poincaré Map of θ_1' vs θ_2' for Small Rate Feedback Gain
(10000 Orbits Sampled at 2π,e=0.5,s=1.0,K=0.7,G_3=0.01) 4-67

4.54. Poincaré Map of θ_1 vs θ_2 for Small Rate Feedback Gain (500 Orbits Sampled at 2π,e=0.5,s=1.0,K=0.7,G_j=0.05) 4-68

4.55. Poincaré Map of θ_1' vs θ_2' for Small Rate Feedback Gain (500 Orbits Sampled at 2π,e=0.5,s=1.0,K=0.7,G_j=0.05) 4-69

4.56. Phase Portrait of ζ vs ζ' for a Family of Orbits of Fixed Eccentricity (e=0.5) 4-71

4.57. Desired Orbit Phase Portrait of ζ vs ζ' (e=0.5) 4-72

4.58. Phase Portrait of ζ vs ζ' for Orbit Equations with Dissipation Term (δ=1.0) 4-74

4.59. Uncontrolled System Multipliers from AUTO ($0.0 \leq e \leq 0.7$,s=1.0,K=0.7) 4-75

4.60. Bifurcation Diagram of K vs θ_1 MAX for Rate Feedback System (e=0.5,s=1.0,G_j=0.85) 4-79

4.61. Branches 3 and 4 of Bifurcation Diagram of K vs θ_1 MAX for Rate Feedback System (e=0.5,s=1.0,G_j=0.85) 4-80

4.62. Bifurcation Diagram of K vs θ_2 MAX for Rate Feedback System (e=0.5,s=1.0,G_j=0.85) 4-81

4.63. Branches 3 and 4 of Bifurcation Diagram of K vs θ_2 MAX for Rate Feedback System (e=0.5,s=1.0,G_j=0.85) 4-82

4.64. Period Doubled Orbit of θ_1 from Branch 3 of AUTO (e=0.5,s=1.0,K=-0.339954,G_j=0.85) 4-84

4.65. Period Doubled Orbit of θ_2 from Branch 3 of AUTO (e=0.5,s=1.0,K=-0.339954,G_j=0.85) 4-85

4.66. Numerically Integrated Period Doubled Orbit of θ_1 (e=0.5,s=1.0,K=-0.339954,G_j=0.85) 4-86

4.67. Numerically Integrated Period Doubled Orbit of θ_2 (e=0.5,s=1.0,K=-0.339954,G_j=0.85) 4-87

4.68. Poincaré Map of θ_1 vs θ_2 from Numerical Integration (50 Orbits Sampled at 2π,e=0.5,s=1.0,K=-0.339954,G_j=0.85) . 4-89

4.69. Poincaré Map of θ_1 vs θ_2 from Numerical Integration (2500 Orbits Sampled at 4π,e=0.5,s=1.0,K=-0.339954,G_j=0.85) 4-90

4.70. Numerically Integrated Period Doubled Orbit of θ_1 with Phase Shift (e=0.5,s=1.0,K=-0.339954,G_j=0.85) 4-91

4.71. Numerically Integrated Orbits of θ_1 at Onset of Chaotic Motion ($e=0.5, s=1.0, K=-0.3485, G_3=0.85$) 4-92

4.72. Numerically Integrated Orbits of θ_2 at Onset of Chaotic Motion ($e=0.5, s=1.0, K=-0.3485, G_3=0.85$) 4-93

4.73. Poincaré Map of θ_1 vs θ_2 from Numerical Integration (1000 Orbits Sampled at 2π, $e=0.5, s=1.0, K=-0.3485, G_3=0.85$) . 4-94

A.1. Coordinate Reference Frames A-2

A.2. Satellite Reference Frame and Orbit Description A-3

List of Tables

Table		Page
3.1.	Classification of Poincaré Maps	3-7
4.1.	Characteristic Multipliers for Control Generation Equations	4-77
4.2.	Summary of Bifurcation Points	4-83

Abstract

Controlled and uncontrolled equations of motion for a spinning symmetric satellite in an elliptical orbit are analyzed using Floquét theory, Poincaré maps, and continuation. The equations of motion for the uncontrolled system are derived via energy methods. A simple feedback controller design and one based on Floquét theory are presented. Parameters varied in the equations of motion include the spin about the symmetry axis of the satellite, the inertia ratio of the satellite, the eccentricity of the orbit, and the controller gains. Floquét analyses determine local stability and bifurcation points. Poincaré maps exhibit some interesting and complex structure in the global phase space. Continuation using a bifurcation analysis computer code (AUTO) reveals a sequence of period doublings, which is verified via numerical integration, for the simple rate feedback controller. The onset of chaotic motion is detected for this sequence of period doublings.

NONLINEAR ANALYSIS OF A SPINNING SYMMETRIC SATELLITE IN AN ELLIPTICAL ORBIT

I. Introduction

The attitude stability of a satellite under less than nominal conditions is the desire of any spacecraft designer. Usually, the nominal conditions include operation of the satellite in the linear regime since most design and stability analysis is easily accomplished there. Yet, there is always a set of initial conditions that define the limit of effectiveness of any attitude stabilization method. These initial conditions usually bring nonlinear effects into the problem. Thus, the goal of the satellite designer is to improve the stability characteristics such that even the less than nominal initial conditions pose no threat to operational effectiveness. Before such a goal can be met, the satellite stability characteristics must be traced from the most basic design to the most complex to include analyses away from the linear regime. In other words, a nonlinear analysis may reveal some critical stability characteristics of the system.

A passive method of gaining attitude stability is to spin the satellite about one of the principal axes similar to a gyroscope or top. Kane and Barba [8] studied such an approach for a symmetric satellite in an elliptical orbit. They found the linearized equations of motion for the satellite to be time periodic; Floquét theory was used to test for

stability. They demonstrated that the attitude stability for a satellite spinning about its symmetry axis is a function of orbit eccentricity, spin rate, and the inertia ratio of the satellite. Wallace and Meirovitch [16] then investigated the stability characteristics of this problem using the Liapounov direct method along with asymptotic expansions as their approach. They found that the nonlinear effects limited the amplitude of resonant oscillations in the attitude motion of the satellite. The nonlinear equations of motion for this problem are derived in Appendix A and the linear equations are summarized in Chapter I.

But, for fine pointing requirements, active control is required. Simple rate and position feedback may be all that is needed. However, more complex control designs are possible and can improve performance. Calico and Yeakel [4] and Calico and Wiesel [3] developed a control method based on Floquét theory utilizing modal coordinates. In simple terms, this approach provides a time periodic, coupled rate and position feedback to stabilize unstable modes (characteristic multipliers outside the unit circle). Myers [12] evaluated some variations of this approach while Shell [14] extended this work to examine what happens away from the linear regime (equilibrium point). Cole [5] investigated in greater detail the global effectiveness of the Floquét controller by using Poincaré maps. He found an attractor present away from the nominal linear conditions as the gain on the controller was increased. The above work has only begun to scratch the surface of the nonlinear phenomena present in this problem. The characterization of such phenomena can help define the boundary for the region of effectiveness of the Floquét and other controller designs.

The origin and characterization of such complex, global nonlinear phenomena is the goal of this thesis. Toward this end, Floquét theory, Poincaré maps, bifurcation theory, and continuation are used to analyze controlled and uncontrolled equations of motion. The uncontrolled equations of motion are analyzed to establish conservative bifurcation points. The complexity of the Floquét controlled equations of motion did not allow for any continuation analyses on this design. Thus, this controller design is evaluated in a cursory fashion in this study. In its place, a simple rate and position feedback controller is used to better understand local and global stability characteristics for the controlled system. The results of this thesis add significantly to the existing knowledge base for the stability and control of the symmetric spinning satellite in an elliptical orbit.

II. Theory

This chapter contains a summary of the equations of motion for a spinning symmetric satellite in an elliptical orbit, Floquét theory, and the controlled equations of motion. The equations of motion are derived in full detail in Appendix A via the energy method approach. When the attitude equations of motion are linearized, they become a set of linear, time-periodic ordinary differential equations. This type of system of equations is essentially the Floquét problem. An extension of Floquét theory to incorporate modal variables allows for the design of a scalar feedback controller. A simplified controller is then defined by using standard rate and position feedback. Again, Floquét theory allows for the determination of linear stability of both the controlled and uncontrolled equations of motion.

2.1 Uncontrolled Equations of Motion

The equations of motion for any dynamical system can be derived by Newtonian dynamics or energy methods using Lagrange's equations. The former is thought of as the brute force approach for dynamical systems described by many rotating coordinate frames referenced to some inertial frame. On the other hand, the latter approach is elegant in that the equations of motion directly result from the expression for the sum of the kinetic and potential energies for the dynamical system. In this case, all conservative forces are included as potentials. All nonconservative forces must be included as generalized forces in Lagrange's equations of

motion. The major difference between the two approaches is that the energy methods do not require the inclusion of constraint forces that do no work in the problem.

I chose to present the energy method approach in this study. Kane and Barba [8] presented the Newtonian derivation in their paper on the stability of the linearized attitude equations of motion. Captain Dale Shell [14:2.23-2.25] and Captain Jim Cole [5:A.1-A.16] presented the Newtonian derivations in their theses also. A detailed presentation of the energy methods approach is provided in Appendix A for the reader. A summary of this is presented here.

The equations of motion are for a spinning symmetric satellite in an elliptical orbit about a symmetric attracting body. The center of mass of the attracting body is considered fixed. An inertial frame is fixed to this point and has the I_1 and I_2 axes in the equatorial plane of the body with the I_3 axis normal to this plane through the north pole. The satellite center of mass has a coordinate reference frame fixed to it such that axis A_1 is in the plane of the orbit and points in the direction of the radius vector to the satellite center of mass. The A_2 axis is perpendicular to axis A_1 and in the direction of the satellite's orbital motion. Finally, the A_3 axis is simply in the direction which completes a dextral, orthogonal coordinate system. This puts the A_3 axis normal to the orbit plane. A 1-2-3 rotation sequence through the angles θ_1, θ_2, and θ_3 measure the attitude orientation of the satellite with respect to the orbital reference frame A. Using these definitions, the equations of motion in nondimensional coordinates are

$$\zeta'' + \frac{1}{\zeta^2} + \frac{e^2-1}{\zeta^3} = 0 \tag{2.1}$$

$$\theta_1'' = 2\theta_1'\theta_2'\tan\theta_2 + 2v'\theta_2'\cos\theta_1 + v''\cos\theta_1\tan\theta_2 + v'^2\cos\theta_1\sin\theta_1 - (K+1)(s+1)(\theta_2' + v'\sin\theta_1)\sec\theta_2 \tag{2.2}$$

$$\theta_2'' = (K+1)(s+1)(\theta_1'\cos\theta_2 - v'\cos\theta_1\sin\theta_2) - \left(\theta_1'^2 - v'^2\cos^2\theta_1 + \frac{3K}{\zeta^3}\right)\sin\theta_2\cos\theta_2 - v''\sin\theta_1 - 2v'\theta_1'\cos\theta_1\cos^2\theta_2 \tag{2.3}$$

where

$$v' = \frac{(1-e^2)^{\frac{1}{2}}}{\zeta^2} \tag{2.4}$$

$$v'' = \frac{-2(1-e^2)^{\frac{1}{2}}}{\zeta^3}\zeta' \tag{2.5}$$

$$\theta_3 = (s+1)\tau - v = (s+1)nt - v \tag{2.6}$$

The dimensionless orbital radius is defined as

$$\zeta = \frac{R}{a} \tag{2.7}$$

with nondimensional time simply as

$$\tau = nt \tag{2.8}$$

which is the mean motion of the satellite times time. The inertia ratio and the spin parameter are defined by

$$K = \frac{C-A}{A} \tag{2.9}$$

and

$$g+1=\frac{P_{\theta_3}}{C} \tag{2.10}$$

respectively. Note that the orbital motion equation given by equation (2.1) drives the attitude equations to be time periodic. See Appendix A for definitions of all other variables.

By inspection, a constant solution to the attitude equations exists and is given by

$$\theta_1=\theta_2=0 \tag{2.11}$$

This equilibrium solution keeps the spin axis of the satellite perpendicular to the orbit plane. If the attitude equations are linearized about this equilibrium point, we get a set of linear, time-periodic, ordinary differential equations. In order to study the stability of these attitude equations, we must use Floquét theory.

2.2 Floquét Theory

Picking a state vector as

$$\vec{x}=\{\theta_1\ \theta_2\ \theta_1'\ \theta_2'\} \tag{2.12}$$

we can write the system of nonlinear equation as

$$\vec{x}'=\vec{f}(\vec{x}',\vec{x},\tau)\vec{x} \tag{2.13}$$

The system of equations can be linearized by

$$\delta\vec{x}'=A(\tau)|_{\vec{x}=\vec{x}_{eq}}\delta\vec{x} \tag{2.14}$$

where

$$\frac{\partial \vec{f}}{\partial \vec{x}} = A(\tau) \tag{2.15}$$

Note that the A matrix is evaluated at the equilibrium condition. The A matrix can be written as

$$A(\tau) = \begin{bmatrix} a_{11} & a_{12} & a_{13} & a_{14} \\ a_{21} & a_{22} & a_{23} & a_{24} \\ a_{31} & a_{32} & a_{33} & a_{34} \\ a_{41} & a_{42} & a_{43} & a_{44} \end{bmatrix} \tag{2.16}$$

The resulting terms of the A matrix for the linearized system are

$$a_{31} = \frac{(1-e^2)}{\zeta^4} - (1+s)(1+k)\frac{(1-e^2)^{\frac{1}{2}}}{\zeta^2} \tag{2.17}$$

$$a_{32} = -a_{41} = \frac{-2\zeta'(1-e^2)^{\frac{1}{2}}}{\zeta^3} \tag{2.18}$$

$$a_{34} = -a_{43} = \frac{2(1-e^2)^{\frac{1}{2}}}{\zeta^2} - (1+s)(1+k) \tag{2.19}$$

$$a_{42} = a_{31} - \frac{3k}{\zeta^3} \tag{2.20}$$

$$a_{13} = a_{24} = 1 \tag{2.21}$$

with the remaining terms being equal to zero. The orbital motion of the satellite causes

$$A(\tau)=A(\tau+T) \tag{2.22}$$

In other words, the A matrix is periodic with a period of T. We now have a set of linear, time periodic, ordinary differential equations. Floquét was the first to describe the solution to such a problem during the last decade of the 19th century [3:671].

The solution to the this type of system of equations can be shown to be

$$x(t)=\Phi(t,0)x(0) \tag{2.23}$$

where $\Phi(t,0)$ is the state transition matrix. The state transition matrix obeys the relationships

$$\frac{d}{dt}\Phi(t,0)=A(t)\Phi(t,0) \tag{2.24}$$

and

$$\Phi(0,0)=I \tag{2.25}$$

where I is the identity matrix [3:671]. Now, from Floquét theory, the state transition matrix becomes

$$\Phi(t,0)=F(t)e^{Jt}F^{-1}(0) \tag{2.26}$$

where J is the constant diagonal matrix of Poincaré/characteristic exponents and F(t) is a periodic matrix with same period T as the original system of equations. Therefore, the periodicity of the F matrix allows us to say that

$$F(0)=F(T) \tag{2.27}$$

at time T. This reduces equation (2.26) to

$$\Phi(T,0)=F(0)e^{JT}F^{-1}(0) \tag{2.28}$$

$\Phi(T,0)$ is an important matrix;it is called the monodromy matrix. Numerical integration over the period T of equation (2.24) with initial conditions given by equation (2.25) will determine the monodromy matrix.

Since the F matrix is periodic, it is bounded and does not affect the stability of the system. So, the only way for the system to be unstable is for the unbounded growth of the exponential term. Since J is a diagonal matrix, it follows that the F matrix is the matrix of eigenvectors for the monodromy matrix. So, the eigenvalues of the monodromy matrix are related to the Poincaré/characteristic exponents by

$$\lambda_i=e^{\omega_i T} \tag{2.29}$$

where the ω_i's are the Poincaré/characteristic exponents and the λ_i's are the eigenvalues of the monodromy matrix. The eigenvalues are called the Floquét/characteristic multipliers. So, if the moduli of all the characteristic multipliers are less than one, the system is linearly stable about the equilibrium condition. If any of the eigenvalues have moduli greater than one, then the system is unstable. If any of the eigenvalues have moduli equal to one, then the system is only stable if the multiplicity of that particular root is equal to the nullity of the monodromy matrix [8:404].

2.3 Controlled Equations of Motion

The controlled attitude equations of motion are

$$\theta_1'' = 2\theta_1'\theta_2'\tan\theta_2 + 2v'\theta_2'\cos\theta_1 + v''\cos\theta_1\tan\theta_2 + v'^2\cos\theta_1\sin\theta_1 - (K+1)(s+1)(\theta_2' + v'\sin\theta_1)\sec\theta_2 + K_1\theta_1 + K_2\theta_2 + K_3\theta_1' + K_4\theta_2' \quad (2.30)$$

$$\theta_2'' = (K+1)(s+1)(\theta_1'\cos\theta_2 - v'\cos\theta_1\sin\theta_2) - \left(\theta_1'^2 - v'^2\cos^2\theta_1 + \frac{3K}{\zeta^3}\right)\sin\theta_2\cos\theta_2 - v''\sin\theta_1 - 2v'\theta_1'\cos\theta_1\cos^2\theta_2 + K_1\theta_1 + K_2\theta_2 + K_3\theta_1' + K_4\theta_2' \quad (2.31)$$

The additional terms added to equations (2.30) and (2.31) provide the necessary feedback to cancel disturbances away from the desired equilibrium condition for an otherwise unstable uncontrolled system. Floquét theory and the use of modal coordinates allow for the design of this time periodic controller. This particular design approach moves one pair of unstable characteristic multipliers into the unit circle. In other words, the controller forced the characteristic multipliers to a stable regime of the phase space. This technique was developed by Calico and Wiesel [3:673-674]. The reader is also referred to [5] and [14] for further reading on this development.

The K_i in equations (2.30) and (2.31) are

$$\begin{aligned} K_1 &= -G_1L_{11} + G_2L_{12} \\ K_2 &= -G_1L_{21} + G_2L_{22} \\ K_3 &= -G_1L_{31} + G_2L_{32} \\ K_4 &= -G_1L_{41} + G_2L_{42} \end{aligned} \quad (2.32)$$

where G_1 and G_2 are gains that determine the location of the characteristic multipliers in the complex plane. The L_{ij} are found by solving the linear, time-periodic matrix differential equation

$$L'(t)=L(t)J-A^{T}(t)L(t) \tag{2.33}$$

where A(t) is given by equation (2.16) and J is the constant matrix of characteristic exponents. This equation is a result of manipulating equation (2.26) from Floquét theory where

$$L^{T}(t)=F^{-1}(t) \tag{2.34}$$

Again, see [3] and [5] for further detail.

A simplified controller is defined by the following equations:

$$\begin{aligned}\theta_1''=&2\theta_1'\theta_2'\tan\theta_2+2v'\theta_2'\cos\theta_1+v''\cos\theta_1\tan\theta_2+v'^2\cos\theta_1\sin\theta_1\\&-(K+1)(s+1)(\theta_2'+v'\sin\theta_1)\sec\theta_2+G_1\theta_1+G_2\theta_2+G_3\theta_1'+G_4\theta_2'\end{aligned} \tag{2.35}$$

$$\begin{aligned}\theta_2''=&(K+1)(s+1)(\theta_1'\cos\theta_2-v'\cos\theta_1\sin\theta_2)\\&-\left(\theta_1'^2-v'^2\cos^2\theta_1+\frac{3K}{\zeta^3}\right)\sin\theta_2\cos\theta_2\\&-v''\sin\theta_1-2v'\theta_1'\cos\theta_1\cos^2\theta_2\\&+G_2\theta_1+G_1\theta_2+G_4\theta_1'+G_3\theta_2'\end{aligned} \tag{2.36}$$

Now, the G_i's in equation (2.36) are simple feedback gains which are arranged such that there can be uncoupled position and rate feedback. These equations are easier to work with since the complexities of the Floquét controller are not included.

Floquét theory is used to determine the stability of both controlled systems of equations. Numerical integration and Poincaré plots are used to study the stability of the local and global solutions. One goal will be to use these techniques to facilitate the design of a control for this problem.

III. Numerical Methods for Nonlinear Analysis

This chapter provides a brief summary of a few selected numerical nonlinear analysis techniques. The discussion starts with an introduction to the nonlinear ordinary differential equations problem. The computer's ability to help investigate such problems is highlighted. The thrust of the remaining nonlinear analysis discussion emphasizes bifurcation theory. Bifurcations due to characteristic multiplier location and movement and their effect on stability are described. The next two sections summarize the selected numerical techniques for nonlinear analysis. These techniques include Poincaré maps and continuation using AUTO [6] which is a computer code used for part of this study. For completeness, a discussion of Hamiltonian (conservative) systems is included. Specific problems encountered with AUTO for Hamiltonian systems are included in the discussion.

3.1 Nonlinear Analysis and the Computer

In many fields of science and engineering, dynamics of motion or processes are modelled by ordinary differential equations. In most cases, these models contain nonlinearities such as equations (2.2) and (2.3). If there is no explicit dependence on time in the differential equation, then the system is said to be autonomous. A general, second order, autonomous differential equation can be written as

$$\frac{d^2\vec{x}}{dt^2} = f\left(\vec{x}, \frac{d\vec{x}}{dt}\right) \tag{3.1}$$

where the vector x contains the states of the system and f is the vector of functions describing the time evolution of the vector x.

Since equation (3.1) is a nonlinear set of differential equations, one would expect nonlinear phenomena in the solutions. However, the solutions to such problems are rarely obtained in closed form. Traditionally, the equations are linearized about some equilibrium point which gives a local picture of the what's going on in the dynamics of a particular system. The objective of such an approach is to stay away from the nonlinearities of the problem at hand. In reality, we can not be assured of initial conditions that keep us in the local (linear) regime. Thus, a global picture away from the equilibrium point is required in order to address the nature of any nonlinear phenomena in the problem.

With the advent of the computer and efficient and accurate numerical integration methods, the study of nonlinear phenomena has become possible for those with little expertise in more rigorous, mathematical approaches. Using this straightforward approach, one can begin to see the nonlinearities effect on the time evolution of a dynamical system. "Jumping between modes, sudden onset or vanishing of periodic solutions, loss or gain of stability, buckling of frames and shells, ignition and combustion, and chaos are but a few examples" [13:ix]. So, through the use of the computer, numerical techniques have opened the door to the study of nonlinear phenomena.

3.2 Bifurcation of Solutions

The introduction of a free parameter into the differential equation modelling the dynamics of system can cause a variety of responses for certain values of the parameter. The dynamical model is now represented by

$$\frac{d^2\vec{x}}{dt^2} = f\left(\vec{x}, \frac{d\vec{x}}{dt}, \lambda\right) \tag{3.2}$$

where λ is a free parameter. A bifurcation occurs when a change in response type is detected as the parameter passes through a critical value called the bifurcation point [7:317]. A bifurcation diagram, which plots the value of the varying parameter versus some scalar measure of one of the system states, allows us to study the effect of the parameter on the system response. In other words, bifurcation of the system response can be detected by looking at the bifurcation diagram. Much of this section follows the presentation in Seydel [13] which is an excellent reference for bifurcation theory.

The characteristic multipliers of a periodic system determine its local (linear) stability. Recall from the discussion on Floquét theory, that the moduli of the characteristic multipliers directly indicate whether or not there is local stability. For a periodic system, there will be one characteristic multiplier with a modulus of unity. If all of the other characteristic multipliers lie in the unit circle, the periodic motion is stable. In order for local stability to be lost, one or more of the characteristic multipliers must depart the confines of the unit circle. This movement of the characteristic multipliers is a result of

varying the free parameter λ. Note that some dynamical systems may have a vector of parameters that can be varied. Figure 3.1, borrowed from Seydel [13:299], depicts three possible ways of leaving the confines of the unit circle.

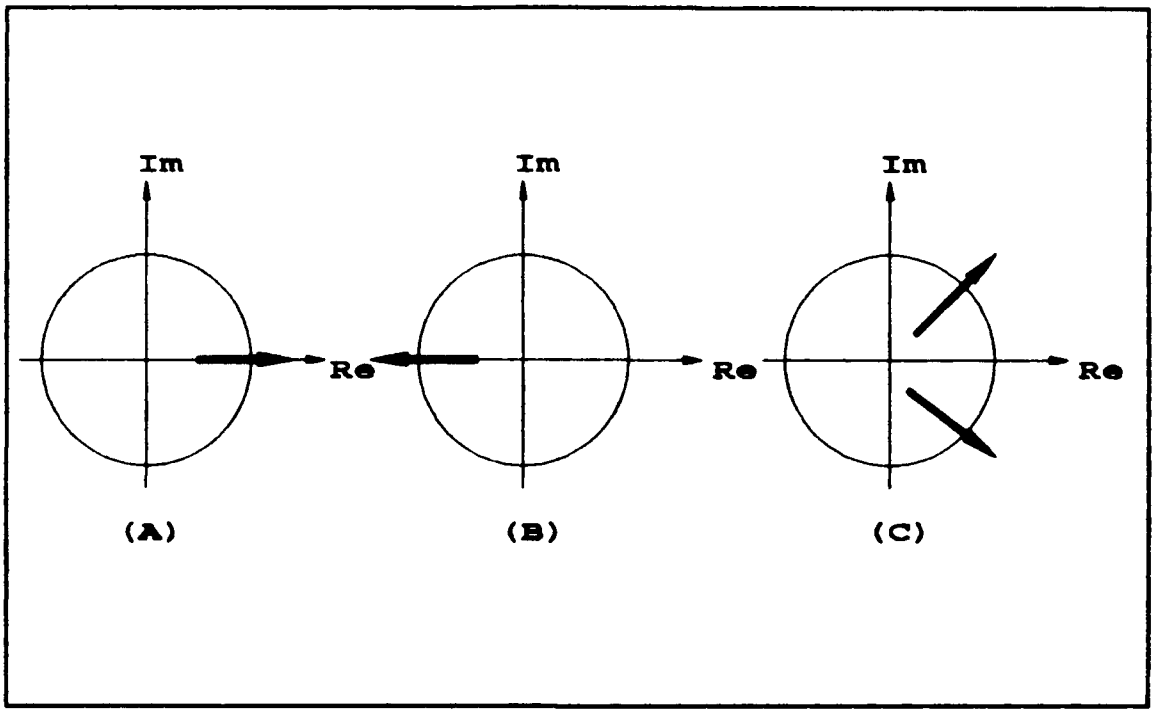

Figure 3.1 Types of Bifurcations

In Figure 2.1 (A), the characteristic multiplier crosses the unit circle at +1. This type of crossing results in one of three possibilities. One possibility is that a limit point is achieved. In other words, for $\lambda > \lambda_{CRITICAL}$, two solutions exist with one being stable and the other being unstable. If $\lambda < \lambda_{CRITICAL}$, then no solutions exist. The other two possibilities are a result of some form of symmetry in the problem

which results in pitchfork or transcritical bifurcations [13:252].

In Figure 3.1 (B), the characteristic multiplier crosses the unit circle at -1. This type of crossing usually results in a period doubling for the dynamical system. This type of bifurcation is only possible for systems with three dimensions or higher. This type of bifurcation, sometimes called a *flip bifurcation*, exhibits a loss of stability for the original stable periodic orbit while a new orbit with twice the period is created [15:127].

In Figure 3.1 (C), a pair of complex-conjugate multipliers cross the unit circle for a critical value of the parameter λ. This type of bifurcation is known as a bifurcation into a torus. Again, such a bifurcation only exits for three dimensions or higher. The original periodic orbit loses stability and remains at the center of the torus. These tori can be attractive or repelling [13:263]. Figure 3.2 depicts motion on a torus. A slice of the torus taken with a Poincaré map yields a closed curve on the map.

Motion on a torus contains two frequencies. One frequency is for motion around the circumference of the torus and the other frequency is for motion around the cross-section of the torus. If these two frequencies are irrational, then the motion is said to be quasiperiodic.

Two less understood but most interesting cases of bifurcation are those that result in a strange attractor or chaos. An attractor is called strange if the trajectory depends sensitively on initial conditions [13:310]. A definition for a strange attractor is "an attractor that is not an equilibrium point nor a limit cycle, nor a quasiperiodic attractor"

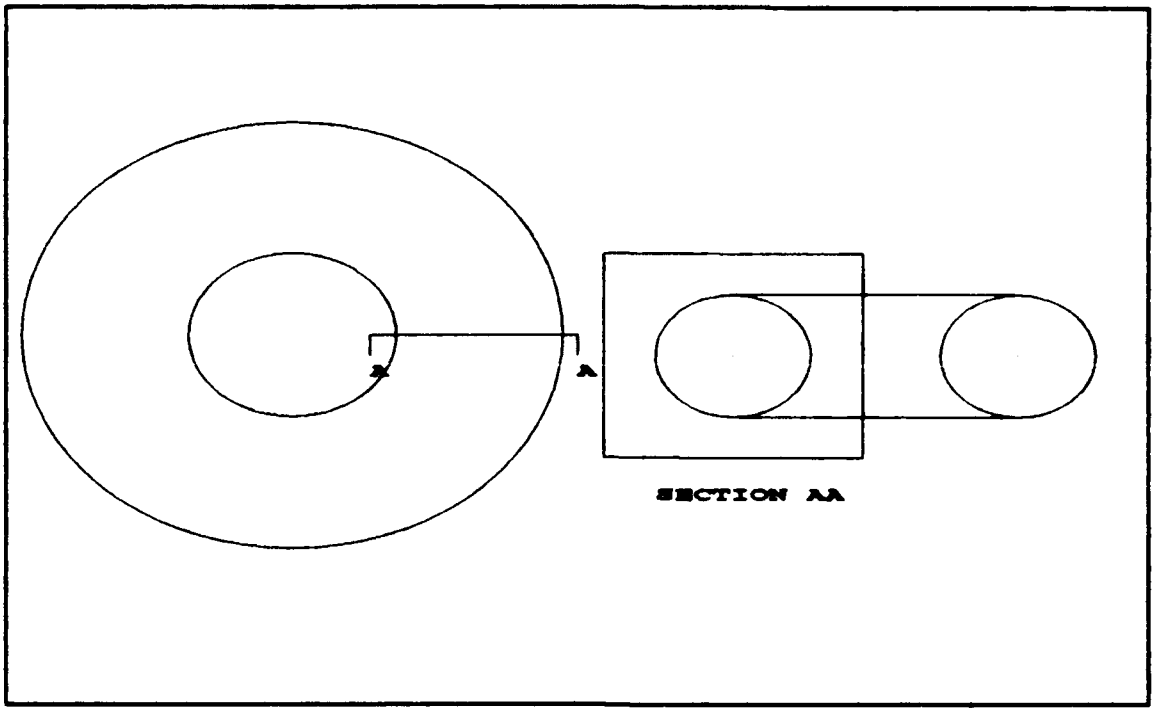

Figure 3.2 Motion on a Torus

[11:267]. Chaos is not far removed from a strange attractor. Both are sensitive to initial conditions. However, trajectories starting from slightly different initial conditions exponentially diverge for chaotic motion [11:262]. It is almost absurd to think that a deterministic differential equation results in an unpredictable type of problem (chaos).

3.3 Poincaré Maps

A technique which is attributed to Henri Poincaré (1854-1912) is the Poincaré map. It is also known in other terms as a first return map, surface of section, and Poincaré section. "Poincaré mapping is often used for analyzing the geometry of trajectories in the phase space" [9:26]. For trajectories in the phase space that are periodic, the Poincaré map is the logical choice to make to identify the structure of any attractors.

An attractor is a portion of phase space that trajectories have an affinity to after the transients have all died out. Classical dynamical attractors include equilibrium points, limit cycles, and toroidal surfaces [11:261].

The Poincaré map is the result of a trajectory in the phase space as it repeatedly passes transversely through a plane or surface that slices through the phase space. The sequence of points plotted on the surface forms the map. The characteristic structure of the Poincaré map can be used to describe the attractor at hand. Table 3.1 derived directly from Moon [11:53] summarizes what particular structures on the Poincaré map might indicate.

Table 3.1 Classification of Poincaré Maps

Finite number of points: periodic or subharmonic oscillation *Closed curve*: quasiperiodic, two incommensurate frequencies present *Open curve*: suggest modelling as a one dimensional map; try plotting x(t) versus x(t+T) *Fractal collection of points*: strange attractor in three phase space dimensions *Fuzzy collection of points*: (i) dynamical system with too much random or noisy input; (ii) strange attractor but system has very small dissipation; (iii) strange attractor in phase space with more than three dimensions; (iv) quasiperiodic motion with three or more dominant incommensurate frequencies [11:53]

A variation of the Poincaré map is the *stroboscopic technique* [15:66]. This approach creates a Poincaré map by plotting points of the trajectory in the phase space at some specified time which is usually a multiple of the period of the system.

In higher dimensional systems, it is difficult to identify the characteristics of the attractor in the phase space using the standard

Poincaré map. The problem here is trying to view more than three dimensions on a two dimensional plot. A technique called the *double Poincaré map* allows one to observe the structure of a three dimensional Poincaré map of a fourth order system [11:142]. The *double Poincaré map* is constructed by sampling the phase space trajectory as done with the *stroboscopic technique* ;however, two frequencies are used instead of one. A point is plotted "when the first frequency is *coincident* with the second frequency" [11:143]. This technique cuts a slice of the three dimensional phase space in order to determine the nature of any attractors present. Any fractal nature in the resulting plot is characteristic of a strange attractor [11:144].

3.4 Hamiltonian Systems

A Hamiltonian system is synonymous with a conservative system; no dissipation is present. Many classical dynamical problems such as those encountered in orbital/celestial mechanics fall into this category of problems. These types of problems are characterized by forces that can be represented by a potential. The uncontrolled equations of motion in this thesis are conservative since the only force in the problem, gravity, is represented by potential as shown in Appendix A.

A Hamiltonian system will always have an even number of phase variables. If a Poincaré plot is used to study the trajectories of a four state Hamiltonian system, the phase trajectories will eventually pass through all points in the remaining three-dimensional subspace. "Chaotic orbits in conservative systems tend to visit all parts of a subspace uniformly; that is they exhibit a uniform probability density over

restricted regions in the phase space" [11:63]. It is important to note that conservative systems "do not exhibit strange attractors" [13:311].

If dissipation is added to a conservative system by some form of control, one would expect a contraction of the trajectories in the phase space into some form of defined structure. Chaotic trajectories in dissipative systems exhibit a fractal structure in the phase space [11:63]. However, a small amount of dissipation in a system can cause it to resemble a Hamiltonian system in the phase space [11:63]. So, it follows that the addition of *enough* dissipation should result in the formation of some sort of attractor.

3.5 Continuation

A numerical method that allows us to compute a family of solutions (algebraic or periodic) as a parameter is varied given an initial solution is a *continuation method.* Another definition is "a numerical technique enabling us to obtain one branch of solutions (or more branches of solutions mutually connected at branch points)" [9:21]. Continuation is also known as branch tracing. So, with continuation, a parameter is systematically varied to compute new solutions from nearby previously computed solutions. Stability of these solutions are available since the Jacobian matrix for the system is also carried along in the solution process. Therefore, it is simply a matter of finding the eigenvalues of the Jacobian matrix to determine stability. As the eigenvalues cross the unit circle, bifurcation points are located.

A FORTRAN digital computer program created by E. Doedel called AUTO [6] performs continuation analysis for moderate sized problems. It

computes families of solutions for both equilibria and periodic solutions. This software package was used in this study in a limited fashion due to the conservative nature of problems studied herein. AUTO was designed to study dissipative systems. In order to handle conservative (Hamiltonian) types of problems, dissipation must be added with caution so that the problem being studied is not altered greatly.

Take for example, equation (2.1), which is the nondimensional differential equation for the satellite's orbital motion. Since this equation is a result of a conservative system, an infinite family of closed trajectories exist. Such a system causes a problem in AUTO. So, dissipation must be added in order for AUTO to run correctly and converge. In other words, a limit cycle about the desired orbit must be created by the addition of a dissipative term to equation (2.1). The question that remains is how to accomplish such a feat.

A chapter in [1] is devoted to such a topic. Let us rewrite equation (2.1) as set of first order differential equations.

$$\zeta' = x' = y = \frac{\partial H}{\partial y} \tag{3.3}$$

$$\zeta'' = y' = \frac{1-e^2}{x^3} - \frac{1}{x^2} = \frac{-\partial H}{\partial x} \tag{3.4}$$

H can be thought of as the Hamiltonian for the system. The elimination of the nondimensional time variable gives us the equation for the phase paths of the system which is

$$\frac{dy}{dx} = \frac{1}{y}\left[\frac{(1-e^2)}{x^3} - \frac{1}{x^2}\right] \tag{3.5}$$

Since equation (3.5) is separable, it is integrated to get

$$H(x,y)=\frac{y^2}{2}+\frac{(1-e^2)}{2x^2}-\frac{1}{x} \tag{3.6}$$

where H is the constant which describes a particular orbit. For the nondimensional variables used, H_o is equal to $-\frac{1}{2}$ for all possible orbits with initial conditions at apogee of y=0 and x=1+e. However, we are interested in the particular case e=0.5. The feature we want the dissipation term to have is a zero contribution when the trajectory is on the desired orbit and an other than zero contribution elsewhere. A dissipative term of the form

$$\delta f(x,y)[H_o-H(x,y)] \tag{3.7}$$

will cleverly do this for us. Now, if we let the new system of equations with the added dissipation be

$$x'=\frac{\partial H}{\partial y} \tag{3.8}$$

$$y'=\frac{-\partial H}{\partial x}+\delta y[H_o-H(x,y]) \tag{3.9}$$

where δ is a parameter, we can show that a limit cycle about the desired orbit is created by the use of the invariant integral

$$\iint tr[J]\,dx\,dy=0 \tag{3.10}$$

where J is the Jacobian matrix for the system. It can be shown that the invariant integral holds for equations (3.8) and (3.9) over the region of the desired orbit. Also, it can be shown that the limit cycle created about the desired orbit is stable.

IV. Results

This chapter contains a variety of results obtained from using the theory and techniques described in chapters II and III. The objective of such a broad approach was to gain enough information about the symmetric satellite in an elliptical orbit problem to characterize some of the local and global phenomena as a function of parameters in the system. The parameters varied included the spin rate about the axis of symmetry (s), inertia ratio (K), eccentricity (e), and controller gains (G_1, G_2, G_3, G_4). Both global and local stability characteristics were examined. However, the local stability characterization was a more tractable problem. As you will see, the nonlinearities in this problem created some interesting results which were at times difficult to explain.

The computer was the primary tool used in generating the results presented in this thesis. All the computer code used was written in FORTRAN 77 using double precision variables. The routines used for the Floquét analysis originated from previous work [14], [12], and [5]. I modified these routines to allow for the cases studied in this thesis as well as automating the program to vary a chosen parameter over a specified range at a user selected step size. These routines were run on a Digital Equipment Corporation (DEC) VAX 8550 computer using the VAX operating system. The numerical integration of the equations of motion was performed using the Hamming integrator. This integration was done on the Elxsi 6400 computer using the EMBOS operating system. The AUTO continuation routines were run on the DEC VAX 8550.

4.1 Floquét Analysis

Floquét theory was used to analyze characteristic multiplier movement on the complex plane to determine possible bifurcation points. It was hoped that any bifurcation points found would lead to some of the complex structure found by Cole [5]. Local stability characterization in a finer detail than presented by Kane and Barba [8] resulted from this analysis.

4.1.1 Uncontrolled Equations of Motion. Kane and Barba [8], Myers [12], and Shell [14] all calculated characteristic multipliers for the uncontrolled equations of motion. However, these multipliers were only calculated at values of eccentricity equal to 0.0, 0.1, 0.3, 0.5 and 0.7 for a set of chosen values of the spin parameter and the inertia ratio. In this thesis, the characteristic multipliers for this problem were calculated over the range $0.0 \leq e \leq 0.7$ with steps in e as small as 1×10^{-8} to determine bifurcation points. The bifurcation points for the uncontrolled equations are termed conservative because the multipliers split away from the unit circle in pairs. These multipliers were plotted on the complex plane along with the unit circle to give a finer picture of what is happening as e is varied.

The first case examined contained the parameter values used in the Floquét controller design and analyses done in the past [12], [14], [5]. Figure 4.1 shows this most interesting case with s=1.0 and K=0.7. At e=0.5, which is the case the Floquét controller stabilized, one multiplier pair is outside the unit circle and one multiplier pair is inside the unit circle. Since one pair of multipliers is outside the unit circle, there

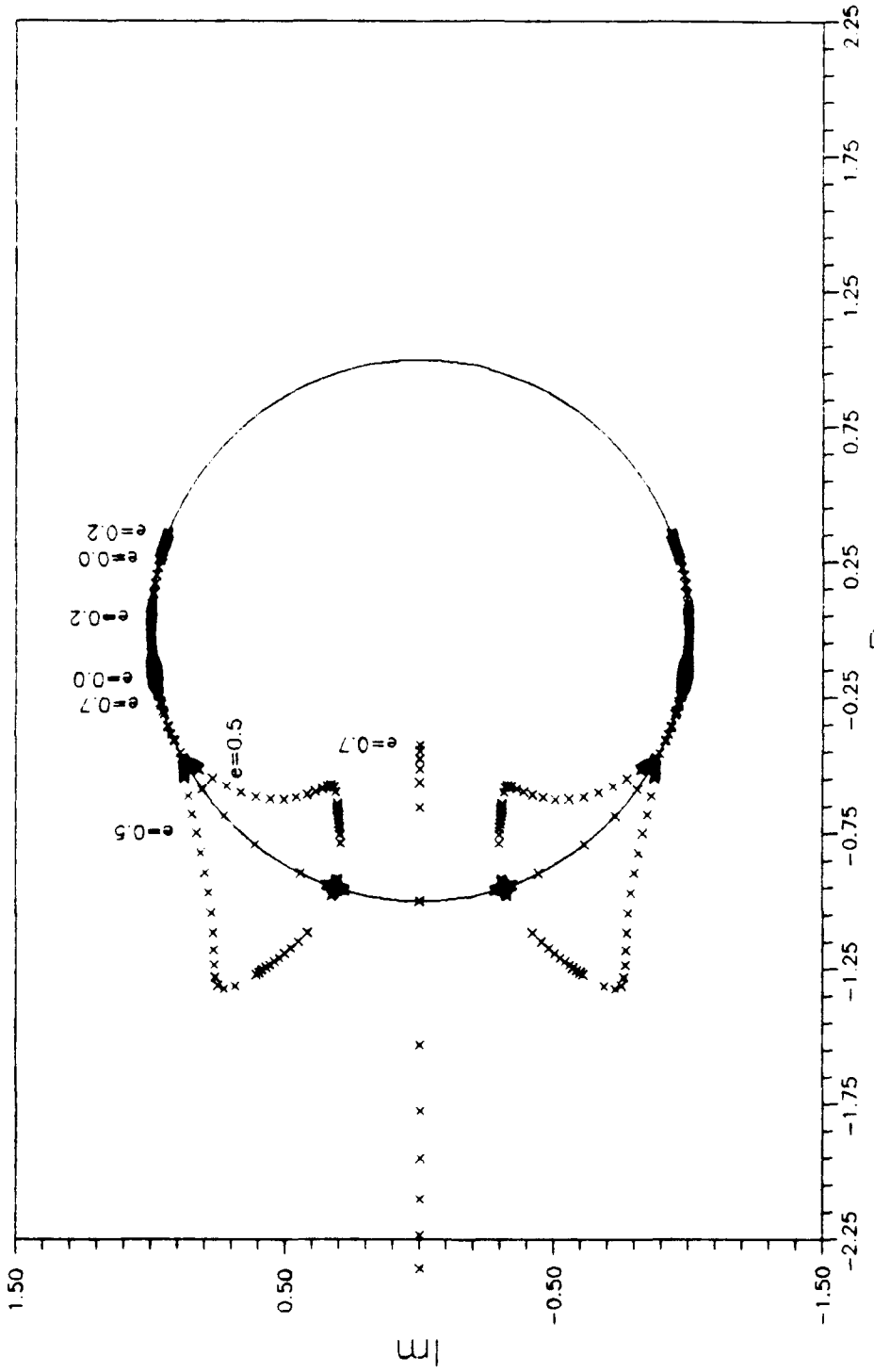

Figure 4.1 Uncontrolled System Multipliers (0.0<e<0.7,s=1.0,k=0.7)

is no local stability for the equilibrium condition. Figure 4.1 exhibits three places where the multipliers leave the unit circle. One place is represented by a dark filled in oval on the unit circle. Figures 4.2, 4.3, 4.4, and 4.5 detail the values of a where the multipliers leave the unit circle; these points locate where local stability is lost. Figure 4.2 shows a plot of the multipliers for $0.38 \leq e \leq 0.41$. This departure from the circle was completely unexpected and not found previously. Figure 4.3 shows that the multipliers leave the unit circle for $0.46 \leq e \leq 0.47$. When a complex pair of multipliers leave the unit circle as in figures 4.2 and 4.3, it usually indicates a bifurcation into a torus. Figure 4.4 shows that the multipliers return to the unit circle for $0.6316 \leq e \leq 0.6317$ where local stability is regained for a very small range of e. This region of local stability was not found previously. Figure 4.5 shows how sensitive the multipliers can be to a very small change in e. For $0.63274217 \leq e \leq 0.63474218$, the multipliers leave the unit circle with a bifurcation point that resembles a local period doubling.

The effect of the spin parameter on figure 4.1 was looked at next. Figures 4.6, 4.7, 4.8, 4.9, 4.10, 4.11, 4.12, and 4.13 show what happens to local stability at different values of the spin parameter s in the range $-3.0 \leq s \leq 3.0$.

First, the spin parameter was increased over the value used in figure 4.1. Figures 4.6 and 4.7 show the movement of the characteristic multipliers for the spin parameters s=1.5 and s=2.0 respectively. The detailed structure of leaving and returning to the unit circle has disappeared. However, the period doubling bifurcation point still

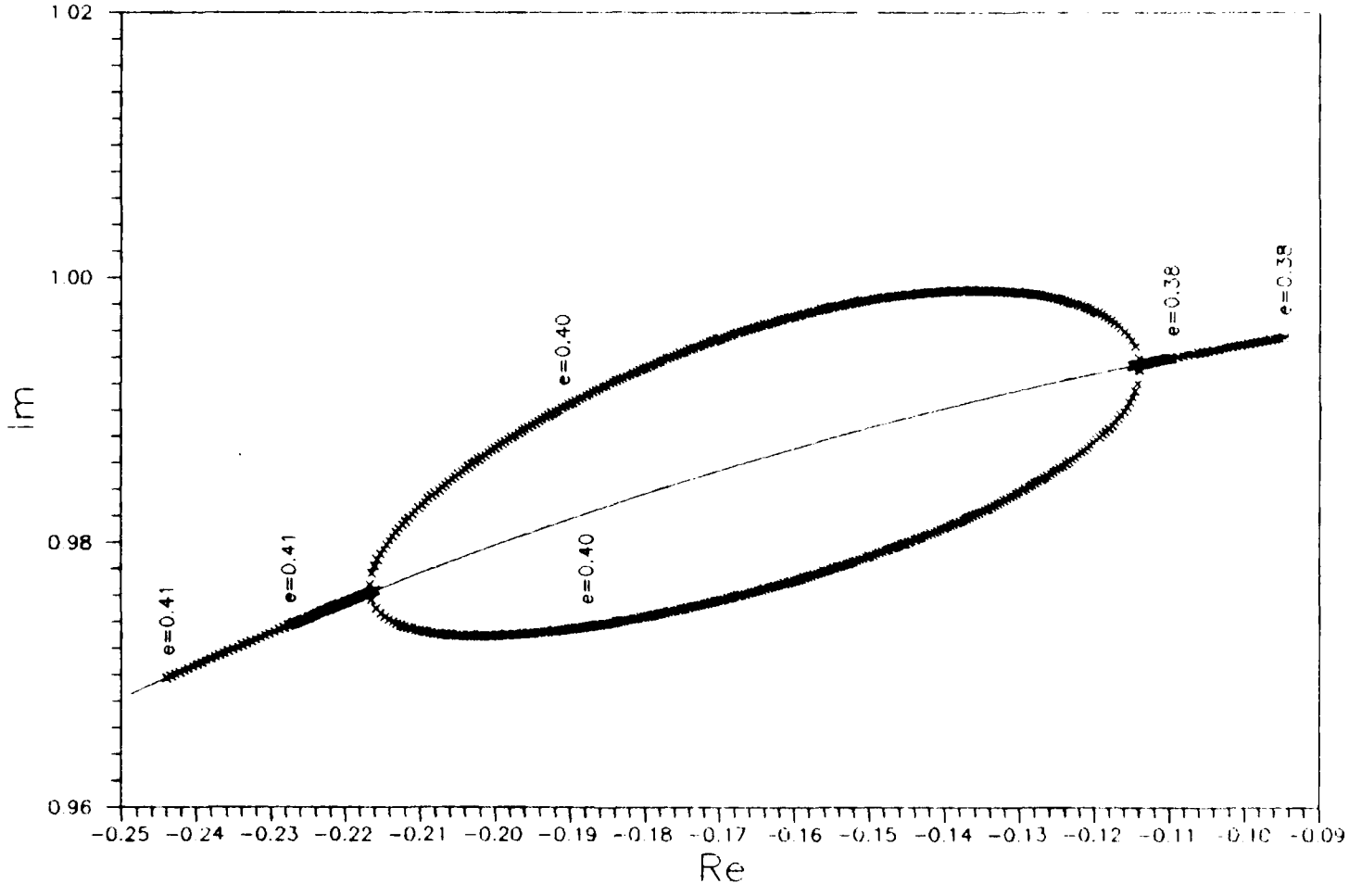

Figure 4.2 Uncontrolled System Multipliers (0.38<e<0.41,s=1.0,k=-0.7)

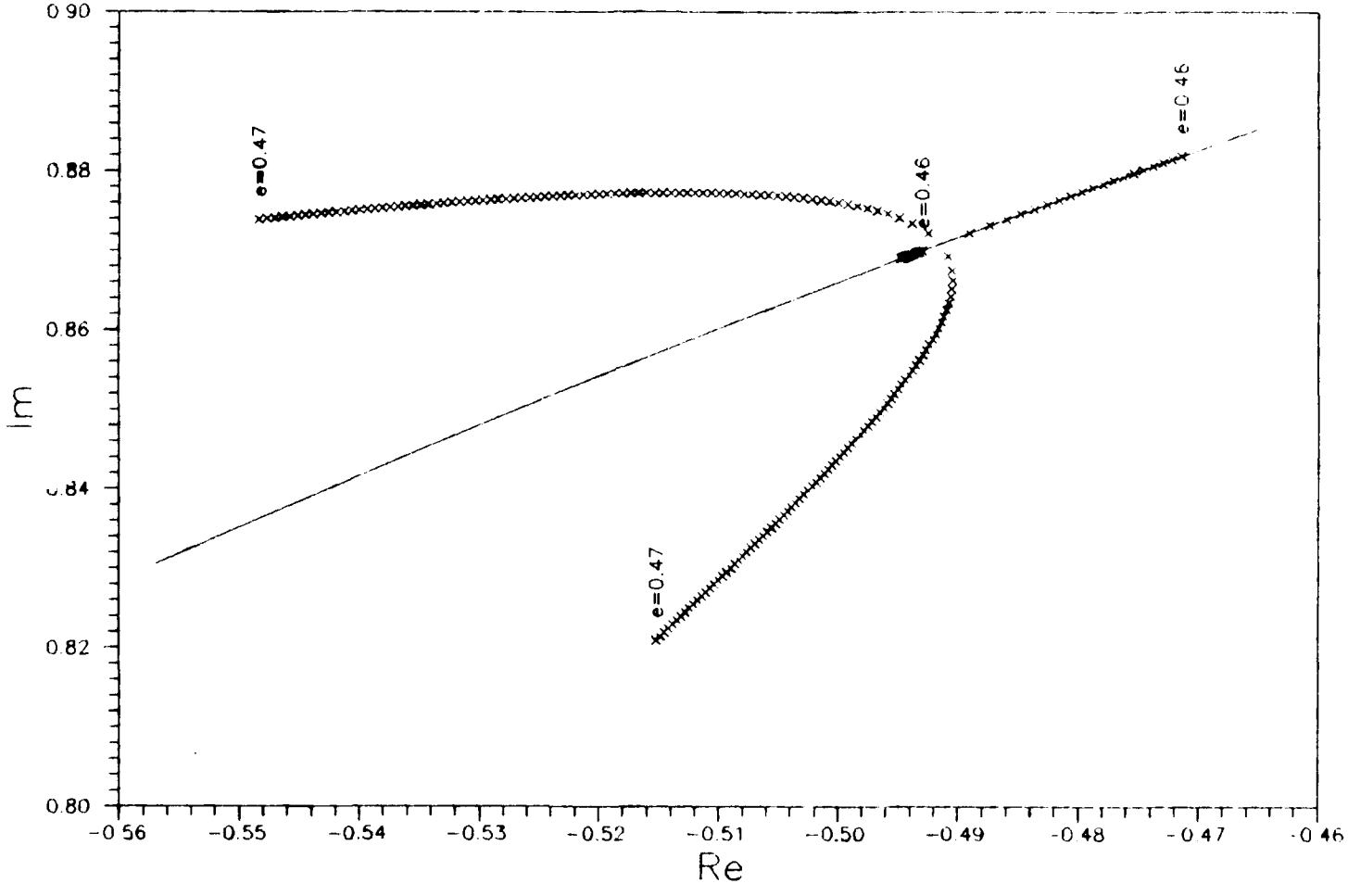

Figure 4.3 Uncontrolled System Multipliers (0.46<e<0.47,s=1.0,K=0.7)

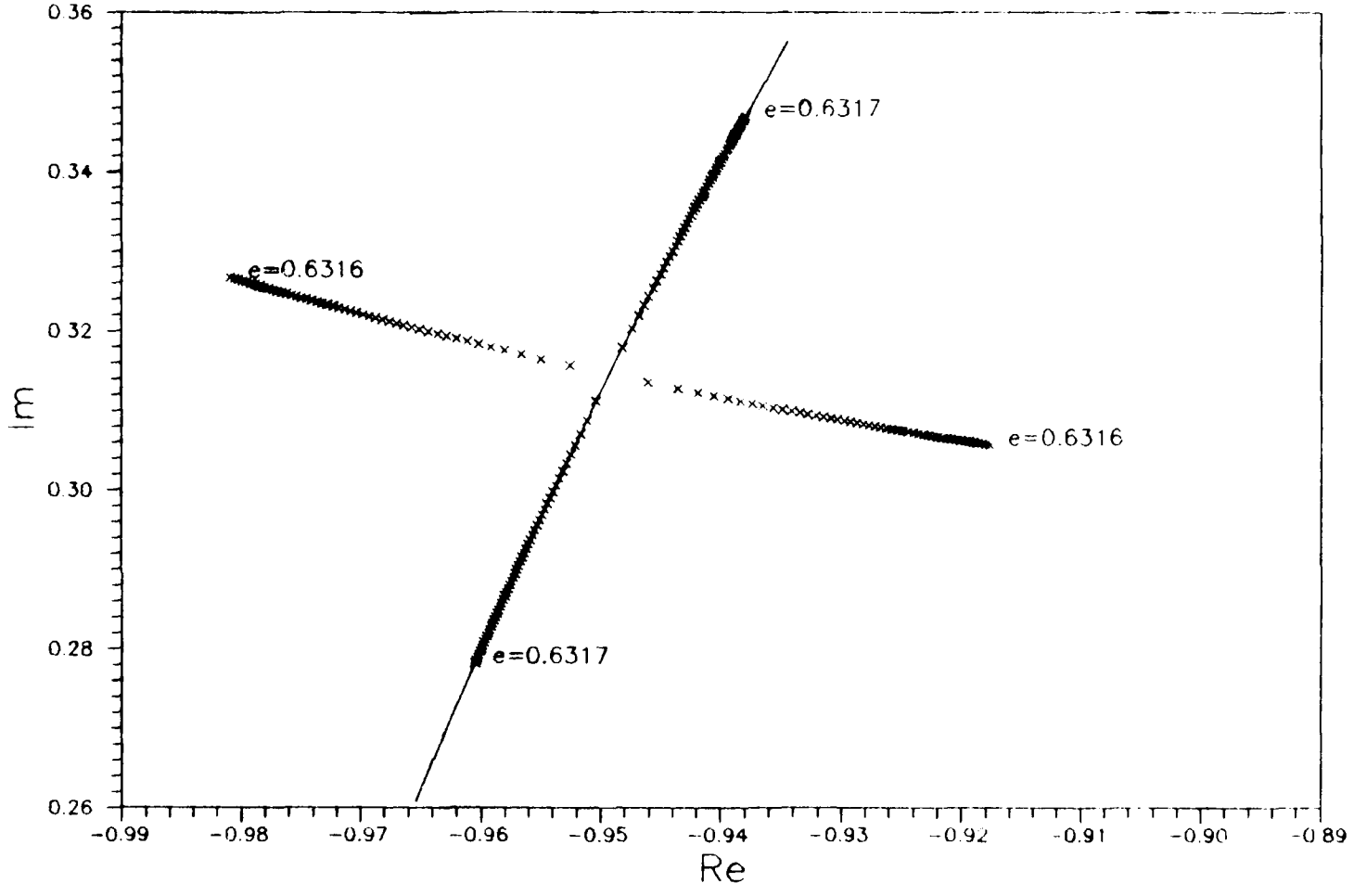

Figure 4 4 Uncontrolled System Multipliers (0.6316<e<0.6317,s=1.0,k=0.7)

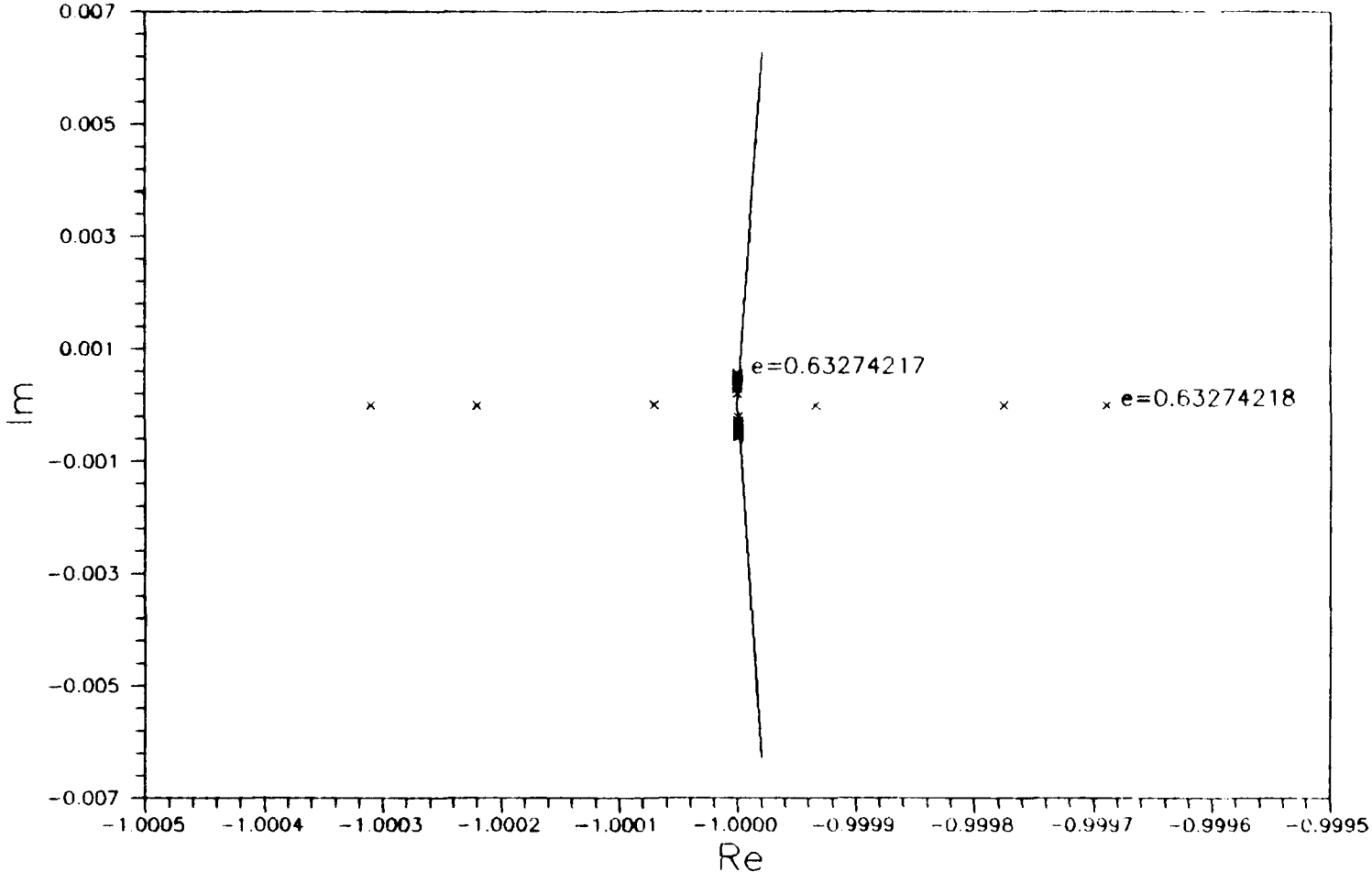

Figure 4.5 Uncontrolled System Multipliers
(0.63274217<e<0.63274218,s=1.0,K=0.7)

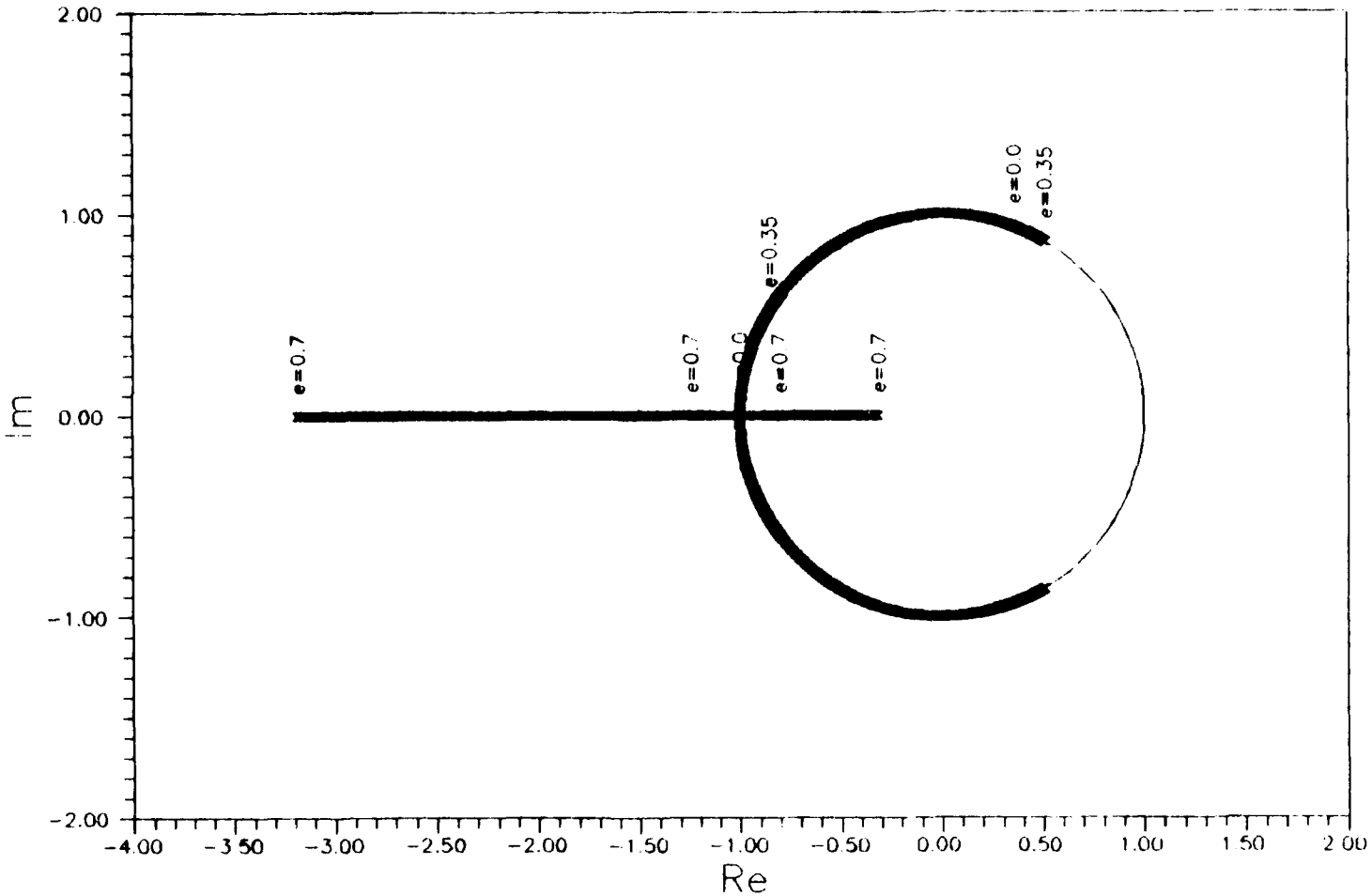

Figure 4.6 Uncontrolled System Multipliers ($0.0<e<0.7, s=1.5, K=0.7$)

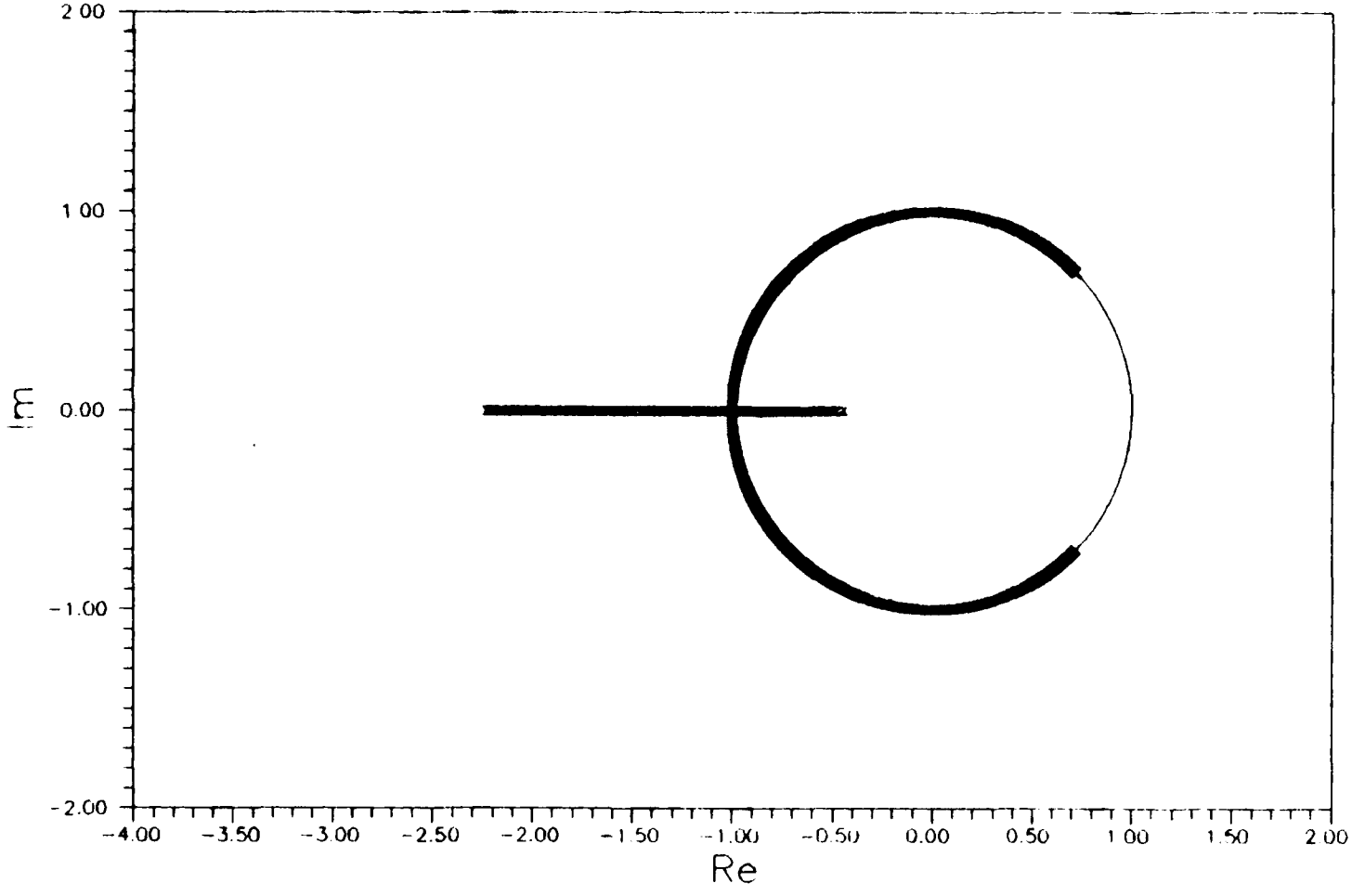

Figure 4.7 Uncontrolled System Multipliers (0.0<e<0.7,s=2.0,k=0.7)

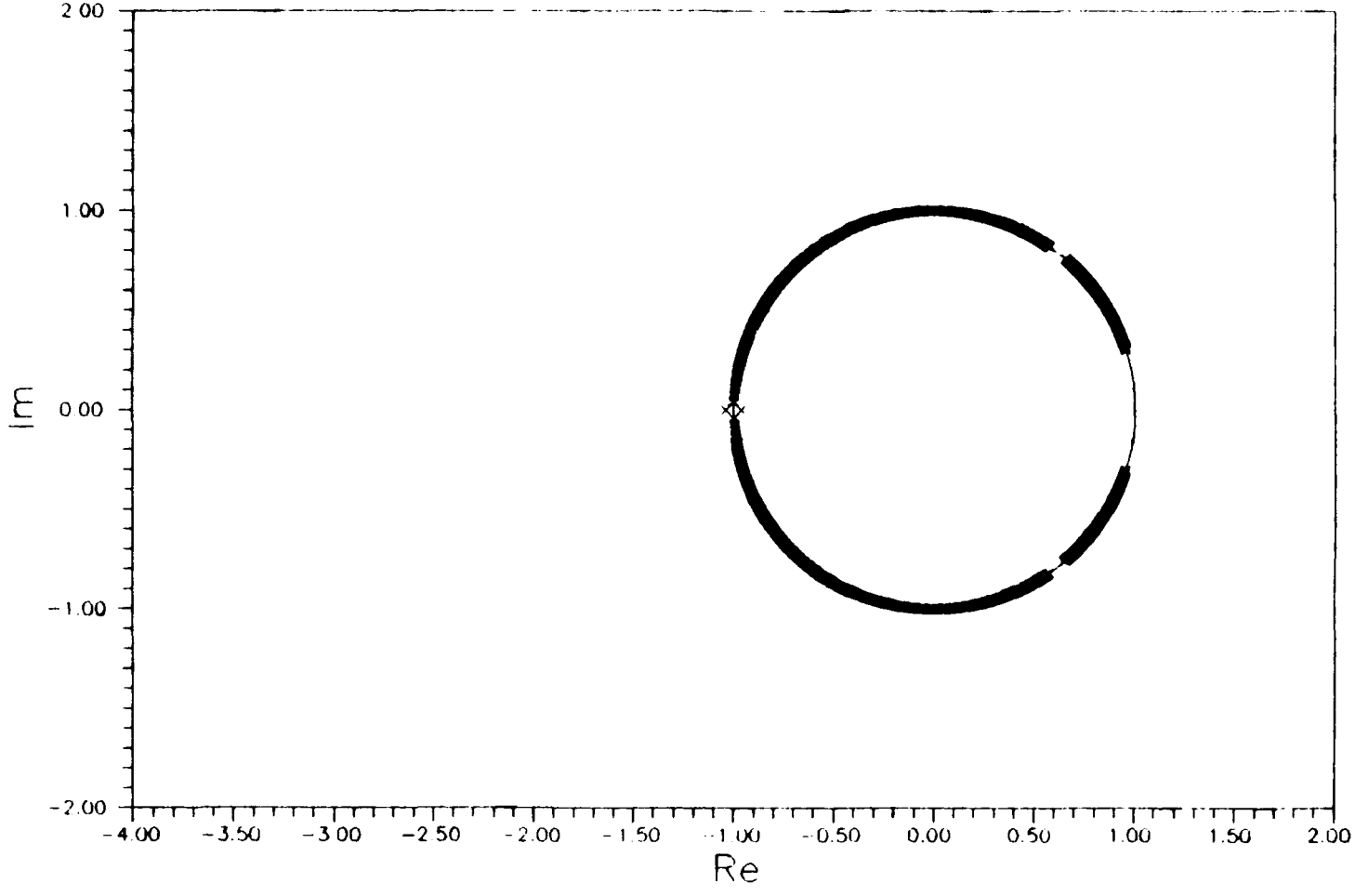

Figure 4.8 Uncontrolled System Multipliers (0.0<e<0.7,s=2.5,k=0.7)

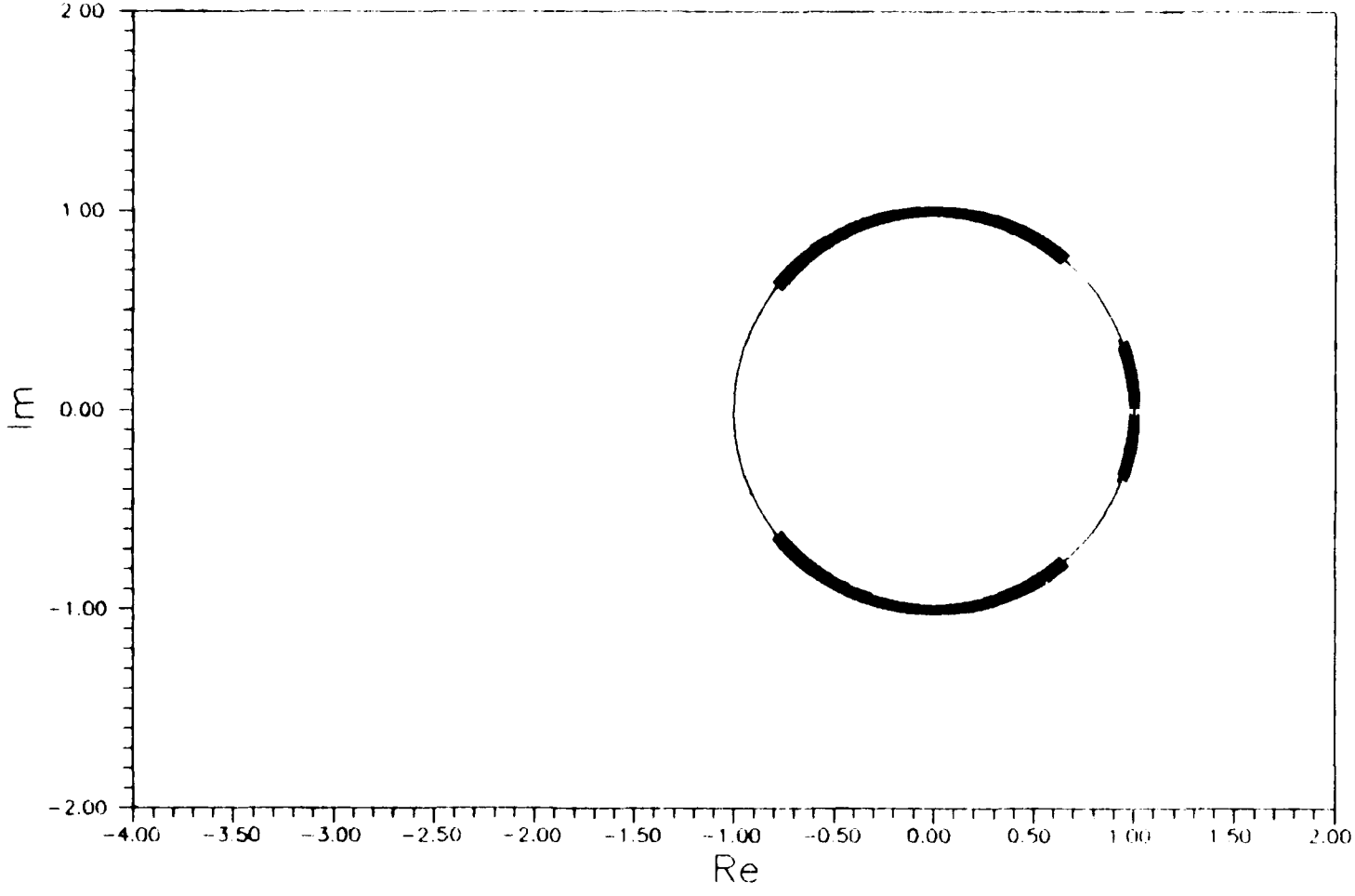

Figure 4.9 Uncontrolled System Multipliers ($0.0<e<0.7, s=3.0, k=0.7$)

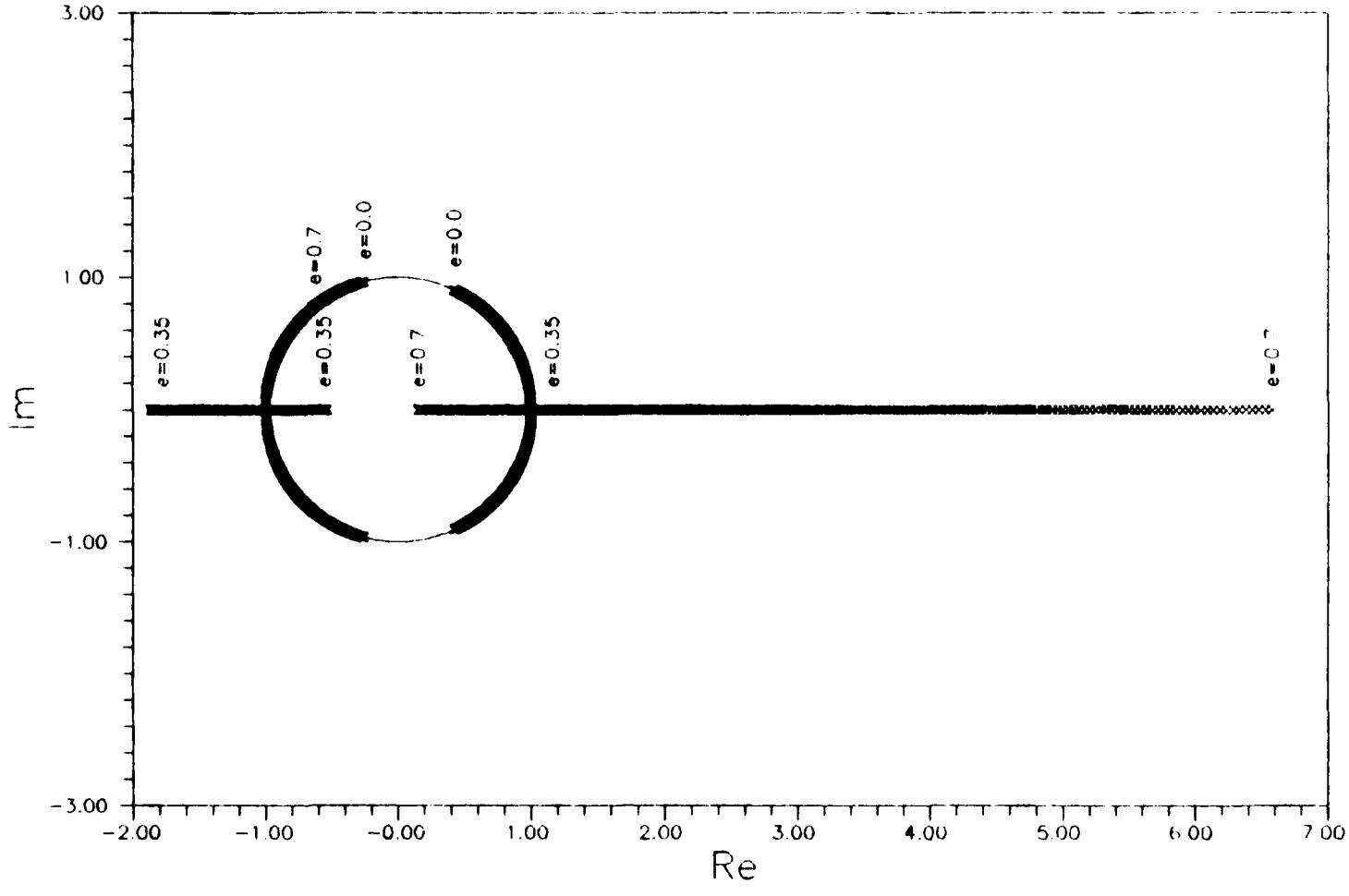

Figure 4.10 Uncontrolled System Multipliers (0.0<e<0.7,s=0.0,K=0.7)

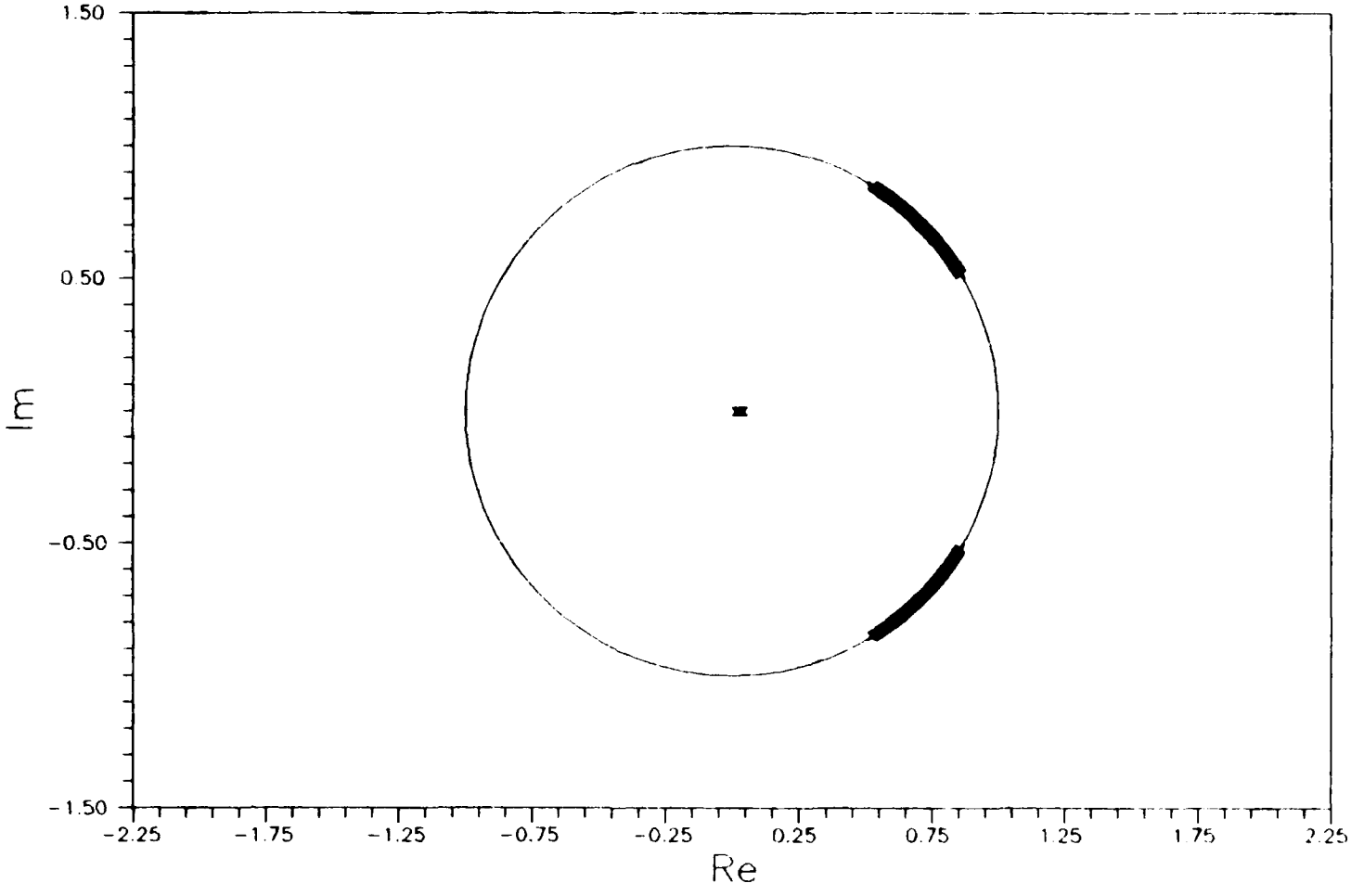

Figure 4.11 Uncontrolled System Multipliers (0.0<e<0.7,s=-1.0,K=0.7)

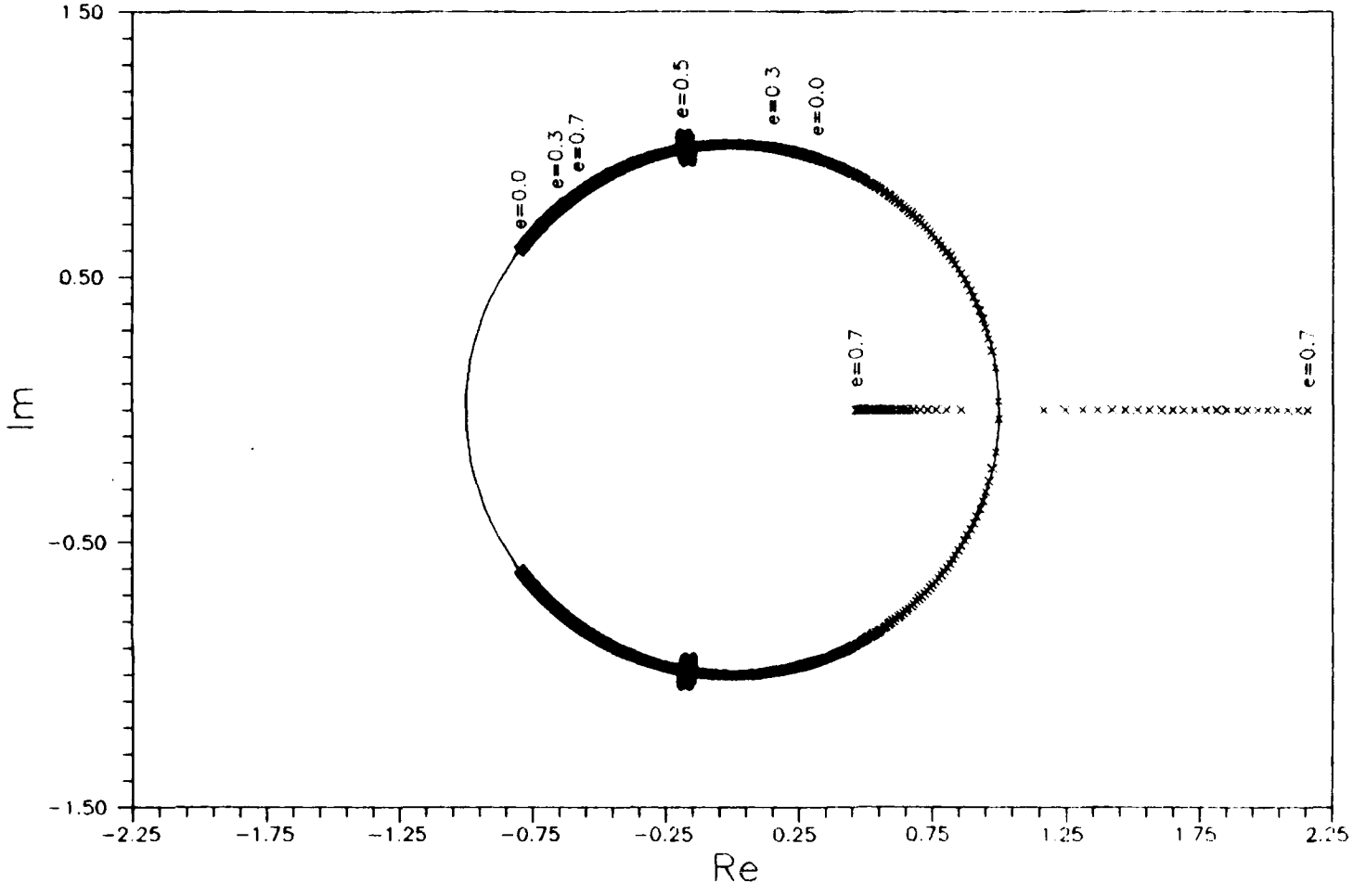

Figure 4.12 Uncontrolled System Multipliers ($0.0<e<0.7, s=-2.0, K=0.7$)

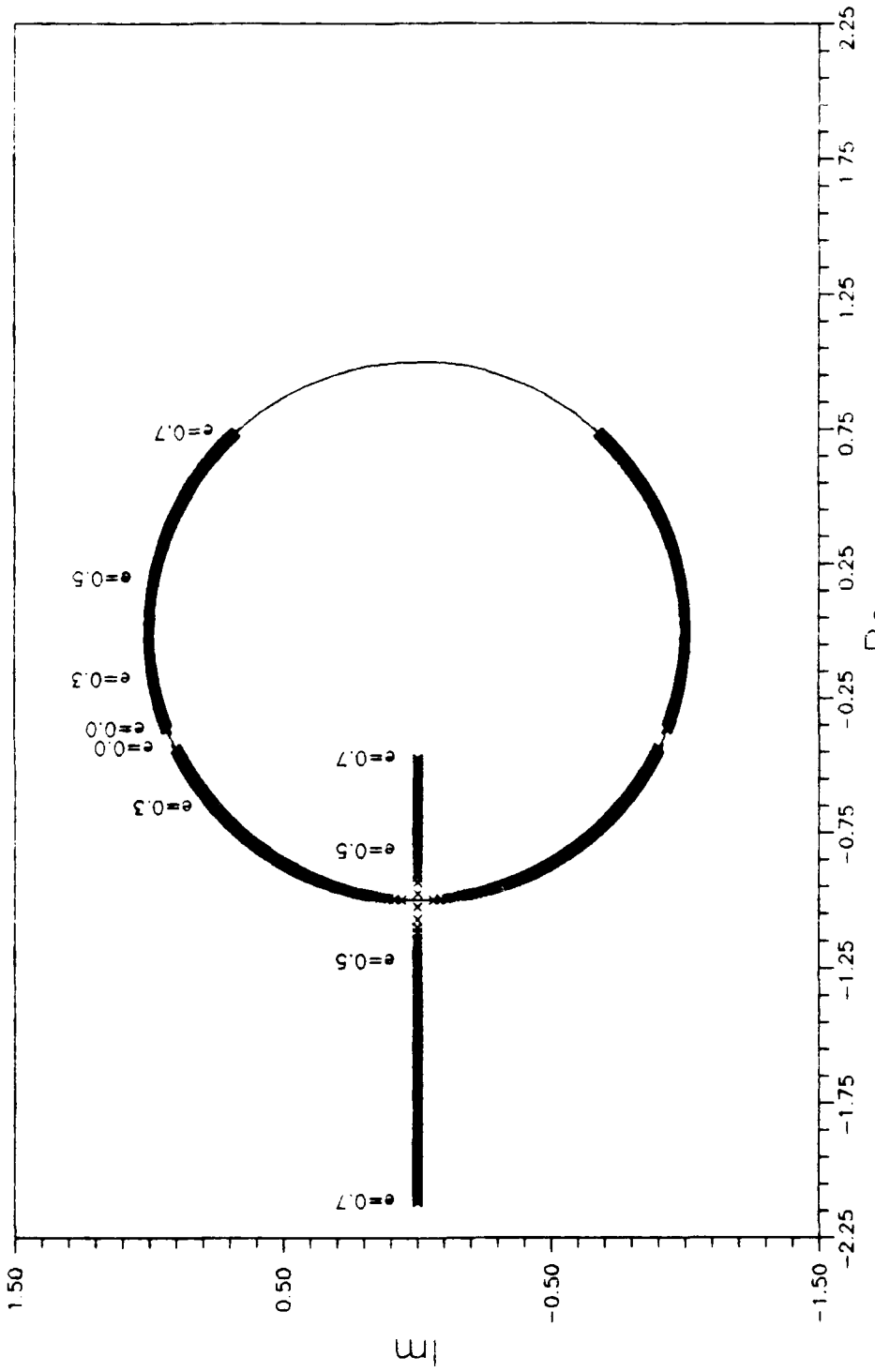

Figure 4.13 Uncontrolled System Multipliers ($0.0<\varepsilon<0.7, s=-3.0, k=0.7$)

remains. This occurs between $0.547 \leq e \leq 0.548$ in Figure 4.6 and between $0.506 \leq e \leq 0.507$ in Figure 4.7. An explanation for the greater stability in this case is that the increased spin has added to the angular momentum, thus increasing stability. Figures 4.8 and 4.9 show a further increase of the spin parameter to the values of s=2.5 and s=3.0 respectively. There is still a period doubling bifurcation for s=2.5 between $0.699 \leq e \leq 0.7$. However, for s=3.0, there is no loss of stability; all characteristic multipliers remained on the unit circle for $0.0 \leq e \leq 0.7$. Again, this is expected for high spin rates about the symmetry axis of the satellite.

Next, the spin parameter was reduced from the baseline value of s=1.0 used in figure 4.1. For s=0.0, the rotation of the satellite about the D_3 axis is simply equal to the mean motion of the satellite. From Figure 4.10, we see two bifurcation points present. One is a period doubling type occurring between $0.25 \leq e \leq 0.251$ and the other is a pitch fork bifurcation or limit point between $0.490 \leq e \leq 0.491$. One pair of multipliers return back to the unit circle for $0.601 \leq e \leq 0.602$. Figure 4.11 shows the characteristic multipliers for s=-1.0. One multiplier is off the graph making the system locally unstable for $0.0 \leq e \leq .0.7$. This agrees with Kane and Barba [8:404-405] and makes sense since the net spin of the satellite is zero here. Figure 4.12 is another interesting case with characteristic multipliers leaving and returning to the unit circle with s=-2.0. The multipliers leave and return to the unit circle for $0.496 \leq e \leq 0.533$. Again, this is a local bifurcation into a torus. There is a pitchfork type bifurcation or limit point for $0.677 \leq e \leq 0.678$ also. This structure disappears for s=-3.0. However, figure 4.13 shows a period doubling

bifurcations for $0.49 \leq e \leq 0.491$. Again, with the larger magnitude spin parameter in these two cases, local stability is maintained over a larger region.

The effect of the inertia ratio was studied next. Figures 4.14, 4.15, 4.16, 4.17, 4.18, 4.19, 4.20, and 4.21 show the effect of the inertia parameter K for $0.0 \leq e \leq 0.7$. The spin parameter was kept at s=1.0 like the baseline case in figure 4.1 A positive K indicates an oblate satellite configuration while a negative K indicates a prolate configuration.

First, the oblate values for K were examined. Figure 4.14 shows the characteristic multipliers for K=1.0 for $0.0 \leq e \leq 0.7$. There is a period doubling loss of stability for $0.268 \leq e \leq 0.27$ and $0.58 \leq e \leq 0.582$. Again, the complex structure of the baseline case in figure 4.1 is not present anymore. Figure 4.15 shows the characteristic multiplier movement for K=0.5 in which the multipliers all stay on the unit circle for $0.0 \leq e \leq 0.7$. This agrees with Kane and Barba except for e=0.7 where they gave a loss of local stability at K=0.4 and K=0.6; one would infer that K=0.5 is also unstable. Figure 4.16 shows a bifurcation into a torus for $0.552 \leq e \leq 0.554$ with K=0.25. Figure 4.17 indicates that an inertia parameter of 0.0 remains locally stable for $0.0 \leq e \leq 0.7$. For such a case, the gravitational potential given by equation (A.58) reduces simply to the potential acting on the center of mass of the system. In other words, there are no torques on the satellite due to gravity.

The prolate satellite configurations were studied next. Figures 4.18 and 4.19 exhibit some very interesting movement of the characteristic

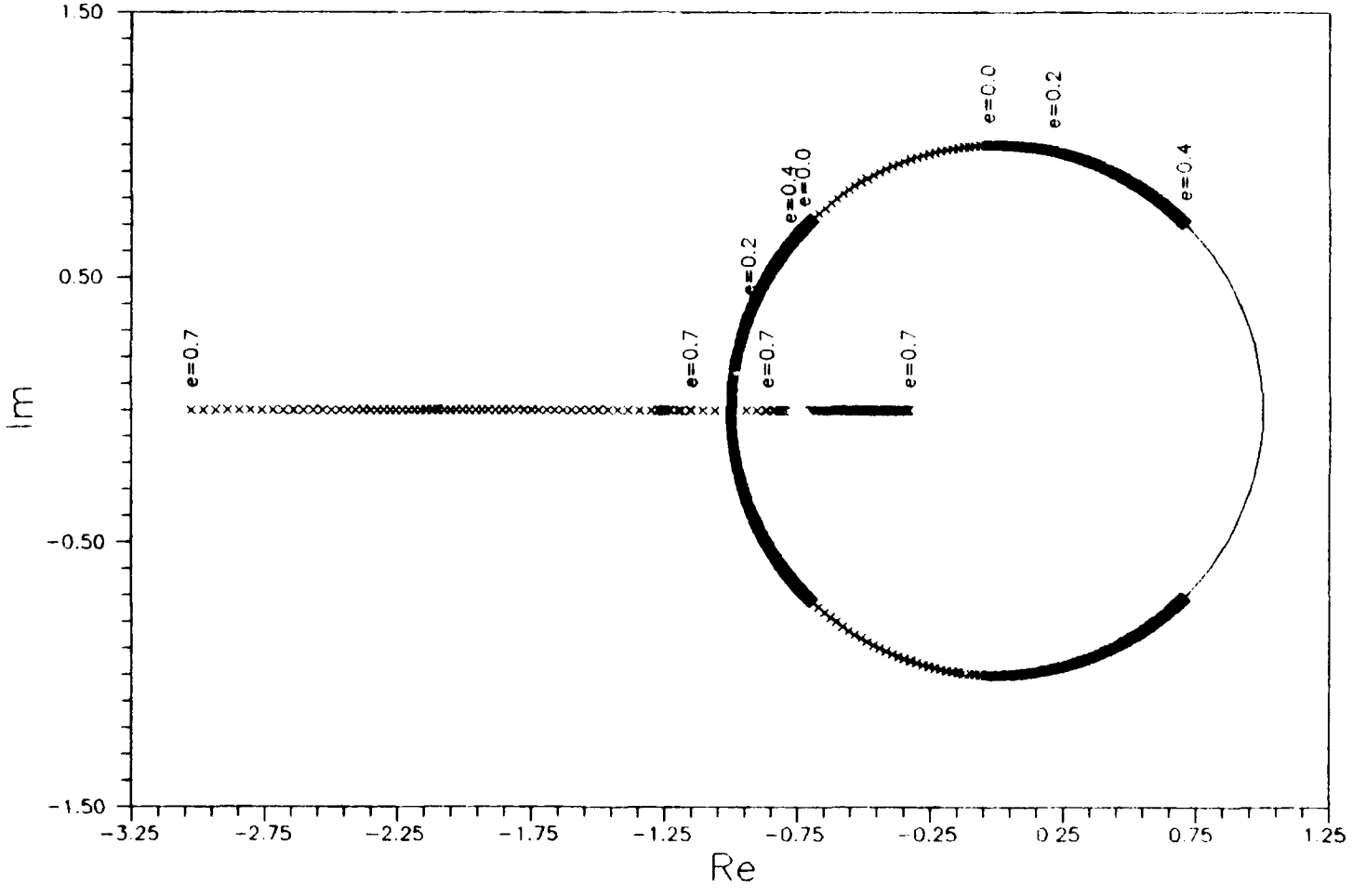

Figure 4.14 Uncontrolled System Multipliers (0.0<e<0.7,s=1.0,K=1.0)

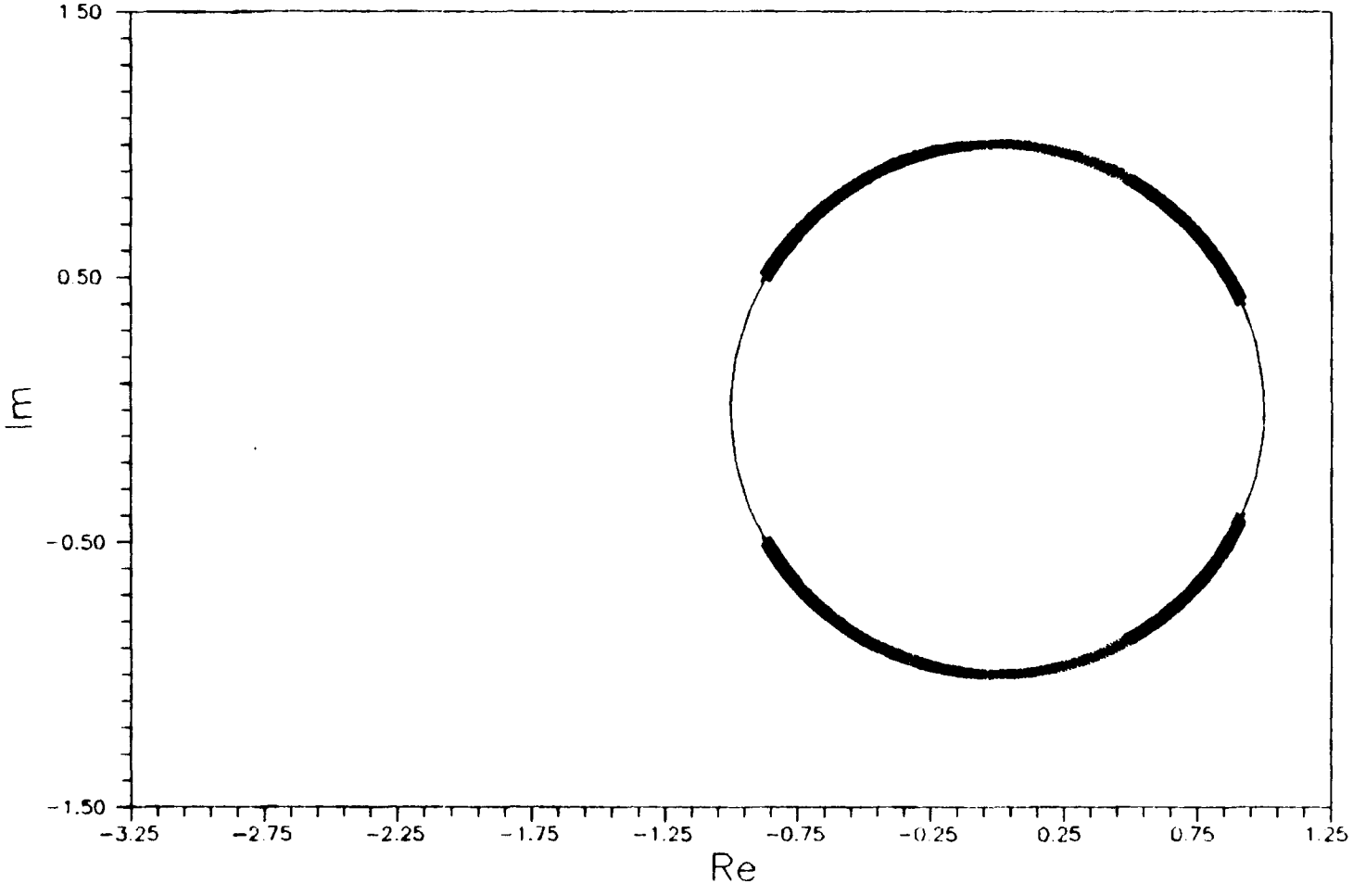

Figure 4.15 Uncontrolled System Multipliers (0.0<e<0.7,s=1.0,K=0.5)

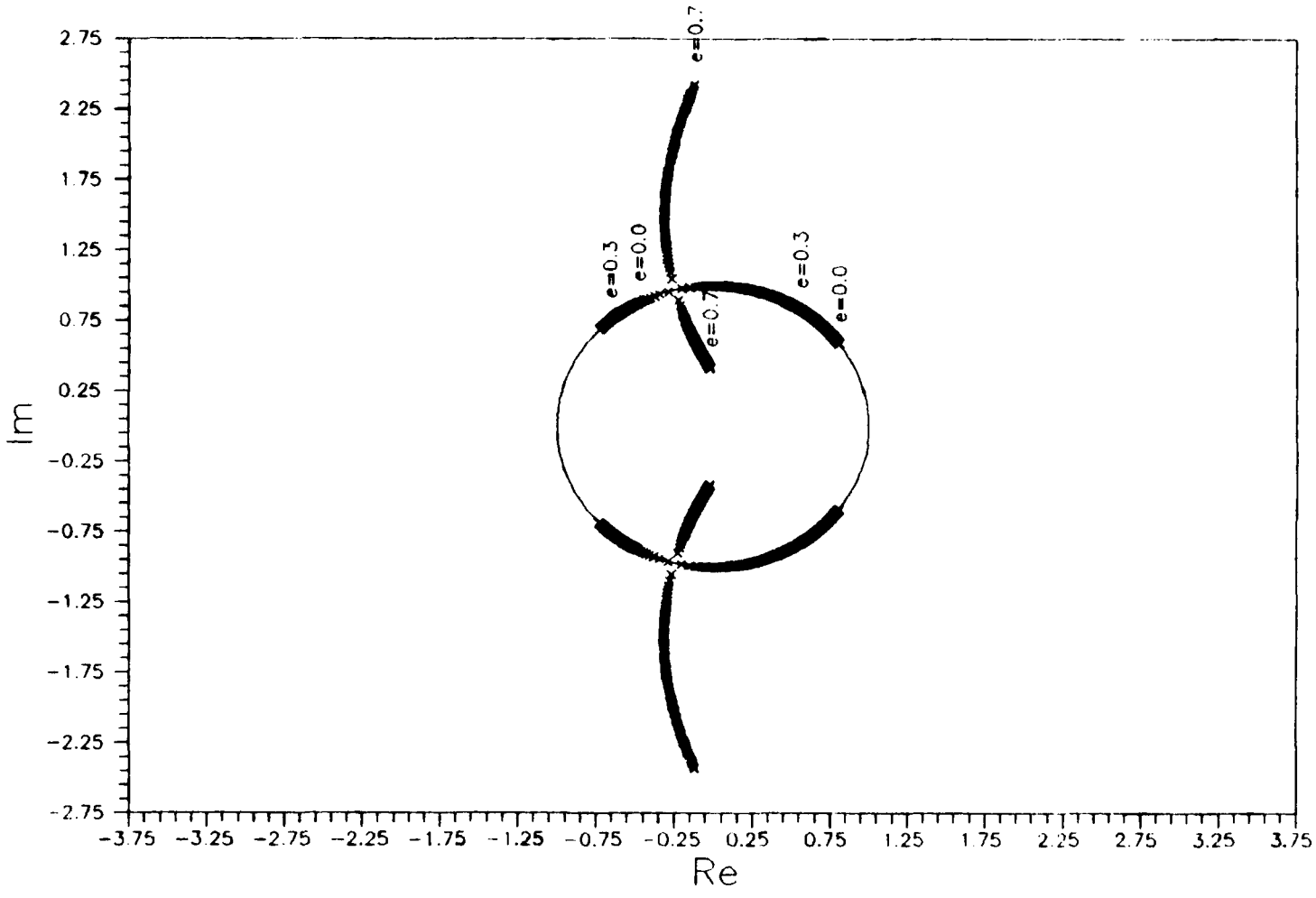

Figure 4.16 Uncontrolled System Multipliers (0.0<e<0.7,s=1.0,K=0.25)

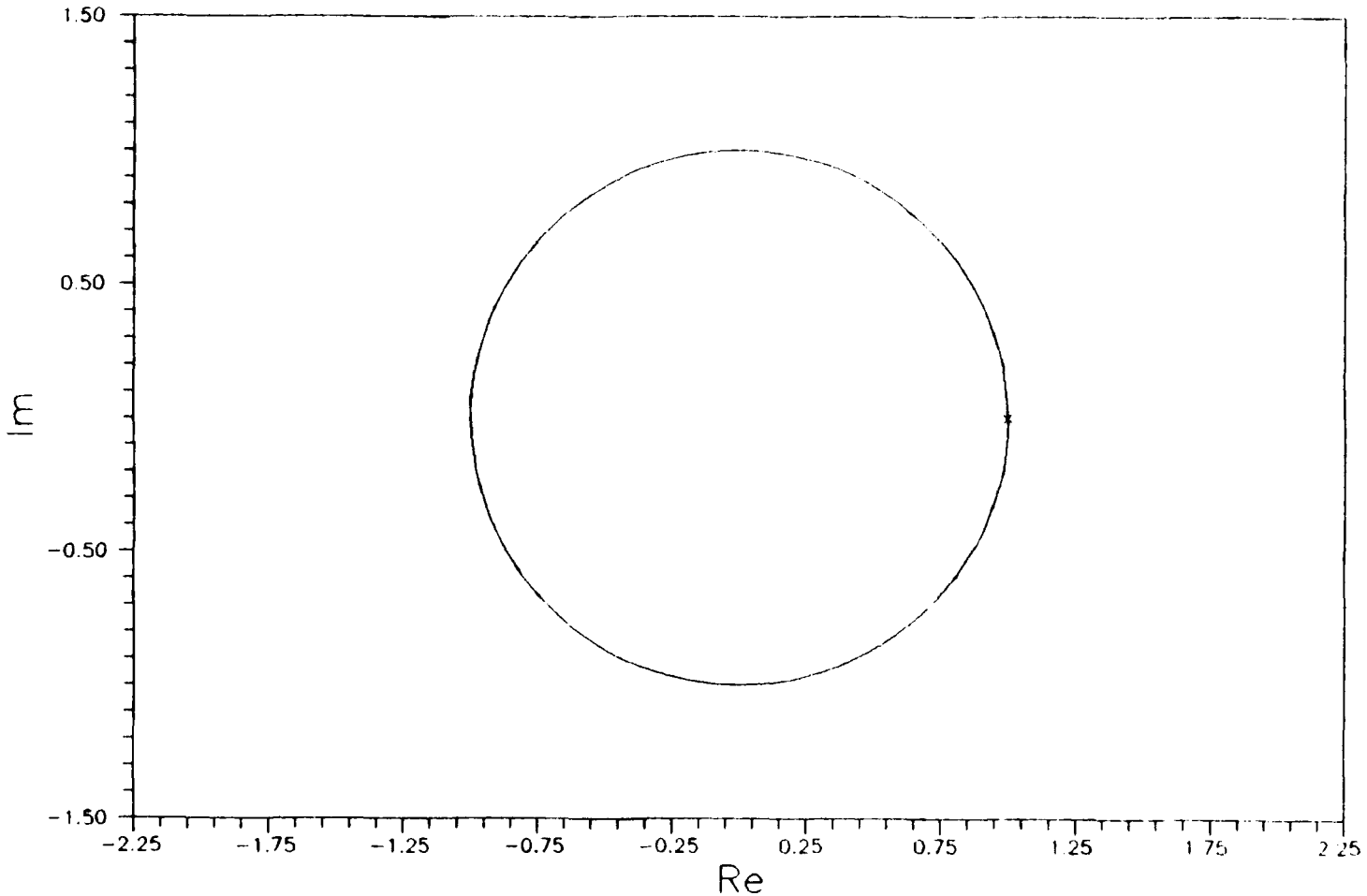

Figure 4.17 Uncontrolled System Multipliers (0.0<e<0.7,s=1.0,k=0.0)

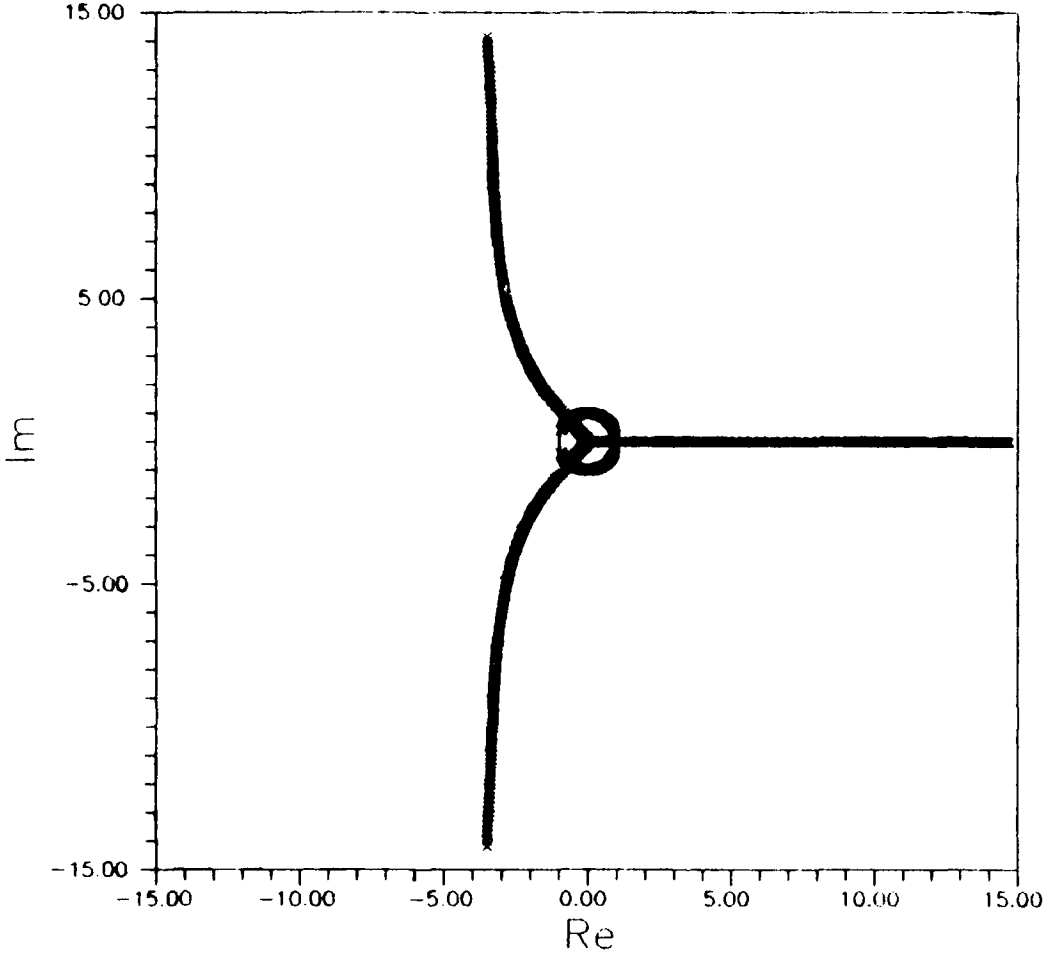

Figure 4.18 Uncontrolled System Multipliers ($0.0<e<0.7, s=1.0, k=-0.25$)

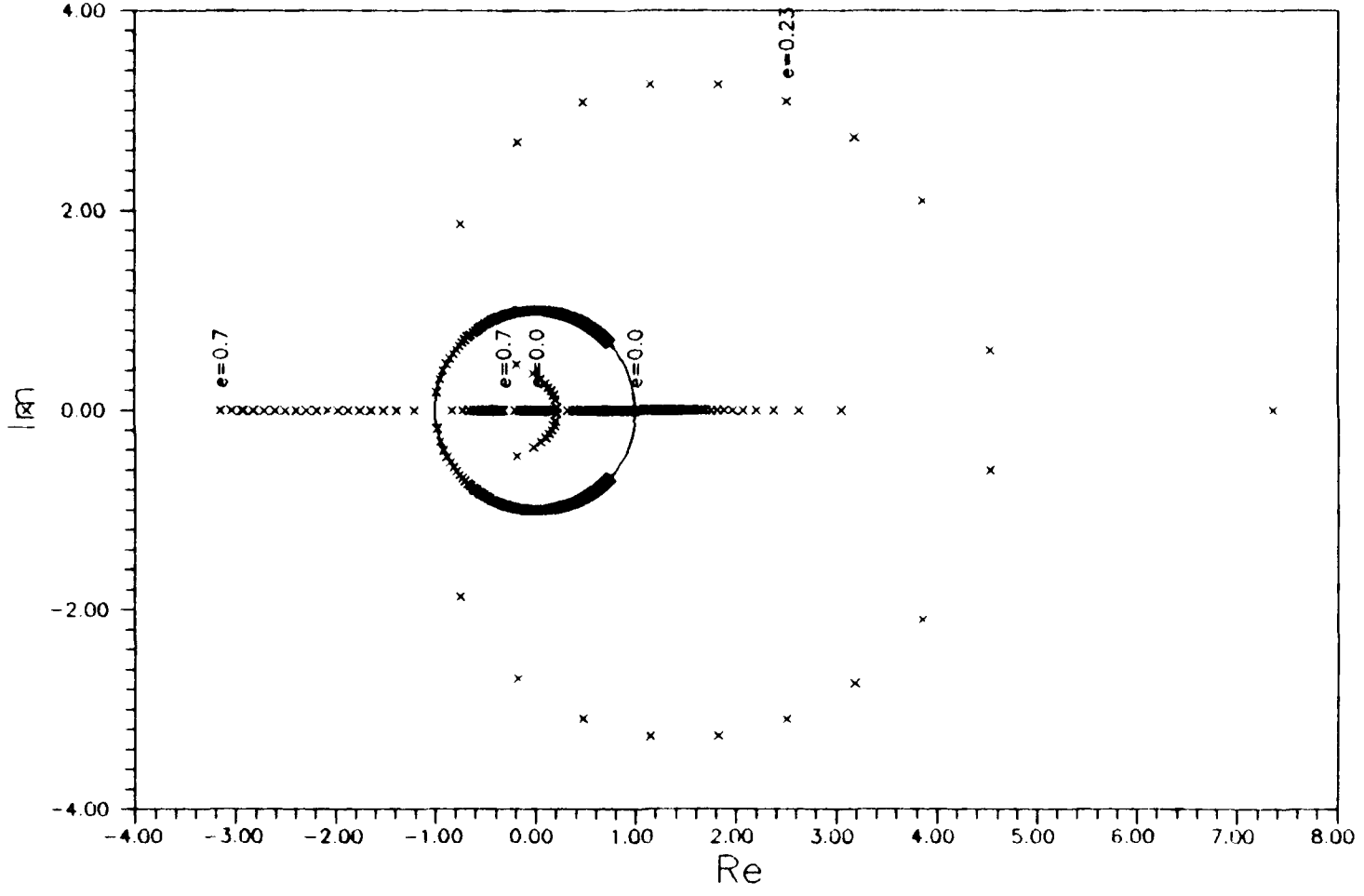

Figure 4.19 Uncontrolled System Multipliers (0.0<e<0.7,s=1.0,K=-0.5)

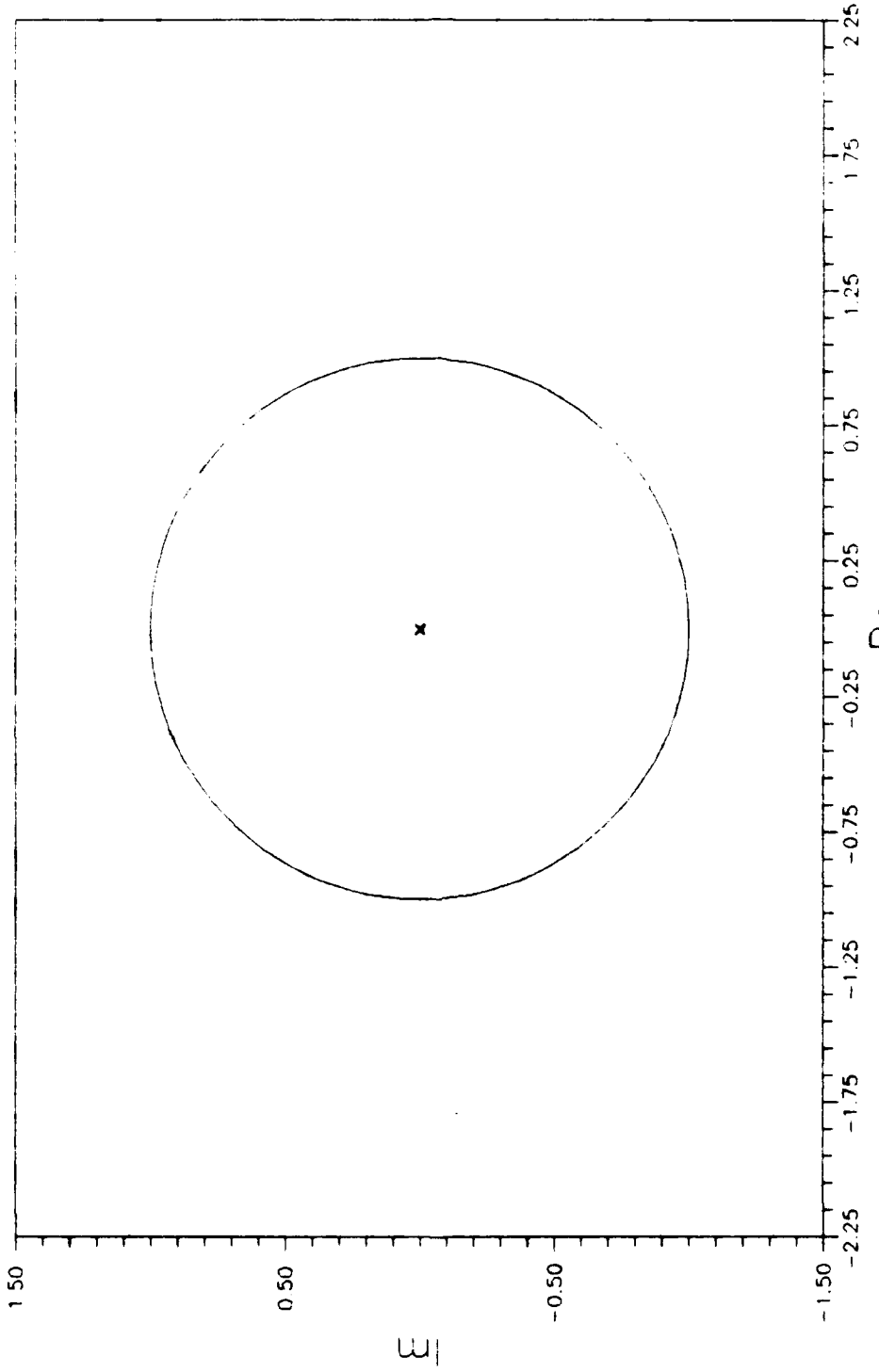

Figure 4.20 Uncontrolled System Multipliers ($0.0 < \epsilon < 0.7, s = 1.0, K = -0.75$)

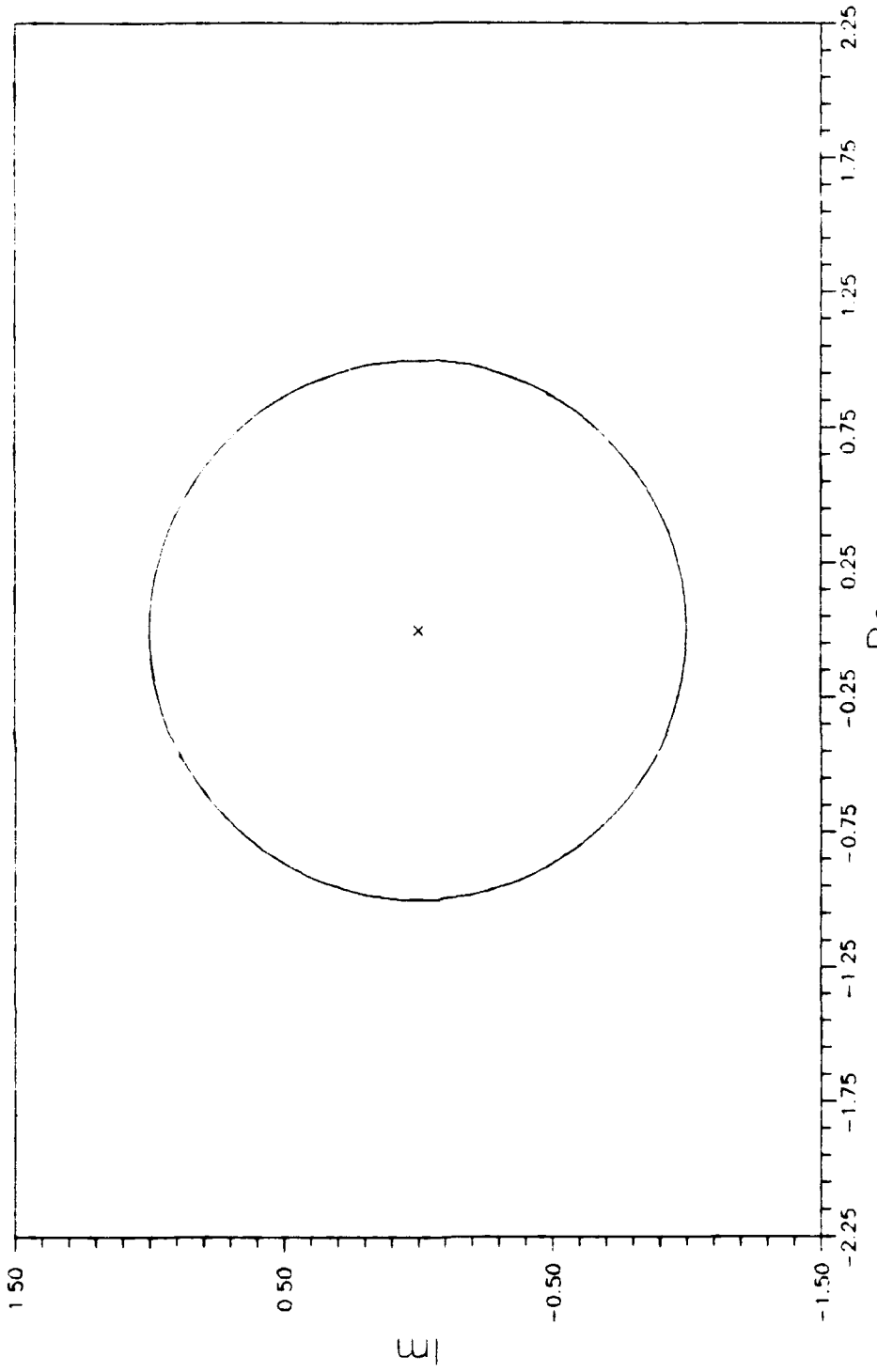

Figure 4.21 Uncontrolled System Multipliers (0.0<e<0.7,s=1.0,K=-1.0)

multipliers at K=-0.25 and K=-0.5 respectively. At K=-0.25, two multipliers meet at +1 on the unit circle between $0.362 \leq e \leq 0.364$ putting all the multipliers on the unit circle. Two complex pairs of multipliers bifurcate into a torus for $0.434 \leq e \leq 0.436$ with one set of multipliers going inside the unit circle and one set going outside. At K=-0.5, we note a period doubling bifurcation between $0.240 \leq e \leq 0.242$ and a pitchfork type bifurcation or limit point between $0.0 \leq e \leq 0.002$. Note how the multipliers move around the outside of the unit circle in figure 4.19. Figures 4.20 and 4.21 have only one pair of characteristic multiplier inside the unit circle for K=-0.75 and K=-1.0 respectively. The other two multipliers in these cases are outside the unit circle and do not appear on these graphs. This indicates local instability for $0.0 \leq e \leq 0.7$ which agrees with Kane and Barba.

In summary, a more complex and detailed structure of local stability characteristics using plots of characteristic multipliers for the various conditions considered herein was revealed. This is certainly more information than previously appreciated for the spinning symmetric satellite in an elliptical orbit problem.

4.1.2 Floquét Controlled Equations of Motion. The Floquét controller was designed to cancel disturbances away from the desired equilibrium condition with the values of the parameters being e=0.5, s=1.0, K=0.7. Figure 4.22 shows how one pair of characteristic multipliers is moved inside the unit circle as the Floquét controller feedback gains G1 and G2 in equations (2.30) and (2.31) are varied between 0.0 and 1.0. The other pair is not affected since this is a "modal

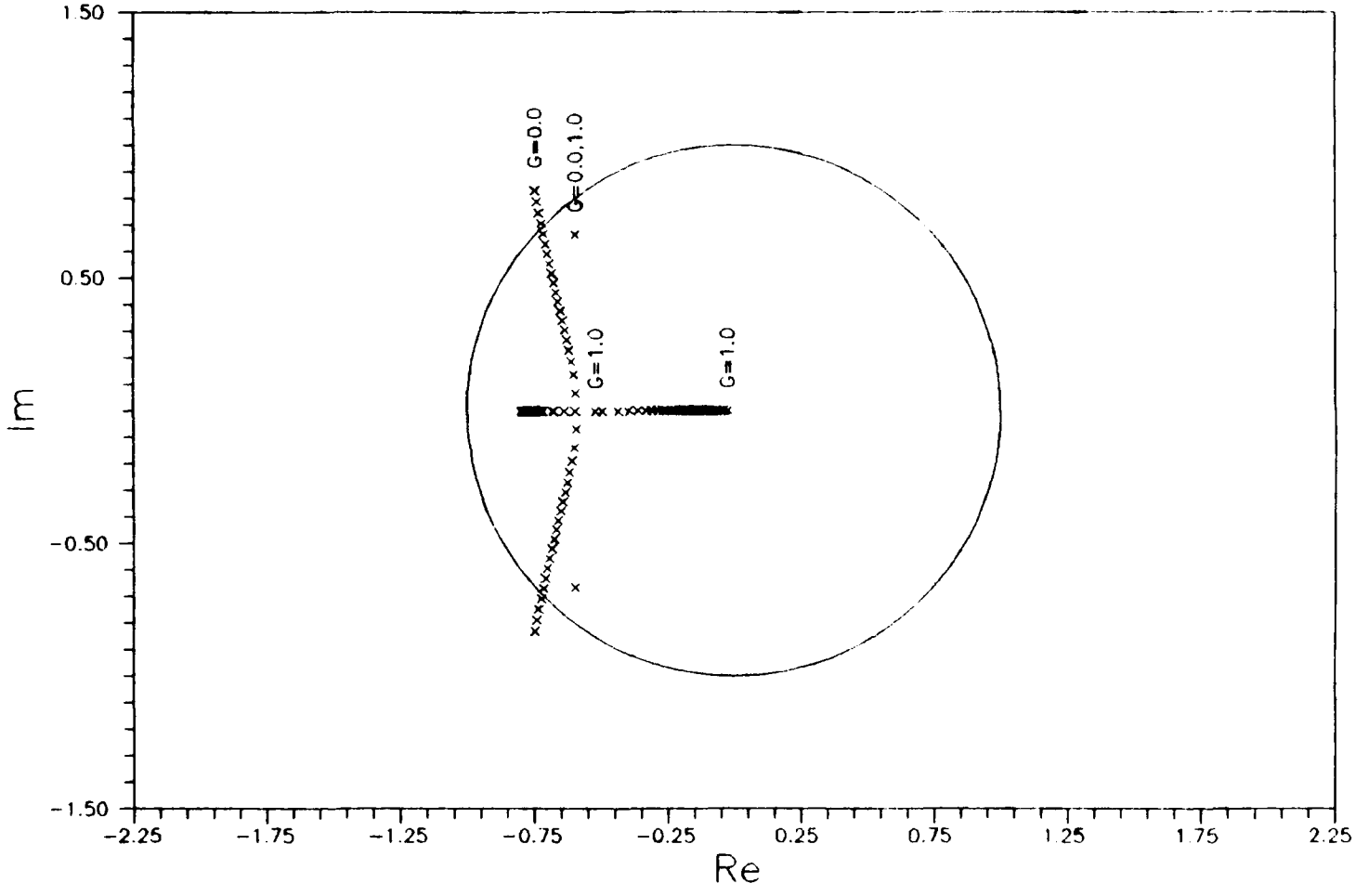

Figure 4.22 Floquet Controlled System Multipliers
(e=0.5,s=1.0,k=0.7,0.0<G_i<1.0)

control" design approach. There is only a torus bifurcation point on this plot of characteristic multipliers. Cole claimed that a period doubling bifurcation existed in a plot he presented of the characteristic exponents [5:4-15-4-16]. However, figure 4.22 does not indicate such a period doubling bifurcation. Even though Cole was in error here, he still may have found a global period doubling as his results seem to suggest. The only conclusion that can be made from figure 4.22 is that local stability is achieved by the movement of the unstable pair of multipliers into the unit circle.

4.1.3 Rate and Position Feedback Equations of Motion. Rather than varying the parameters in the Floquét controlled equations of motion, a simple rate and position feedback controller was designed. This was done to allow for the use of the continuation software (AUTO) and is explained later. In order to save time in intializing the continuation software, I performed a Floquét analysis on the simple controller design to locate any existing bifurcation points. Once any bifurcation points were found, it was easy to start the continuation software up with the correct initial conditions for parameters in the equations of motion.

First, only uncoupled rate feedback was added to the equations of motion given by equations (2.35) and (2.36). The gain G_j was varied for $0.0 \leq G_j \leq 1.0$ to achieve local stability. Figure 4.23 indicates how effective this simple controller was in moving the unstable pair of multipliers into the unit circle. In comparison with figure 4.22, we see a similar movement of the unstable pair of multipliers. But, as exhibited by figure 4.23, the simple controller also moved the stable pair of multipliers

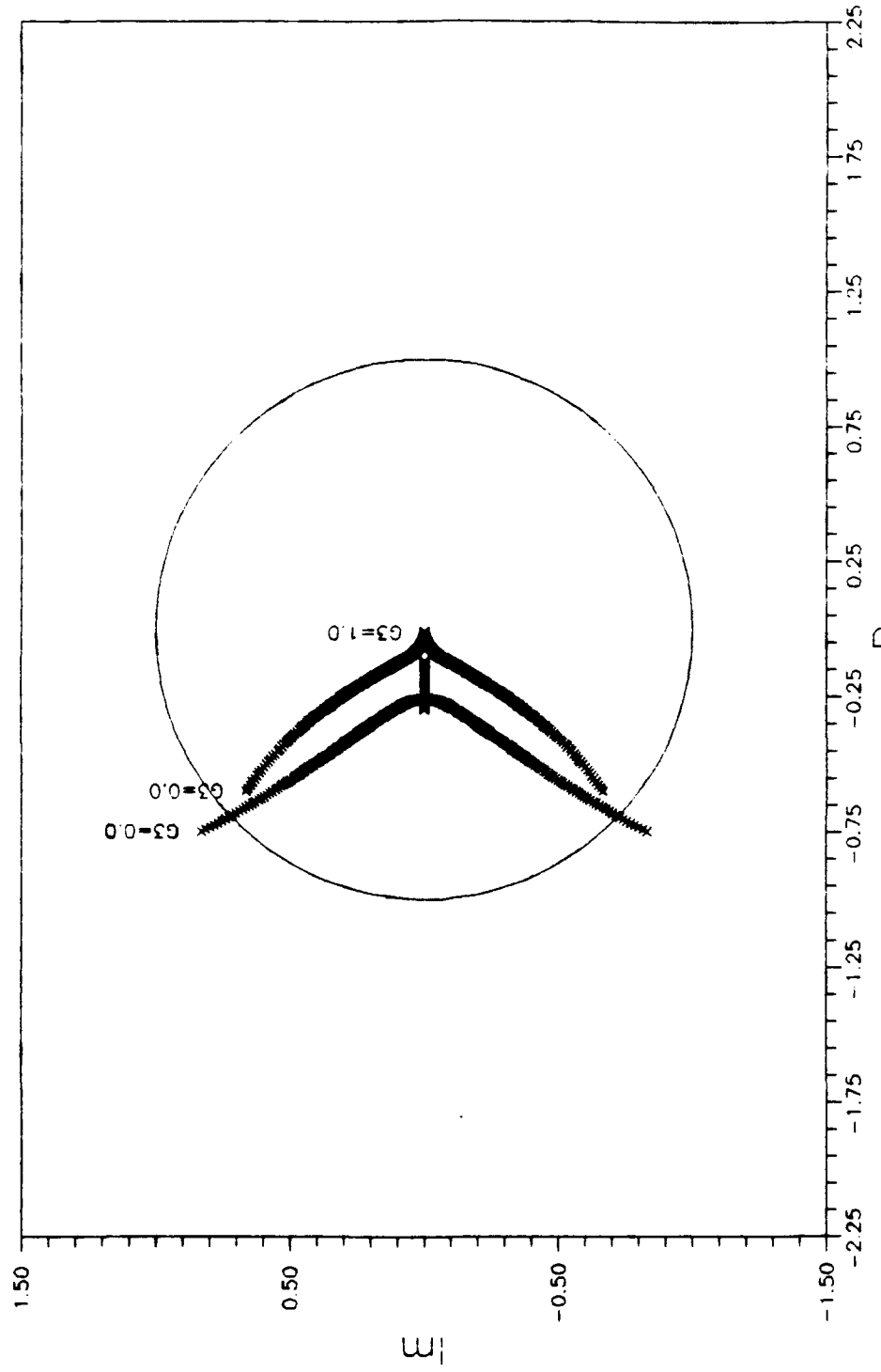

Figure 4.23 Rate Feedback System Multipliers ($e=0.5, s=1.0, K=0.7, 0.0<G_3<1.0$)

further into the unit circle. The Floquét controller left this multiplier's location unchanged. Note that there is a torus bifurcation point as a complex pair of multipliers cross the unit circle.

The uncoupled rate feedback gain was fixed to G_j=0.85 so that all the characteristic multipliers would just lie on the real axis in figure 4.23. This condition of local stability was now analyzed as other parameters in the equations were varied. Figure 4.24 plots the movement of the characteristic multipliers as the inertia ratio went from $-1.0 \leq K \leq 1.0$. When K was varied through this range, two crossings of the unit circle at +1 occurred. These pitchfork type bifurcations happened in the ranges of $-0.36 \leq K \leq -0.35$ and $-0.29 \leq K \leq -0.28$. Both of these crossings moved a multiplier into the unit circle for a positive change in K. The other two multipliers stayed in the unit circle over the range K was varied. So, after the second crossing into the unit circle, local stability was achieved. We can conclude that the simple rate feedback controller with G_j=0.85 is locally stable for $-0.28 \leq K \leq 1.0$. The second crossing was analyzed using the continuation software with the results presented later in this thesis.

Figure 4.25 depicts characteristic multiplier movement as the spin parameter is varied from $-3.0 \leq s \leq 3.0$. As with the previous case, two multipliers remain inside the unit circle and two start outside the unit circle. Again, there are two crossings into the unit circle at +1. One occurred for $-1.82 \leq s \leq -1.81$ and the other between $-0.23 \leq s \leq -0.22$. These two bifurcations are pitchfork type bifurcations. All the multipliers entered inside the unit circle after the second crossing, thus indicating local

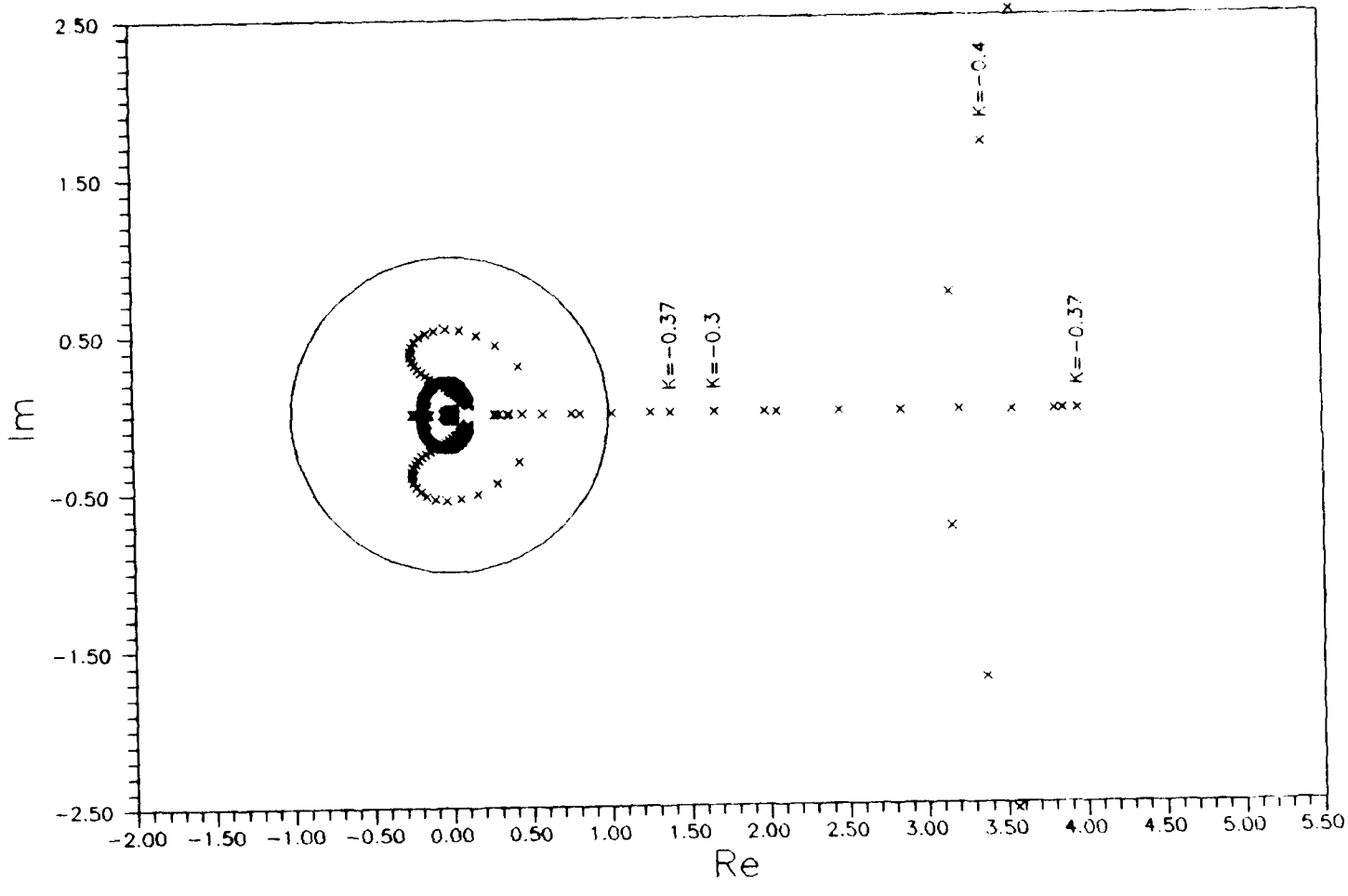

Figure 4.24 Rate Feedback System Multipliers ($e=0.5, s=1.0, -1.0<K<1.0, G_3=0.85$)

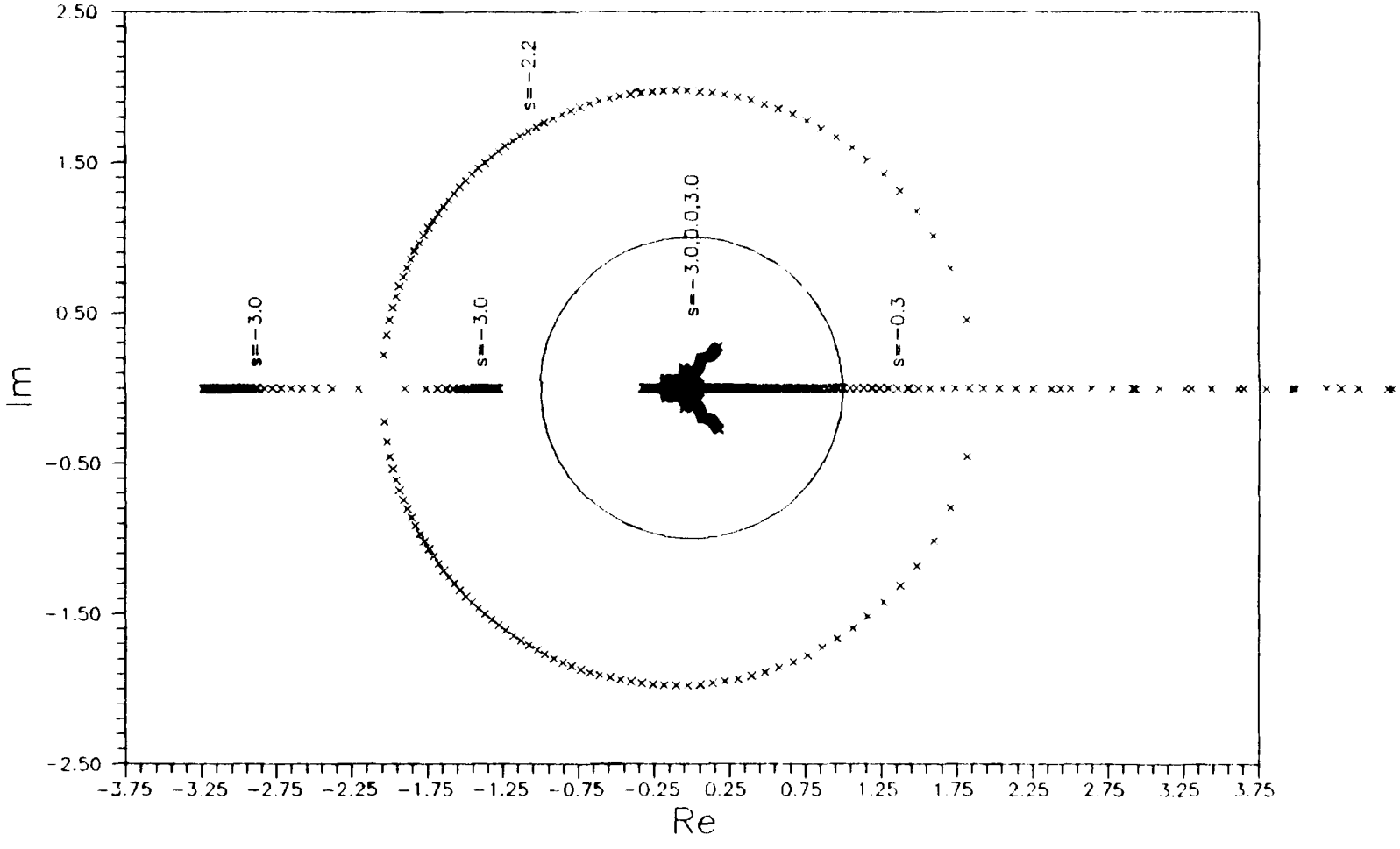

Figure 4.25 Rate Feedback System Multipliers ($e=0.5, -3.0<s<3.0, k=0.7, G_3=0.85$)

stability for $-0.22 \leq s \leq 3.0$.

Next the eccentricity was varied for $0.0 \leq e \leq 0.7$. Figure 4.26 shows that for s=1.0, K=0.7 and G_3=0.85, local stability is maintained over the total range of eccentricity. So, the simple rate feedback eliminated any effect that eccentricity might have on this particular case.

Finally, coupled rate feedback and position feedback were added to the equations of motion given by equations (2.35) and (2.36). These gains are G_4 and G_1 respectively in the equations of motion. They were both varied individually between 0.0 and 1.0. Again, the fixed parameters were G_3=0.85, e=0.5, s=1.0, K=0.7. Figures 4.27 and 4.28 both indicate that coupled rate feedback by itself and coupled position feedback by itself have little effect on the stability of the system.

Uncoupled rate feedback with G_3=0.85 was chosen to be the baseline design for fixed parameters of e=0.5, s=1.0, K=0.7. Figures 4.29, 4.30, 4.31 ,4.32 show that this gain selection returns the system to equilibrium from an initial disturbance of $\theta_1=\theta_2=0.4$. Note that it took between two and three orbits to cancel the disturbance.

4.2 Poincaré Maps

Poincaré maps were plotted for the uncontrolled, Floquét controlled, and rate feedback controlled equations of motion. These maps were plotted to give a snapshot of the global phase space at a variety of initial values for the parameters in the equations of motion. It was hoped that some of the cases selected would shed some light on the origin of the attractor found by Cole in [5]. The *stroboscopic technique* for creating Poincaré maps was used. Most cases plotted a point on the map at

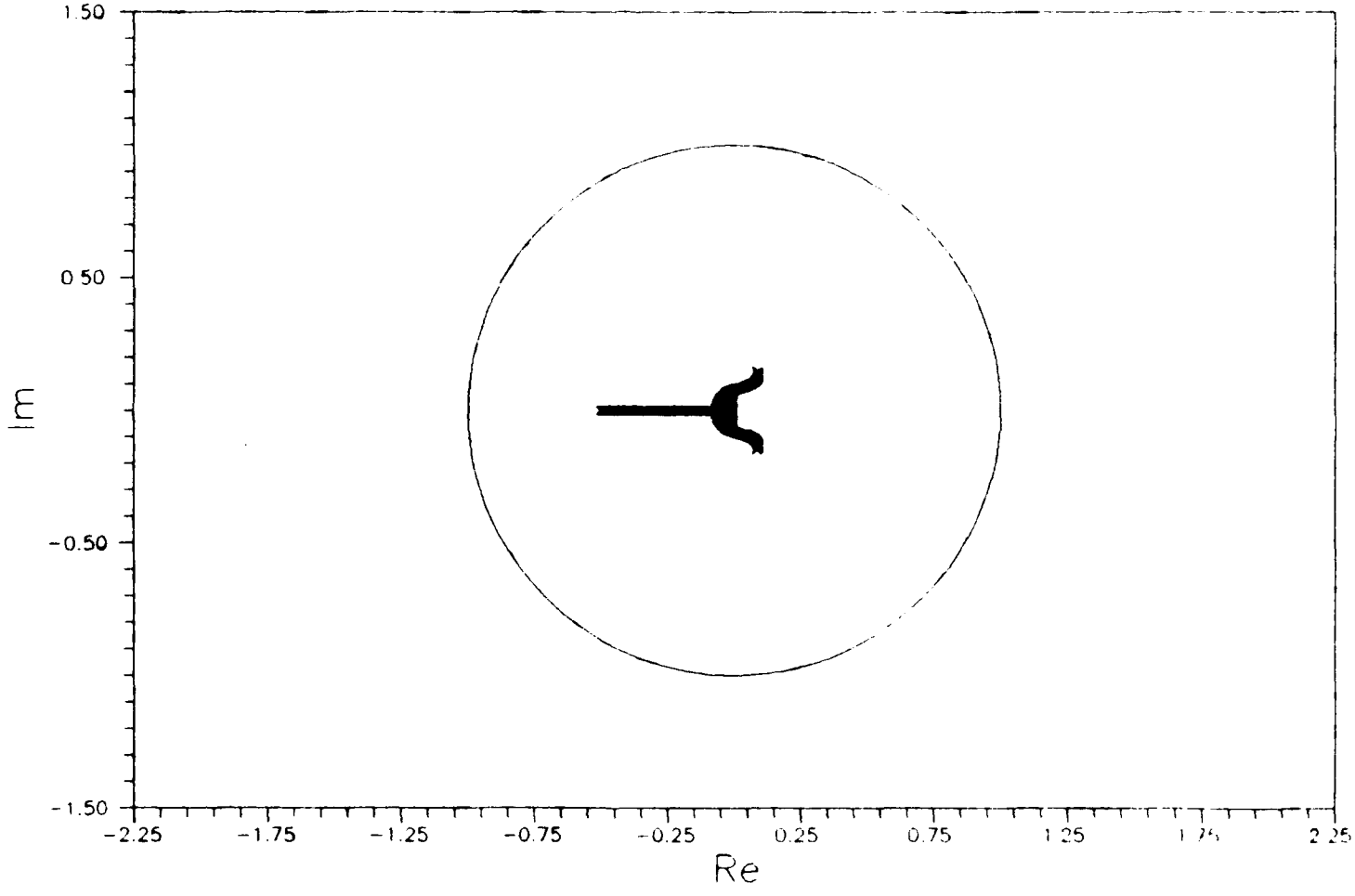

Figure 4.26 Rate Feedback System Multipliers ($0.0<\epsilon<0.7, s=1.0, k=0.7, G_3=0.85$)

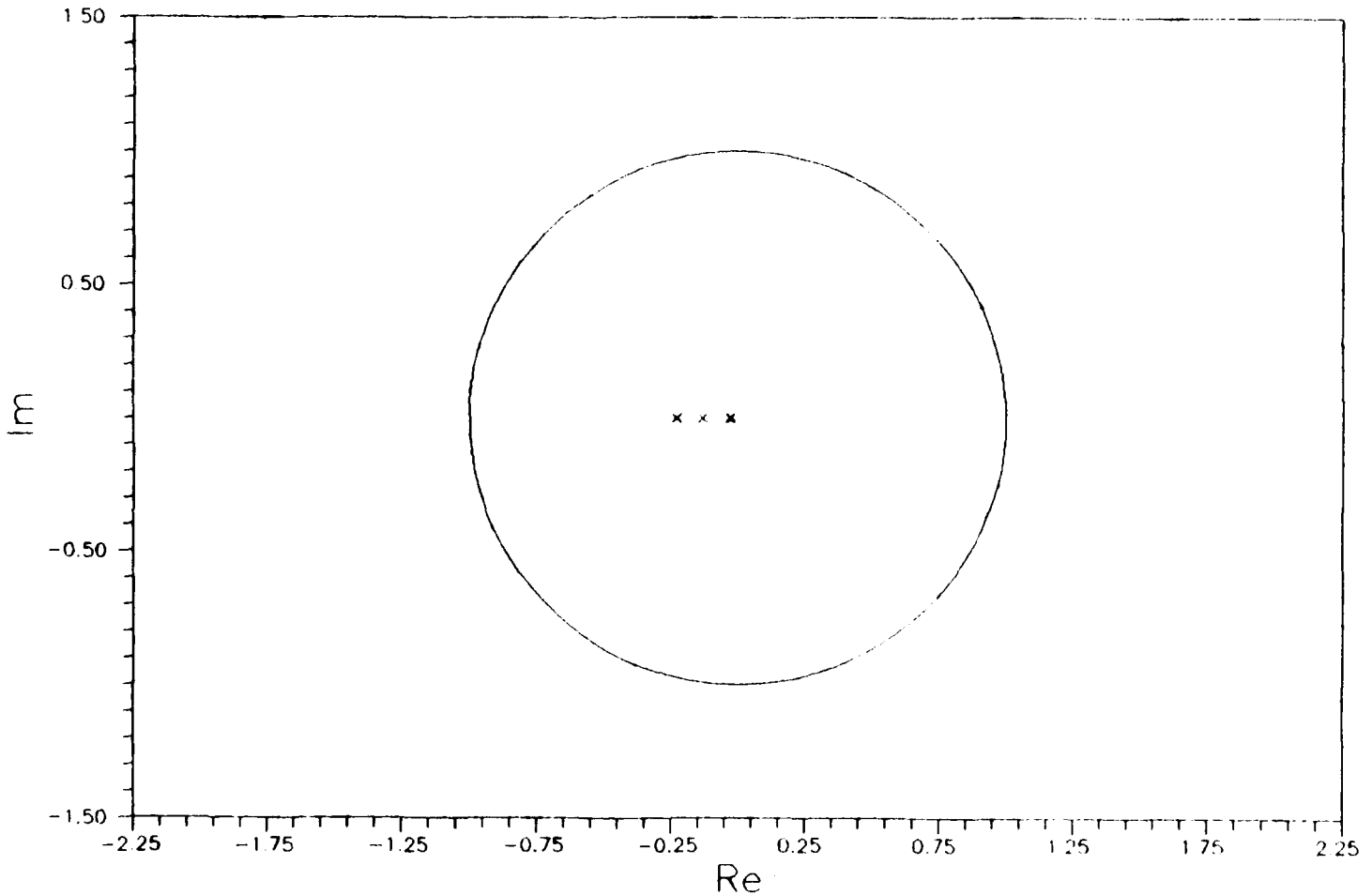

Figure 4.27 Rate and Position Feedback System Multipliers
($e=0.5, s=1.0, K=0.7, G_3=0.85, 0.0<G_1<1.0$)

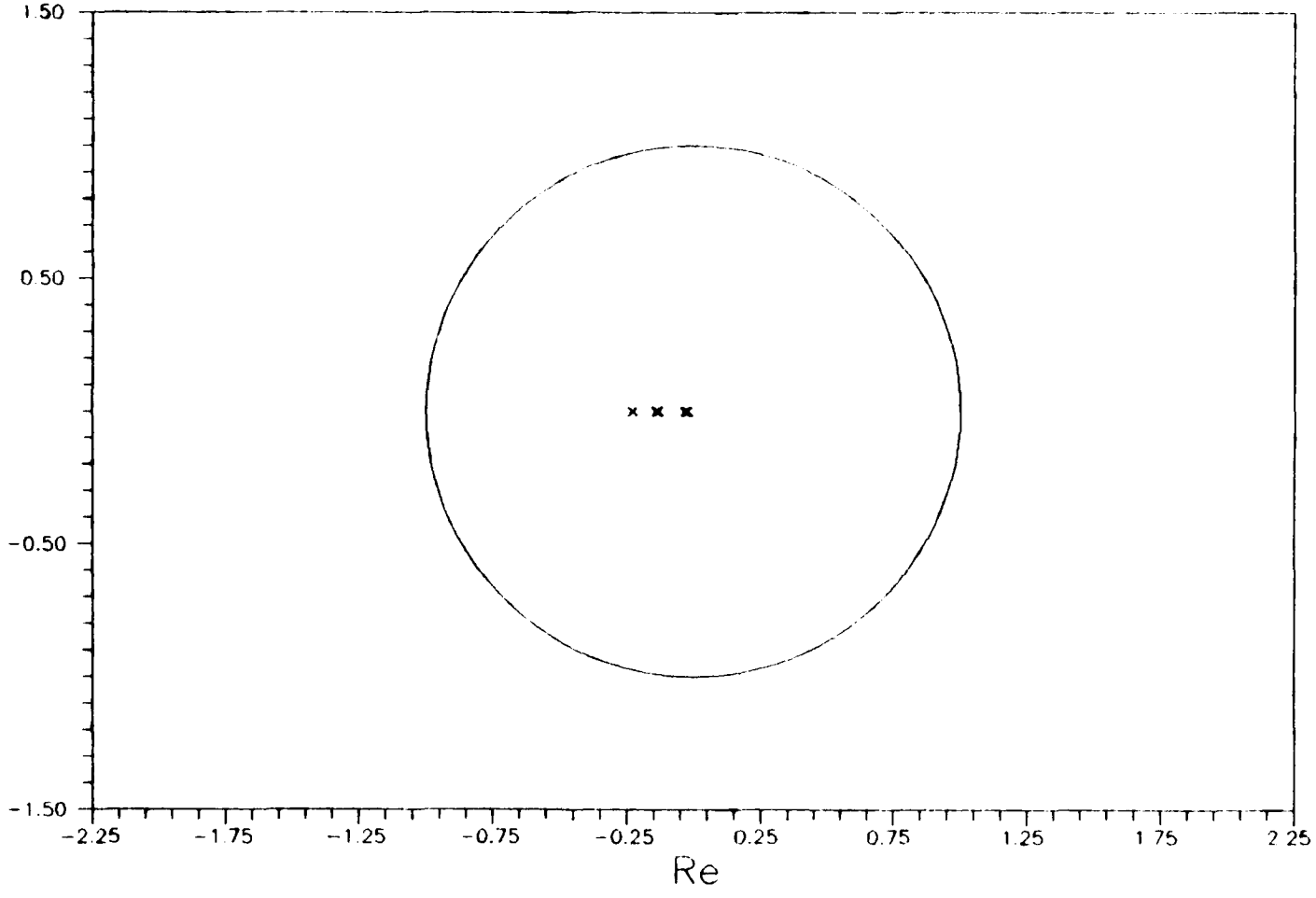

Figure 4.28 Rate Feedback System Multipliers
($e=0.5, s=1.0, K=0.7, G_3=0.85, 0.0<G_4<1.0$)

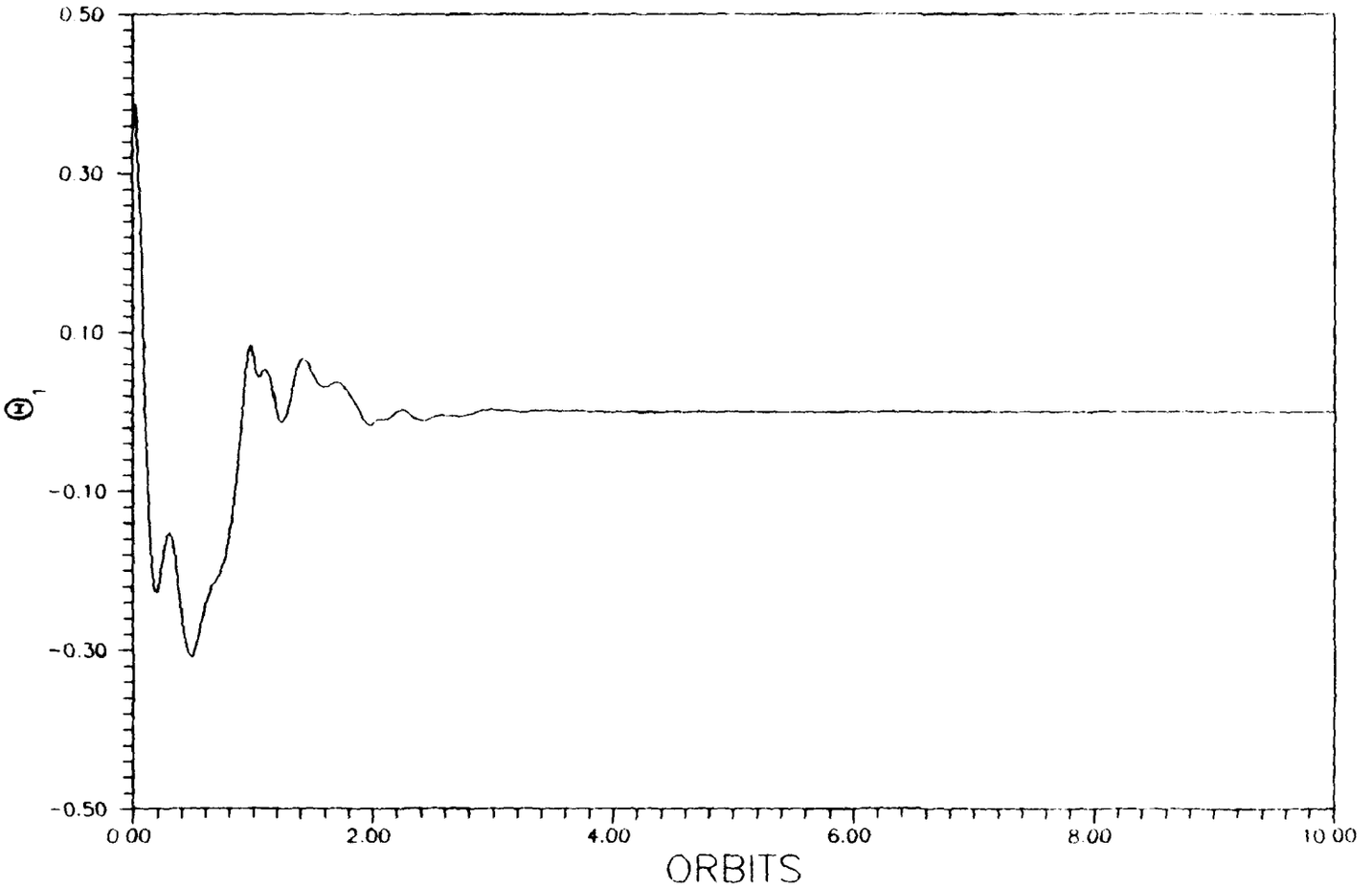

Figure 4.29 Rate Feedback System Time Response for θ_1 ($e=0.5, s=1.0, K=0.7, G_3=0.85$)

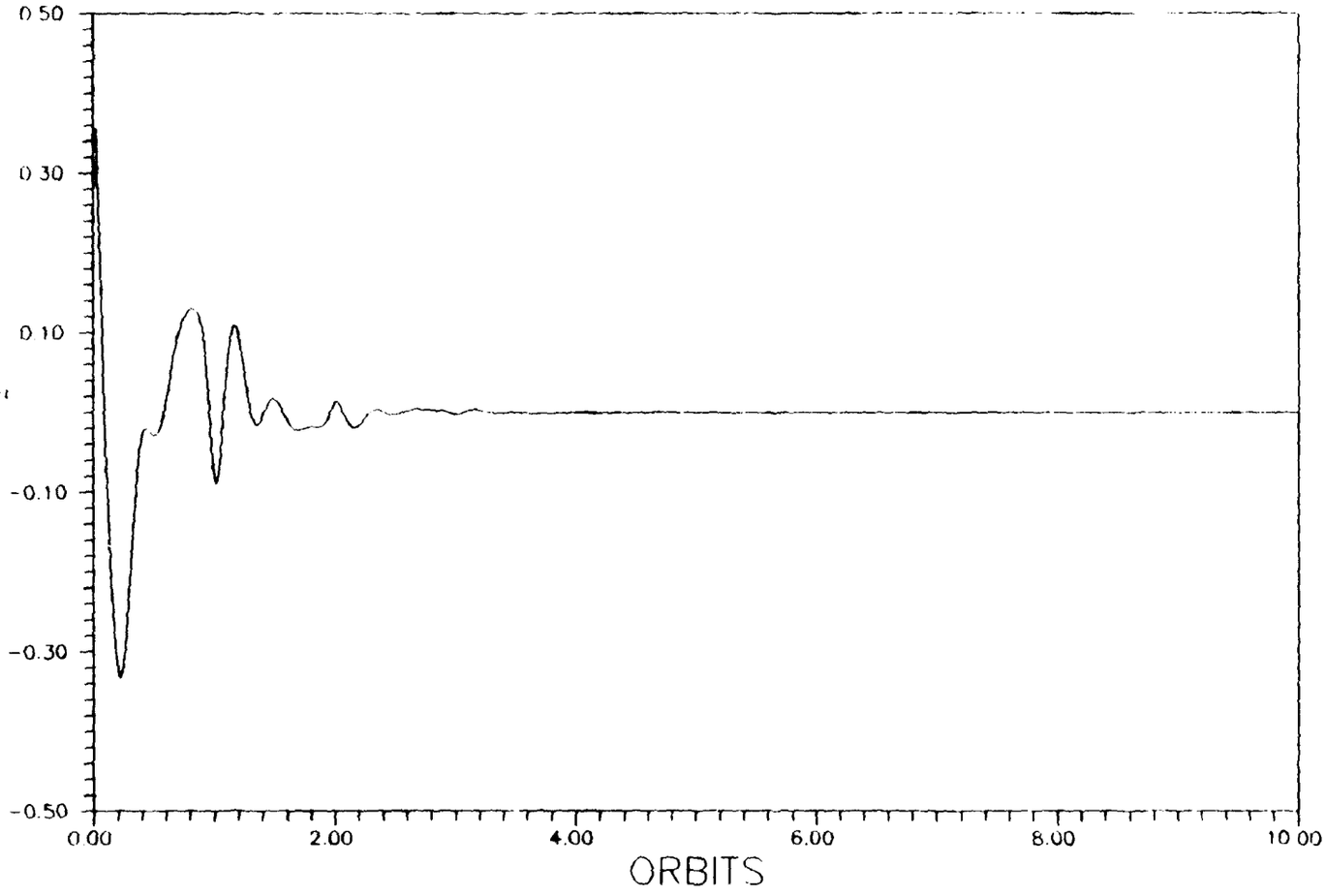

Figure 4.30 Rate Feedback System Time Response for θ_2 ($e=0.5, s=1.0, K=0.7, G_3=0.85$)

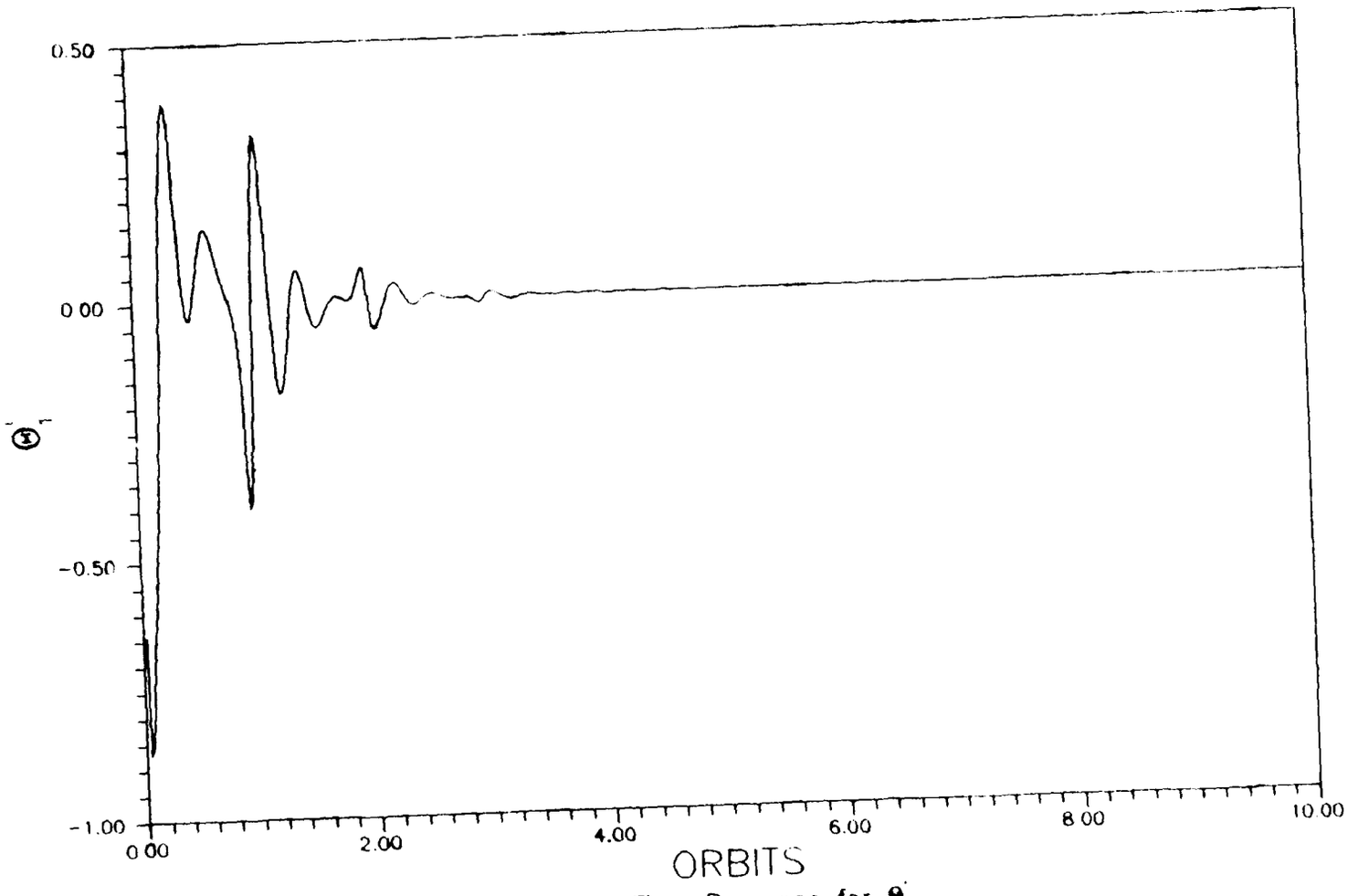

Figure 4.31 Rate Feedback System Time Response for $\dot{\theta}_1$
($e=0.5, s=1.0, K=0.7, G_3=0.85$)

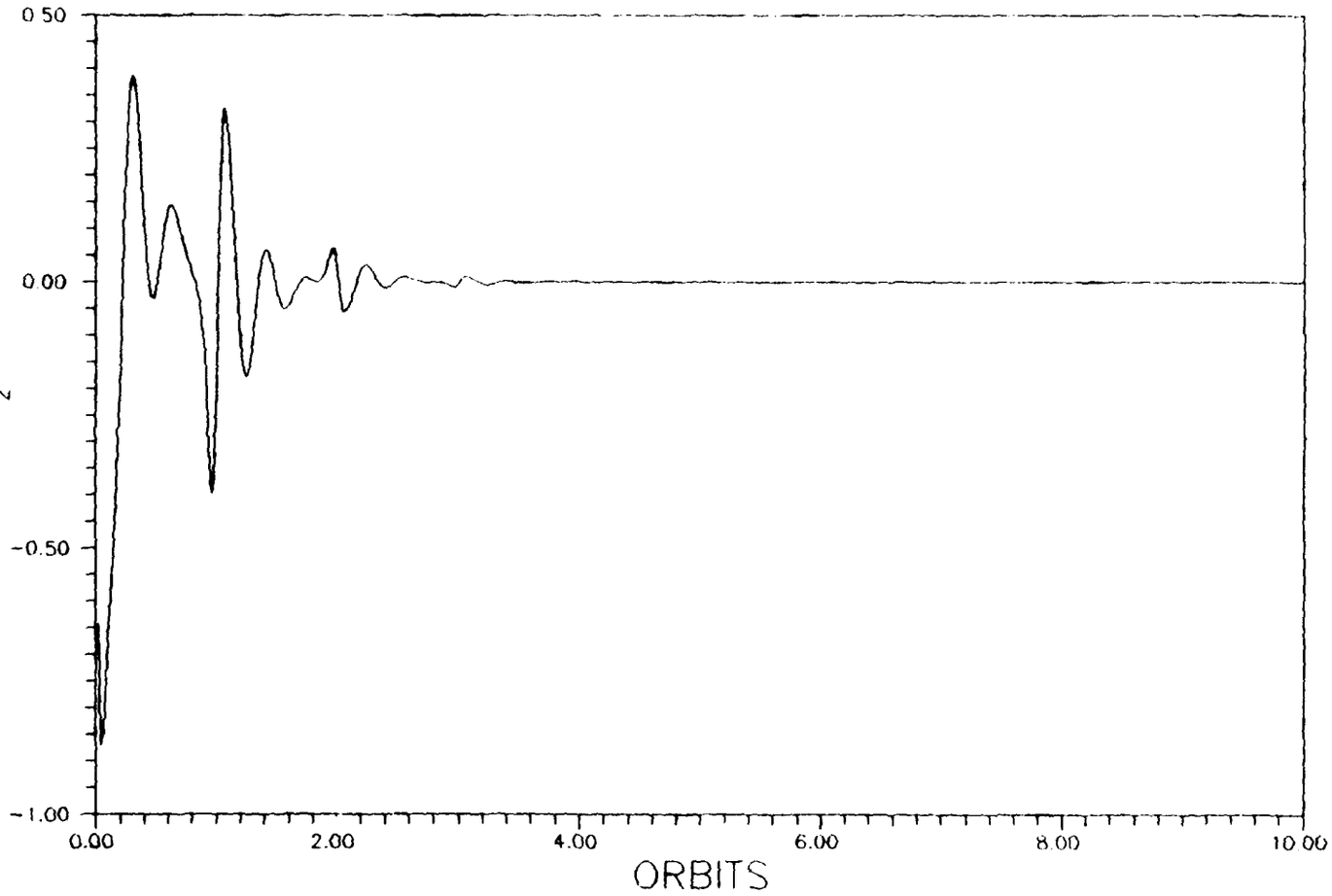

Figure 4.32 Rate Feedback System Time Response for $\dot{\theta}_2$ ($e=0.5, s=1.0, K=0.7, C_3=0.85$)

a 2π interval since the orbital period is 2π. But, some cases used a 4π interval instead. The technique produced maps depicting some interesting and complex structure in the global phase space.

4.2.1 Uncontrolled Equations of Motion. Two cases were looked at for the uncontrolled equations of motion. One case was locally stable with all of the characteristic multipliers on the unit circle with e=0.15. The other case was locally unstable with e=0.5. These two cases were chosen for two basic reasons. One is that the stable case occurs before the torus bifurcation point and the unstable case occurs after the torus bifurcation point. This bifurcation point is shown by figure 4.3. The second reason is that the Floquét controller was studied at e=0.5. The hypothesis here is that the global phase space structure found by Cole originated from the uncontrolled system. The maps plotted 2500 orbits at a 2π interval with fixed parameter values of s=1.0 and K=0.7. Both cases used a disturbance of $\theta_1=\theta_2=0.005$ to create the maps.

The Poincaré maps for the e=0.15 case exhibit an identifiable structure. Figure 4.33 shows a map for θ_1 vs θ_2 and figure 4.34 shows a map for the rates. The trajectories seem to have two frequencies plus the orbital frequency which is characteristic of motion on a 3-torus. This makes sense since only a small step was taken away from the locally stable periodic orbit and both sets of multipliers are complex with a modulus of unity. The structure in both of these maps is confined to a region in the phase space.

On the other hand, the e=0.5 case shows no identifiable structure on the Poincaré maps. These maps are shown in figures 4.35 and 4.36. Note

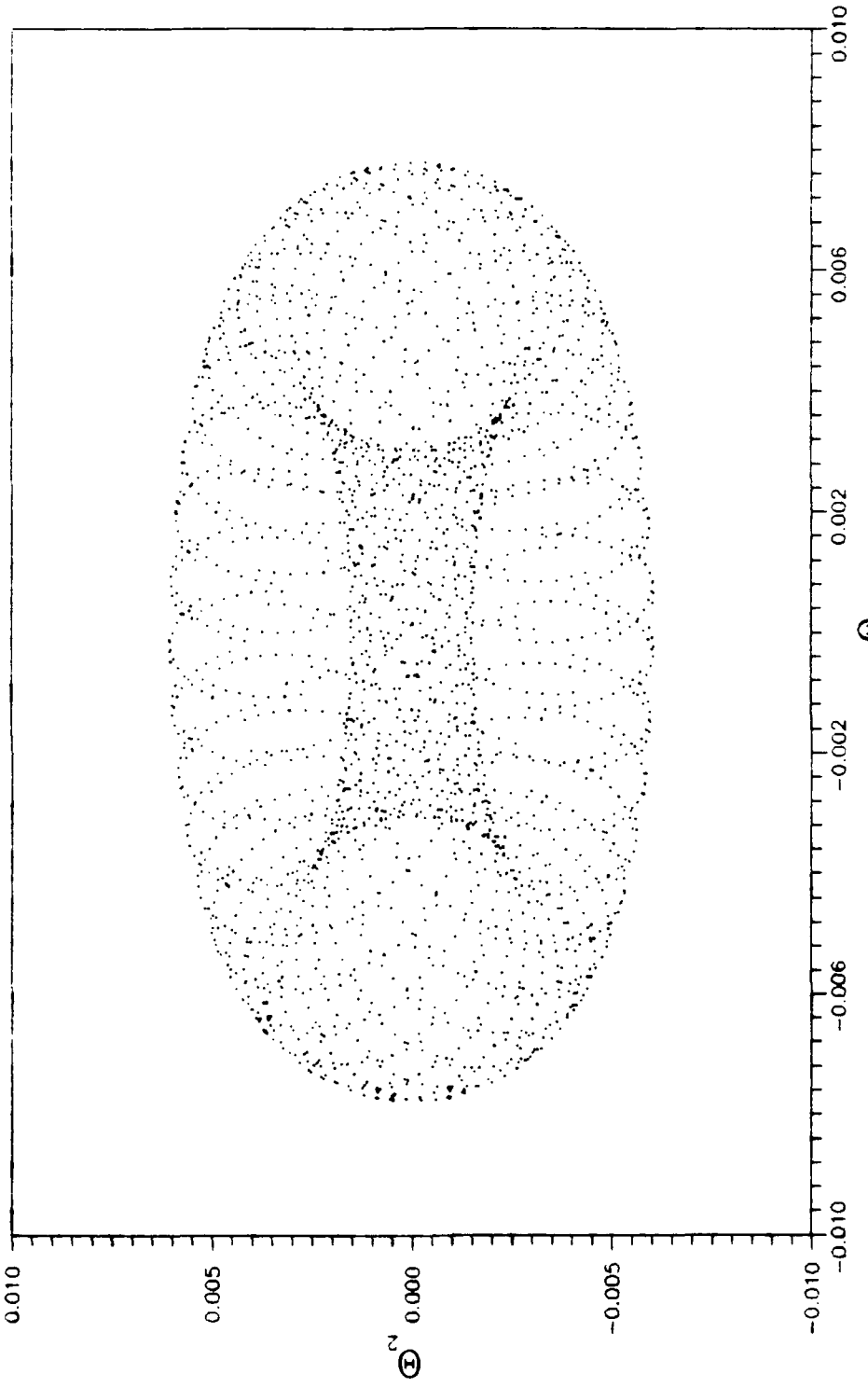

Figure 4.33 Poincare Map of Θ_1 vs Θ_2 for Uncontrolled System (2500 Orbits Sampled at 2π, e=0.15, s=1.0, K=0.7)

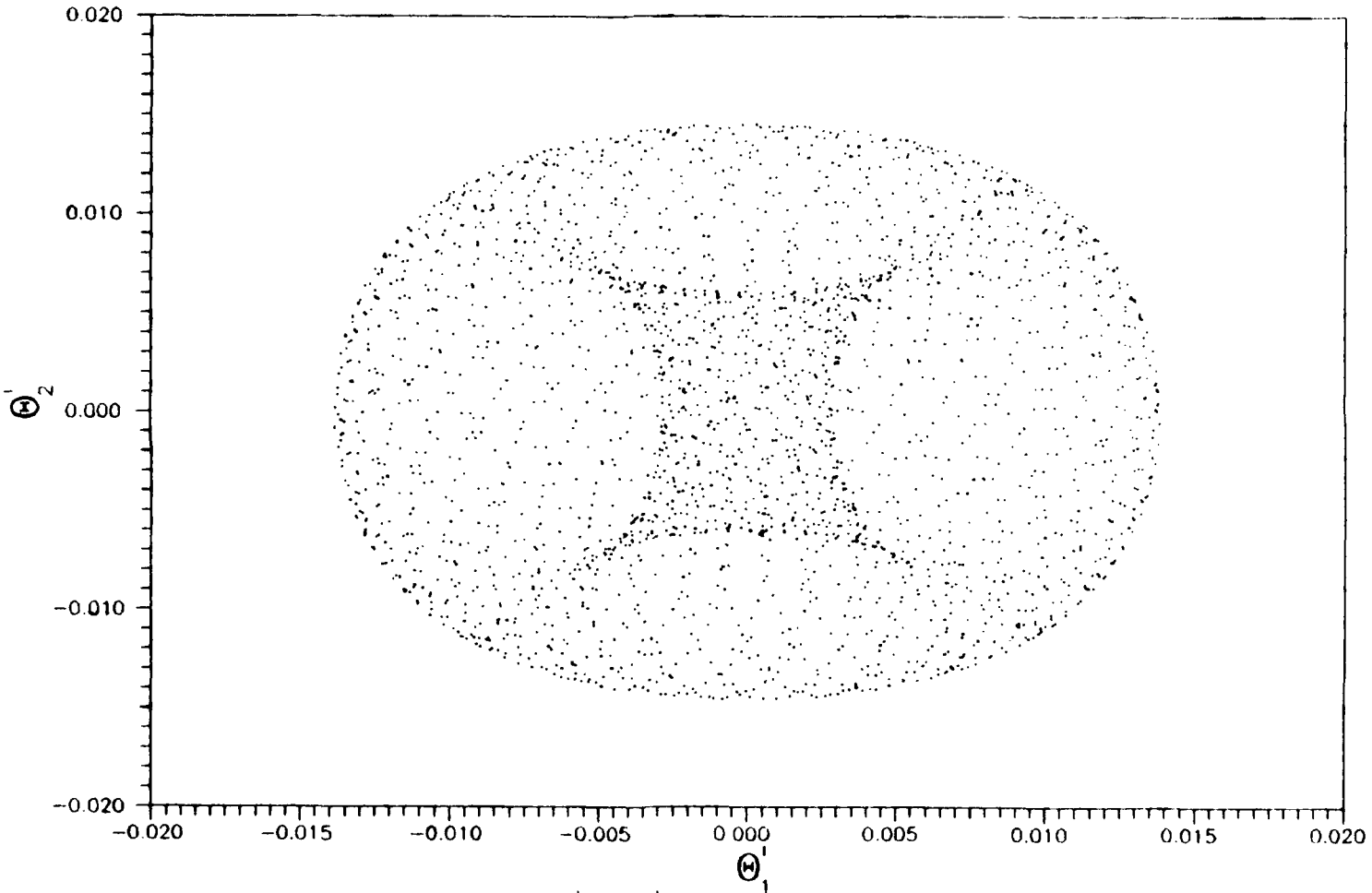

Figure 4.34 Poincare Map of $\dot{\theta}_1$ vs $\dot{\theta}_2$ for Uncontrolled System (2500 Orbits Sampled at 2π,e=0.15,s=1.0,K=0.7)

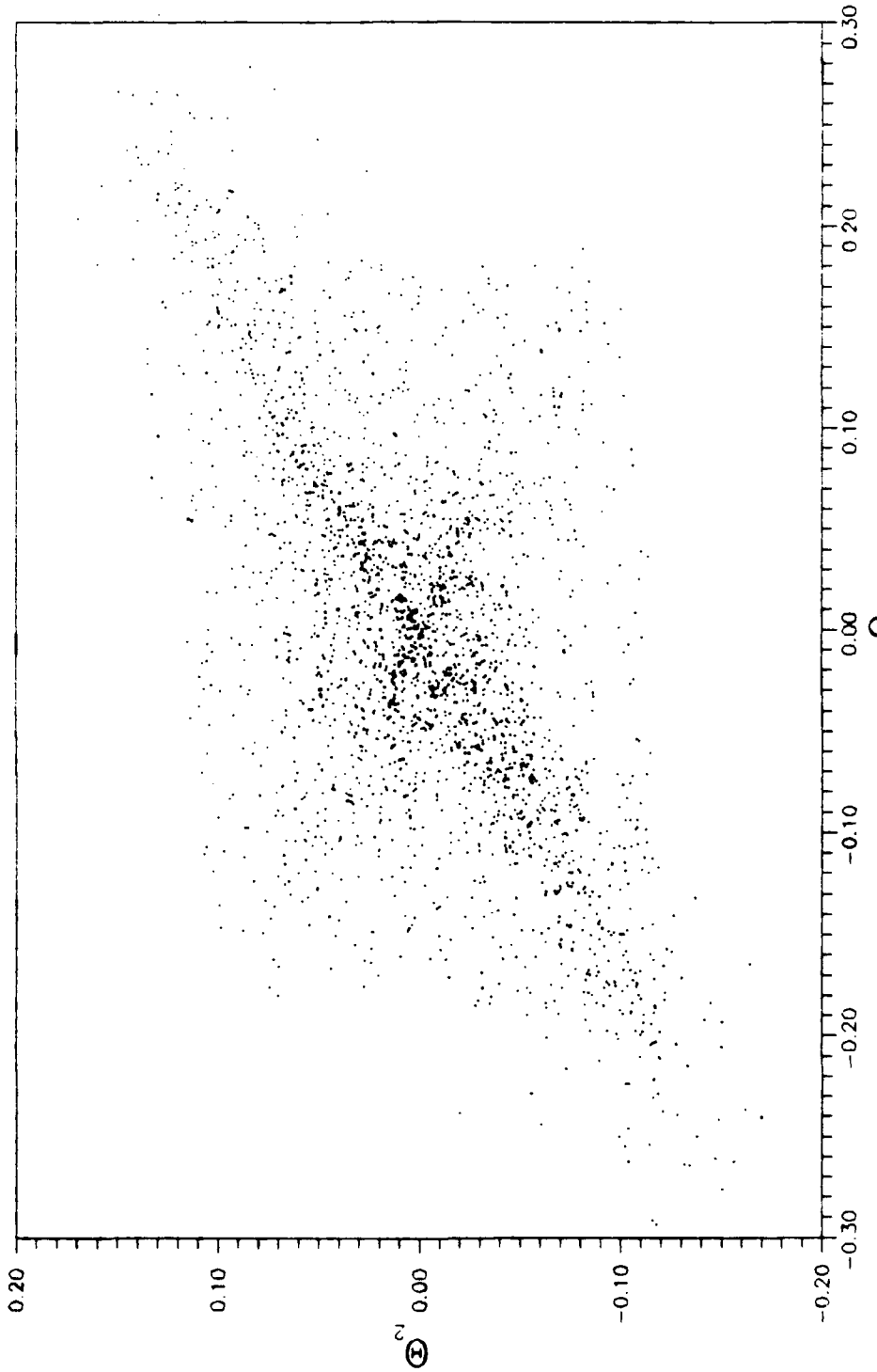

Figure 4.35 Poincare Map of Θ_1 vs Θ_2 for Uncontrolled System (2500 Orbits Sampled at 2π, e=0.5, s=1.0, K=0.7)

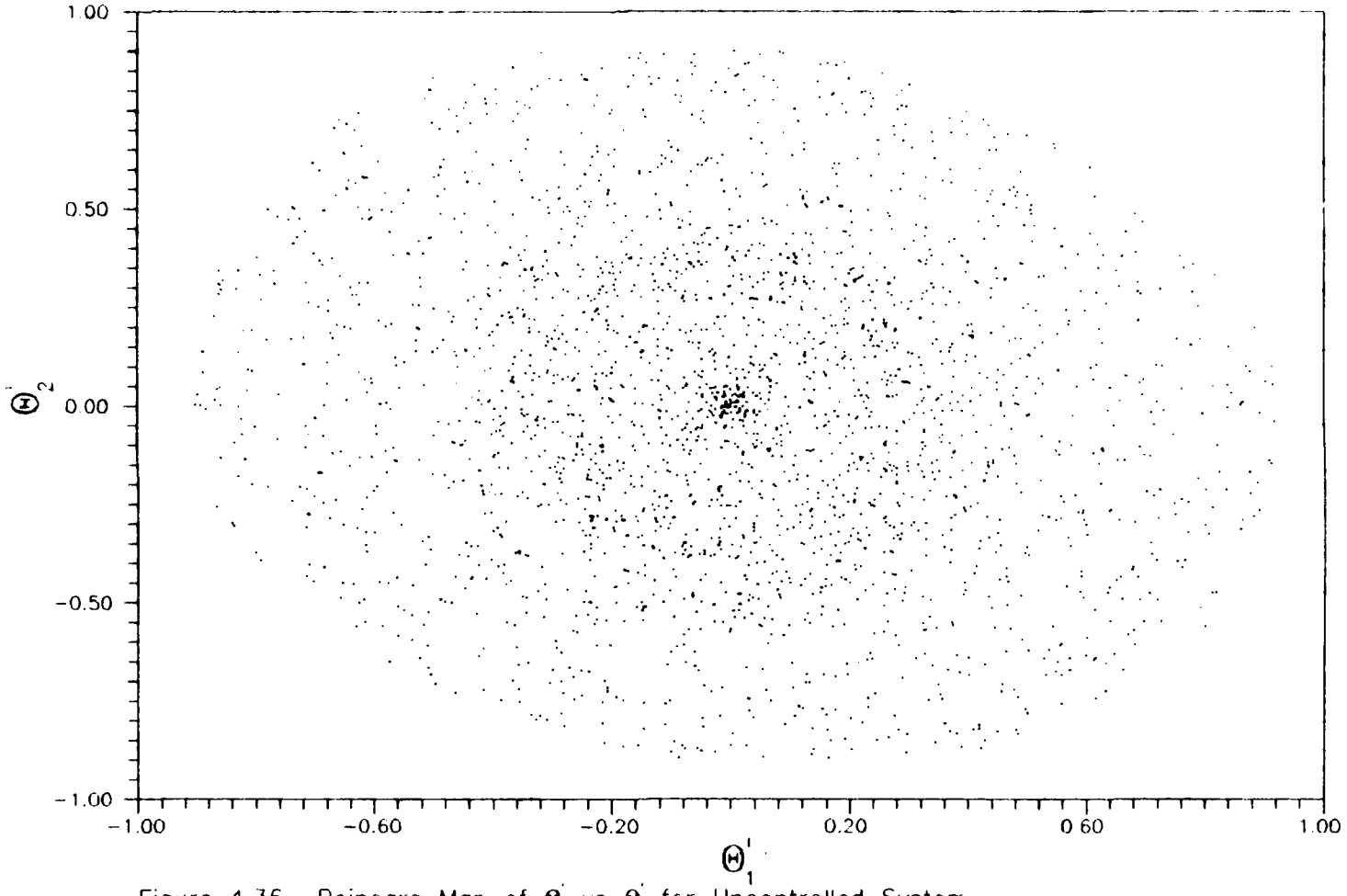

Figure 4.36 Poincare Map of θ_1' vs θ_2' for Uncontrolled System (2500 Orbits Sampled at 2π,e=0.5,s=1.0,K=0.7)

that the maps are still confined to a region of the phase space. This result is typical of a Hamiltonian system since the map fills the space occupied without any preferred structure. If damping is added to the system, one expects this region to collapse into an attractor though.

4.2.2 Floquét Controlled Equations of Motion. A few selected Poincaré maps were generated for the Floquét controlled equations of motion. The parameter values, which were identical to the values used by Cole, were selected as e=0.5, s=1.0, K=0.7, and $G_1=G_2=0.4$. These maps were plotted to see if any additional information could be gained. The initial disturbance put into the system was $\theta_1=0.0851$, $\theta_2=0.0576$, $\theta'_1=-0.1569$, and $\theta'_2=0.95$. In modal variables used by Cole, this was equivalent to $\eta_1=\eta_2=\eta_3=0.0$ and $\eta_4=0.95$. All the maps in this case were sampled at a 4π interval since Cole claimed the system had period doubled [5].

The attractor found by Cole is recreated here. Figures 4.37 and 4.38 show the attractor which was created by the first 400 orbits mapped in the modal variables. These maps contain two apparently closed curves instead of four as demonstrated by Cole in [5]. The shapes in the figures match Cole's identically. The reason for Cole having four closed curves is that he actually plotted at a 2π interval rather than 4π.

When 2500 orbits are mapped, a different picture is created. Figures 4.39 and 4.40 show the original closed curves embedded in some other structure in the phase space. There are now also what seems to be solid lines appearing on the maps. The points which created these solid lines came from the very last portion of the 2500 points plotted. It appears that the initial closed curves are transients that disappear over

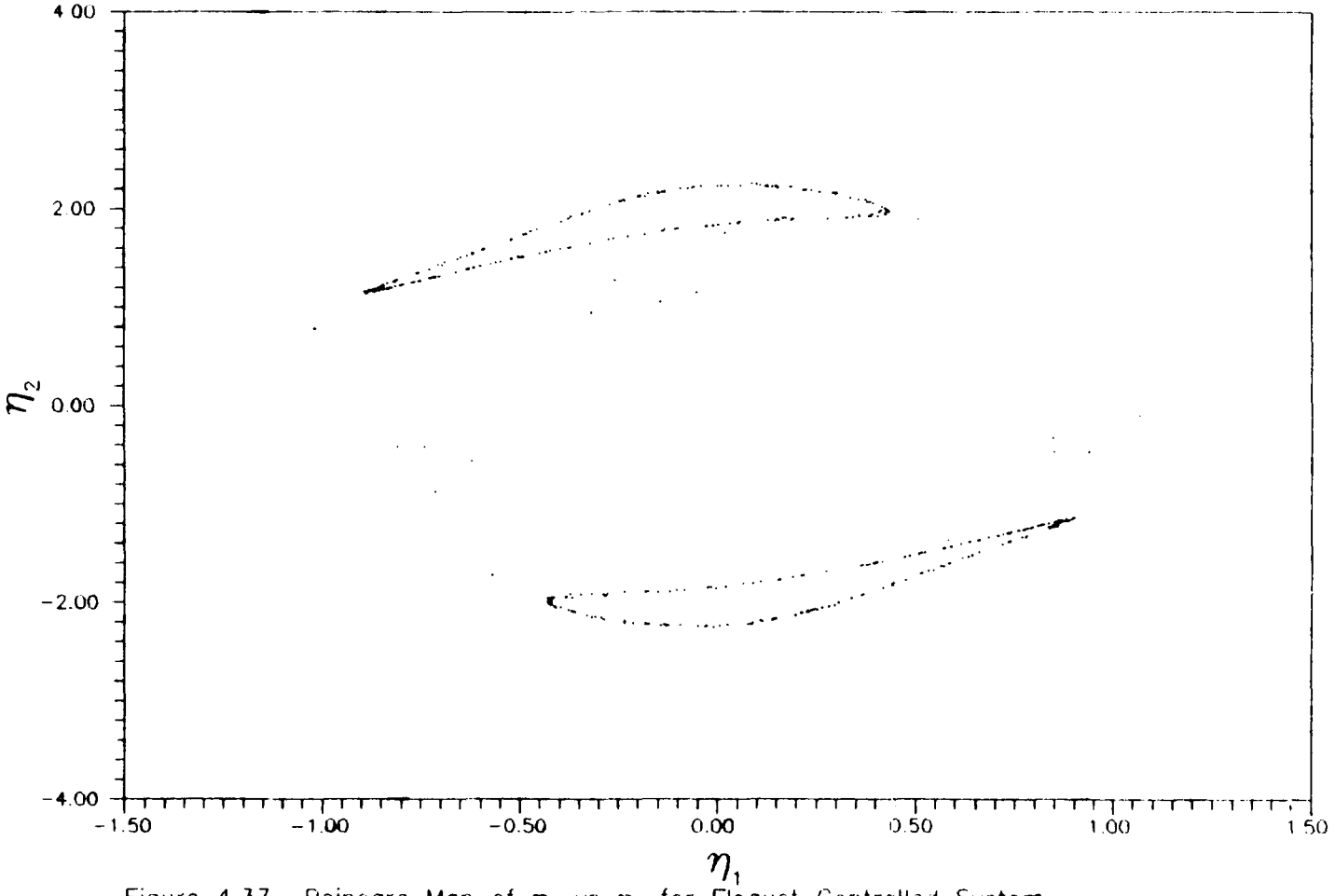

Figure 4.37 Poincare Map of η_1 vs η_2 for Floquet Controlled System (400 Orbits sampled at 4π,e=0.5,s=1.0,K=0.7,G_1=G_2=0.4)

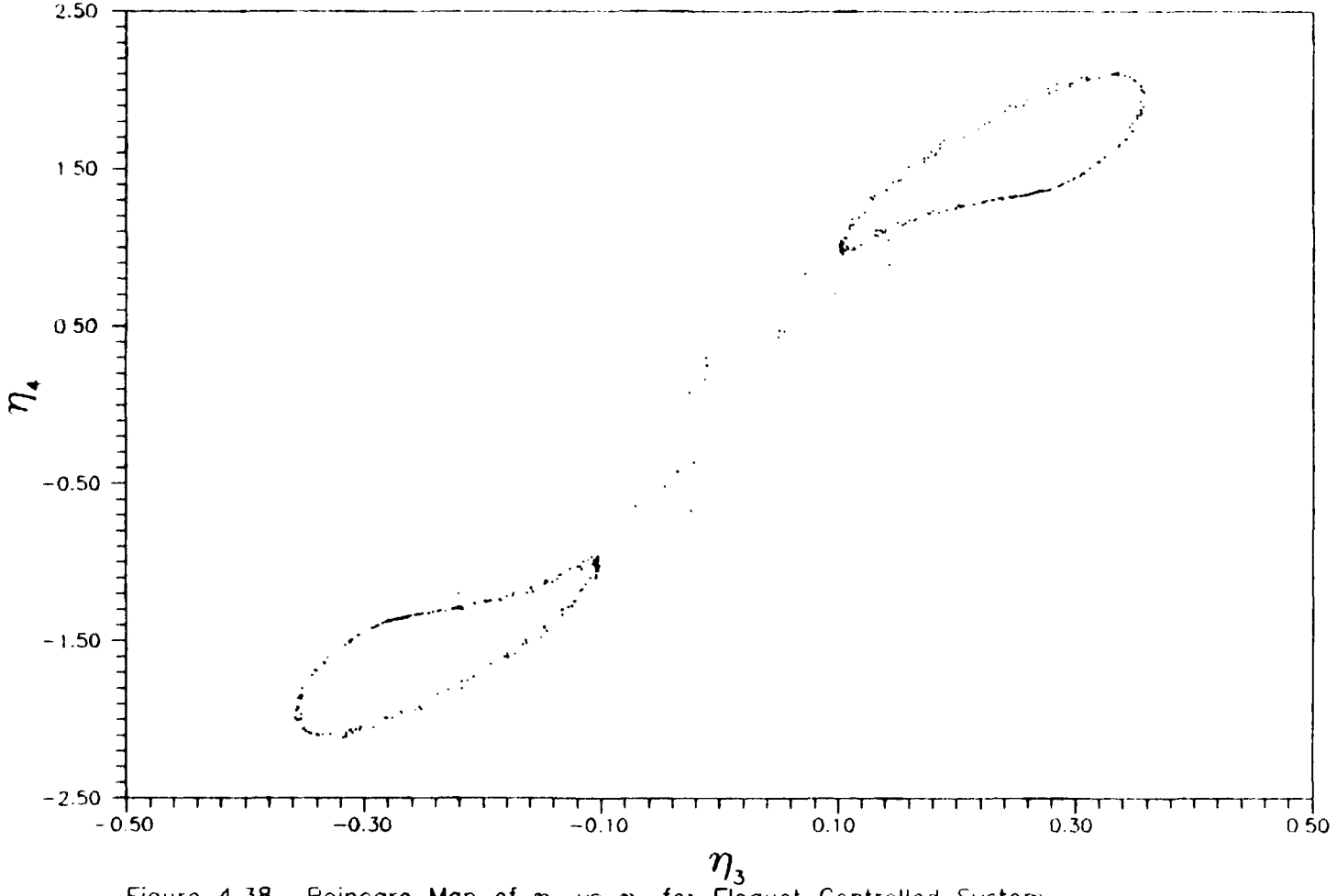

Figure 4.38 Poincare Map of η_3 vs η_4 for Floquet Controlled System (400 Orbits sampled at 4π,e=0.5,s=1.0,K=0.7,G_1=G_2=0.4)

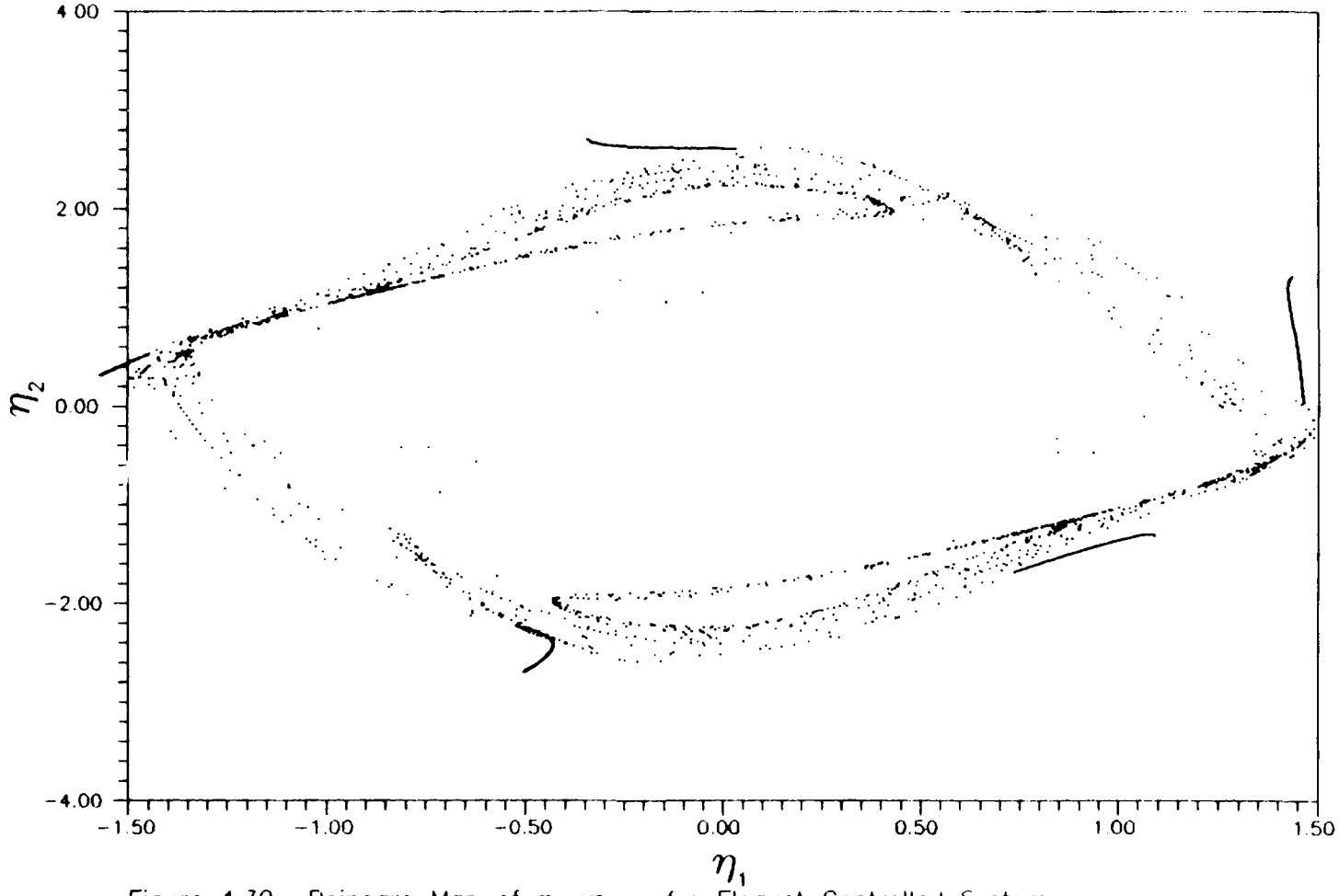

Figure 4.39 Poincare Map of η_1 vs η_2 for Floquet Controlled System (2500 Orbits sampled at 4π,e=0.5,s=1.0,K=0.7,G_1=G_2=0.4)

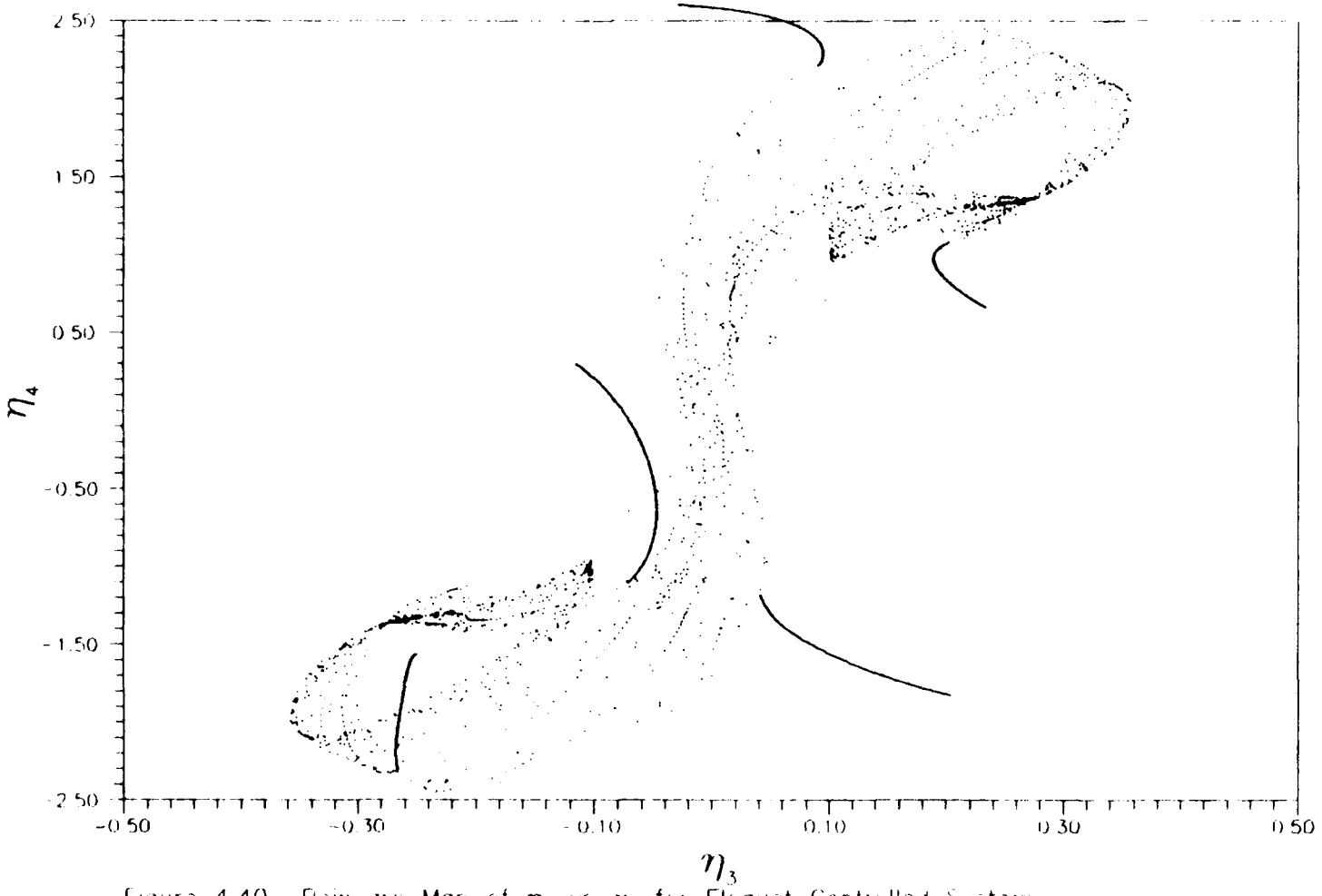

Figure 4.40 Poincare Map of η_3 vs. η_4 for Floquet Controlled System (2500 Orbits sampled at 4π, e=0.5, s=1.0, K=0.7, $G_1=G_2=0.4$)

the long time scale and maybe re-visited over an even longer time scale.

The same type of structure appeared in the nondimensional variable phase space. Figures 4.41 and 4.42 map the nondimensional physical variables using the same parameter values as for the modal variables. However, these figures map an angle versus its corresponding rate for 2500 orbits. Again, there are two closed curves embedded in some other structure in the phase space. Also, the solid looking lines are present.

The solid lines seemed to indicate that another attractor was present. It is possible that this attractor is a limit cycle that is wandering a little due to numerical accuracy problems in the integration. So, the integration was restarted using the end points of figures 4.41 and 4.42 for 2500 more orbits. The results of this integration are mapped in figures 4.43 and 4.44. Figure 4.43 shows two different closed curves embedded in some other structure in the phase space. Again, the solid lines appear. Figure 4.44 is a little harder to visualize. However, two closed curves are present inside the structure on the map. These curves occurred during the first part of the mapping. The same solid lines appear again. If the first 2500 orbit and the 2500 restarted orbits are combined onto one map, we see four closed curves. This is easily seen in figure 4.45. Yet, there is still other structure present on the map. Notice that the solid lines fall on top of one another. The same phenomenon occurs in figure 4.46. These maps show that the trajectory visits two weakly unstable structures (one like a torus and the other like a limit cycle) with transients between the two leading to a complicated attractor. An explanation of this may be that the trajectories in the

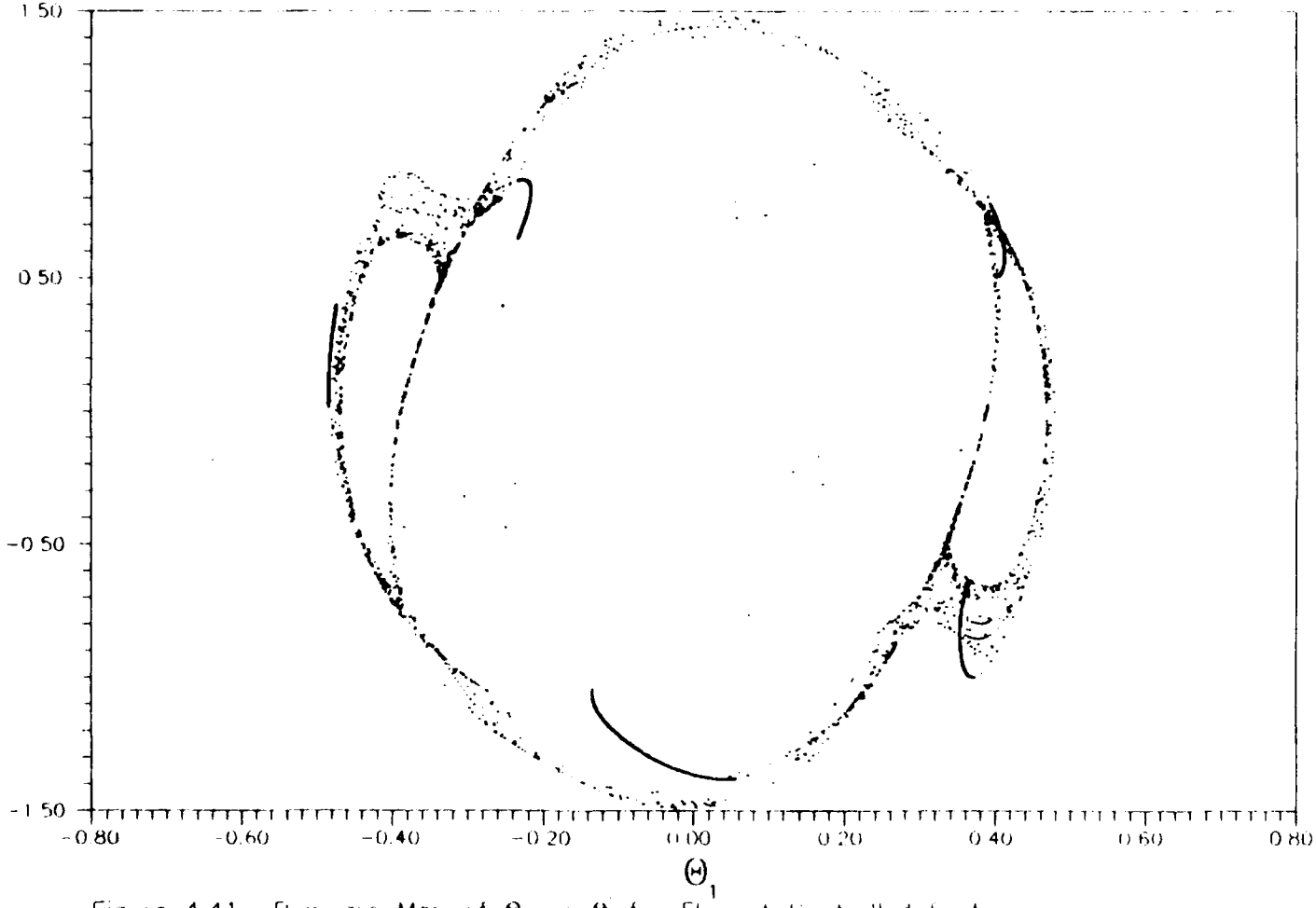

Figure 4.41 Poincare Map of Θ_1 vs Θ_1' for Floquet Controlled System (2500 Orbits sampled at 4π, e=0.5, s=1.0, K=0.7, G_1=G_2=0.4)

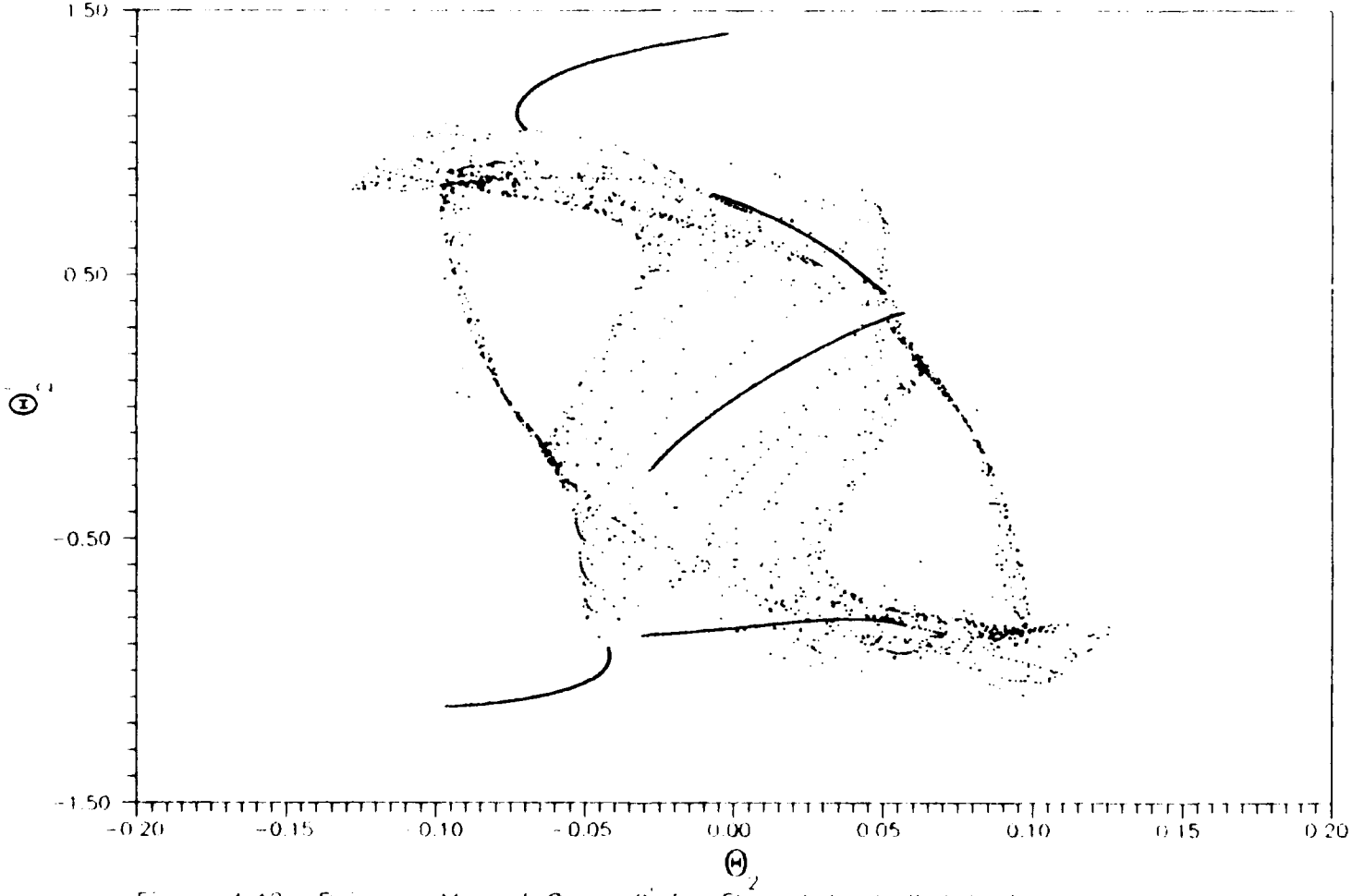

Figure 4.42 Poincare Map of Θ_2 vs $\dot{\Theta}_2$ for Floquet Controlled System (2500 Orbits sampled at 4π, e=0.5, s=1.0, k=0.7, $G_1=G_2=0.4$)

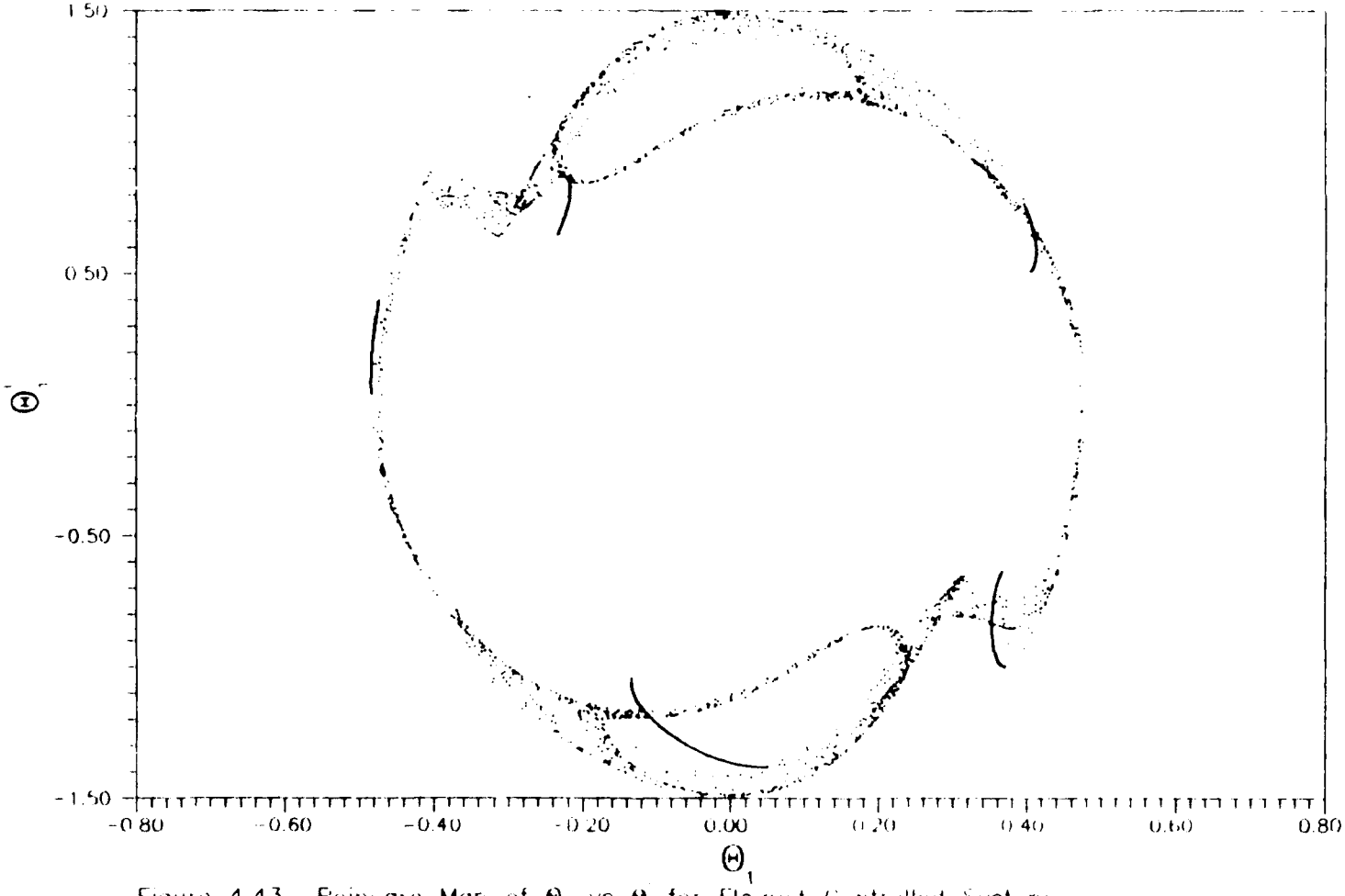

Figure 4.43 Poincare Map of Θ_1 vs Θ_1 for Floquet Controlled System (2500 Orbits Sampled at 4π, e=0.5, s=1.0, K=0.7, $G_1 = G_2$ = 0.4)

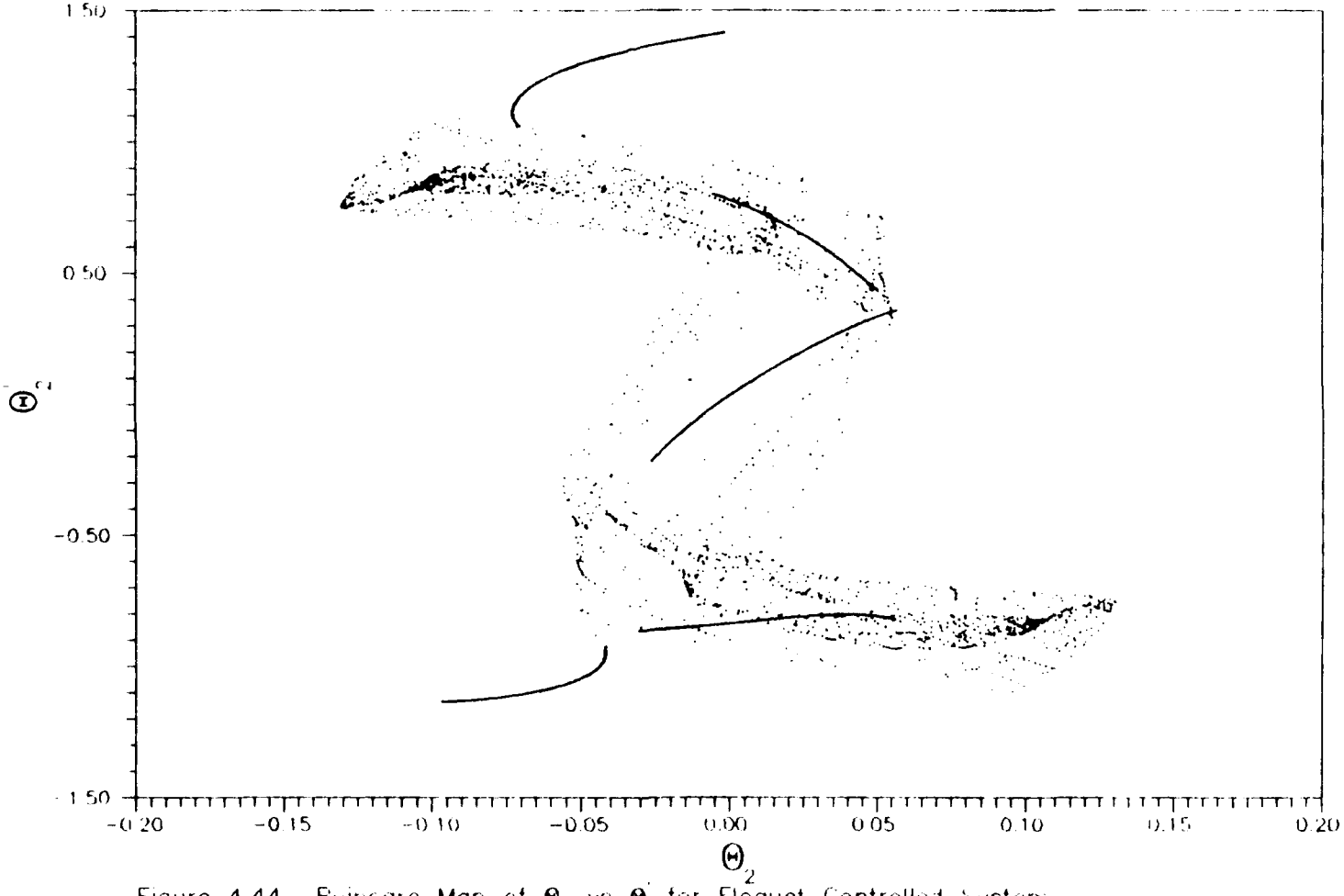

Figure 4.44 Poincare Map of Θ_2 vs Θ_2' for Floquet Controlled System (2500 Orbits Sampled at 4π, e=0.5, s=1.0, K=0.7, $G_1=G_2=0.4$)

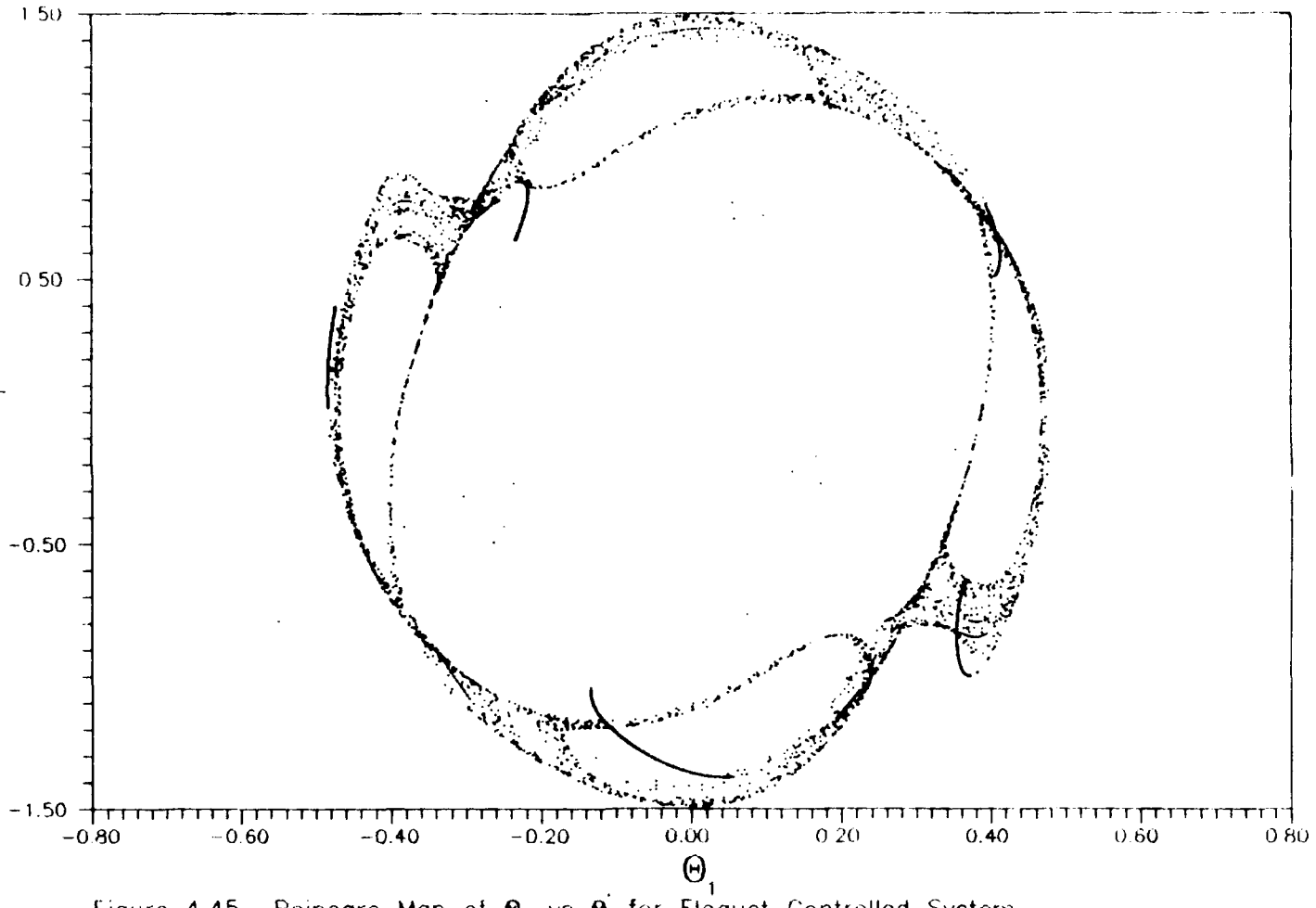

Figure 4.45 Poincare Map of Θ_1 vs $\dot{\Theta}_1$ for Floquet Controlled System (5000 Orbits Sampled at 4π, e=0.5, s=1.0, K=0.7, $G_1=G_2=0.4$)

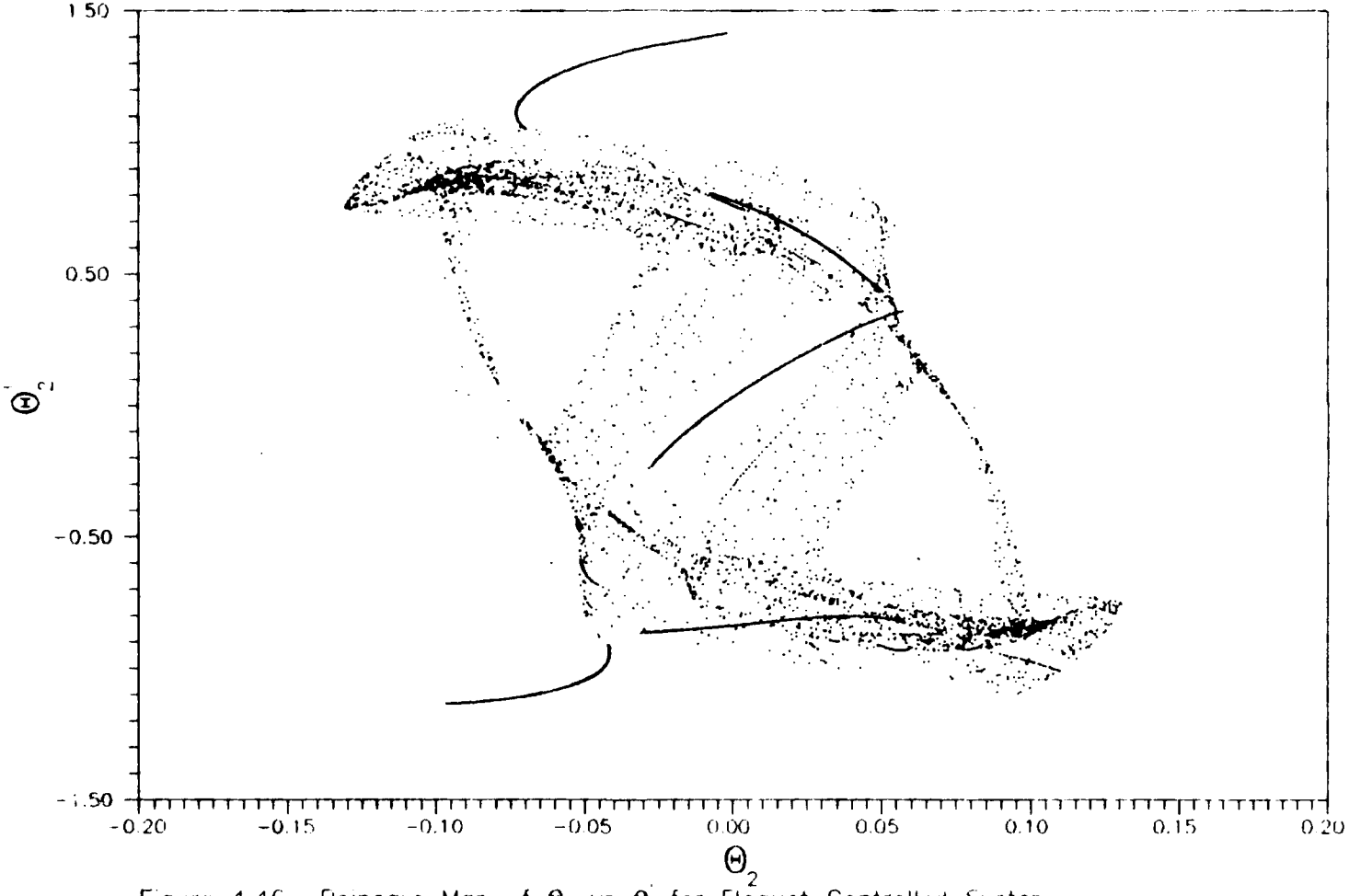

Figure 4.46 Poincare Map of Θ_2 vs $\dot{\Theta}_2$ for Floquet Controlled System (5000 Orbits Sampled at 4π, e=0.5, s=1.0, K=0.7, G_1=G_2=0.4)

phase space are trapped between the surface of an unstable torus and an unstable limit cycle. The solid lines on the plot may indicate the approach of the trajectories to the limit cycle.

4.2.3 Rate and Position Feedback Equations of Motion. A small amount of damping was added to the uncontrolled equations of motion here through the uncoupled rate feedback term. Again, the case we are interested in here is when e=0.5. Recall that the uncontrolled equations of motion showed no structure on the Poincaré map at this particular eccentricity. See figures 4.35 and 4.36. With the added damping, we were looking for the formation of an attractor similar in structure to that of the Floquét controlled equations. But, there was no guarantee that this would be the case.

The problem here was set up by plotting the characteristic multipliers for the rate feedback gains of G_j=0.0, G_j=0.01, and G_j=0.03 for $0.46 \le e \le 0.5$, s=1.0, K=0.7. Figure 4.47 shows the plot for these three rate feedback gains. The solid line in the plot is a portion of the unit circle. The location of the characteristic multipliers for e=0.5 is the first point on left of each plotted line. For G_j=0.01, the multipliers are still outside the unit circle. It can be deduced from figure 4.47 that all the multipliers are inside the unit circle for G_j=0.05 and e=0.5. These two cases were looked at with the Poincaré map.

The maps for G_j=0.01 indicate an initial transient attractor as shown earlier. Figures 4.48, 4.49, 4.50, and 4.51 show this for 500 orbits. The disturbance for figure 4.48 and 4.49 was $\theta_1=\theta_2$=0.005. The initial disturbance for figures 4.50 and 4.51 was $\theta_1=\theta_2$=0.4. Note that the same

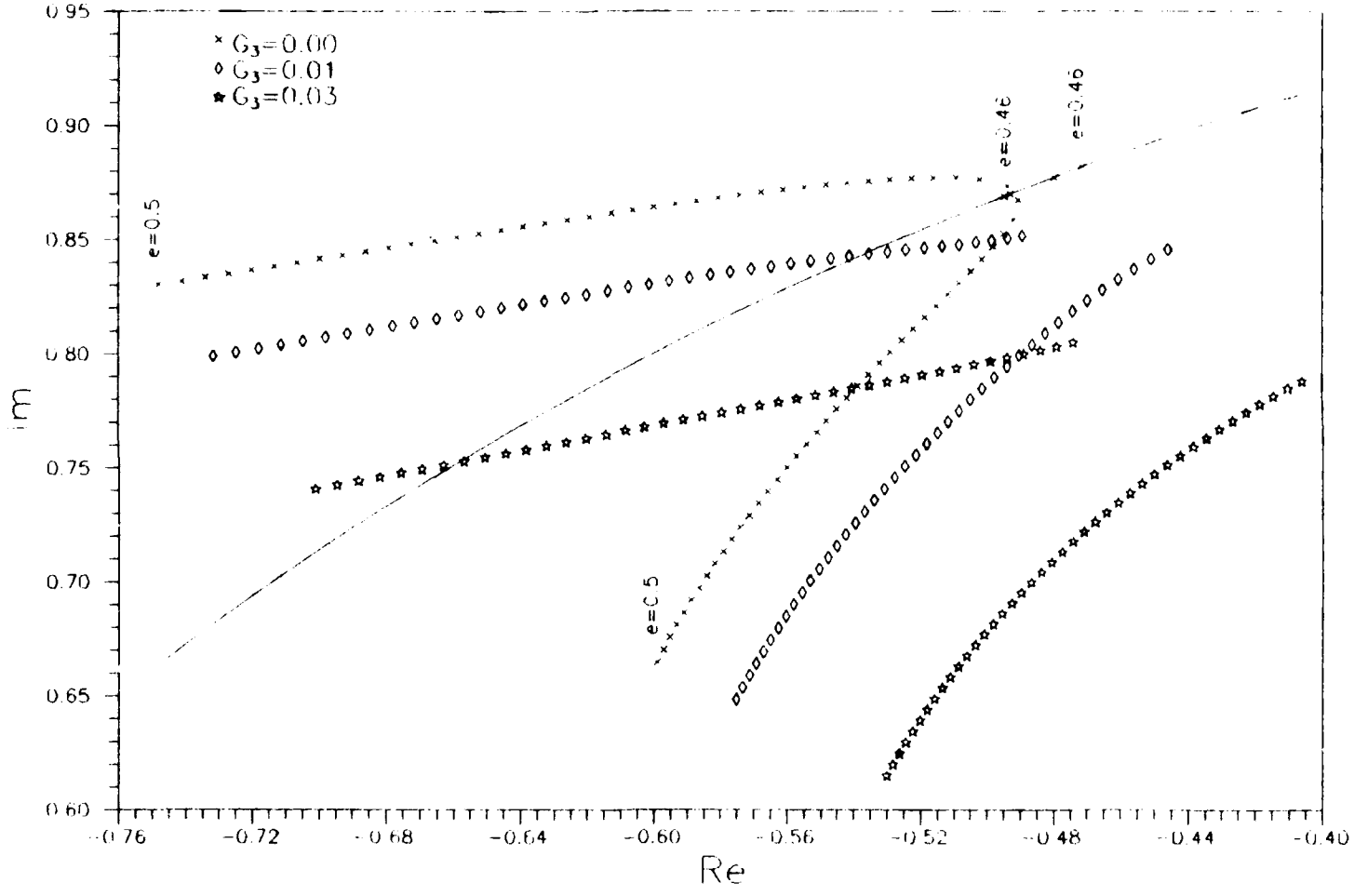

Figure 4.47 Rate Feedback Gain Effect on Multipliers (0.46<e<0.50,s=1.0,K=0.7)

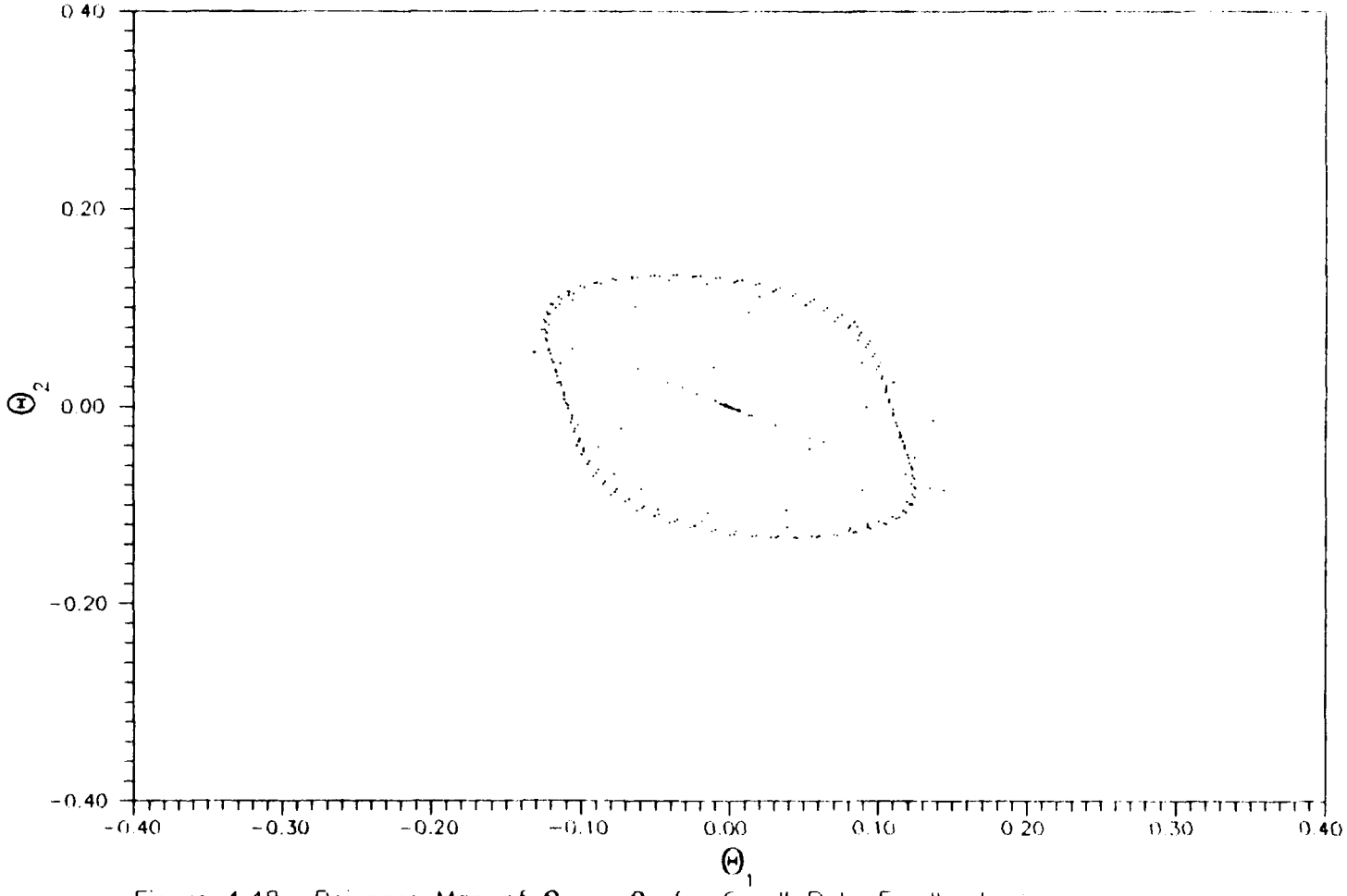

Figure 4.48 Poincare Map of Θ_1 vs Θ_2 for Small Rate Feedback Gain (500 Orbits Sampled at 4π, e=0.5, s=1.0, k=0.7, G_3=0.01)

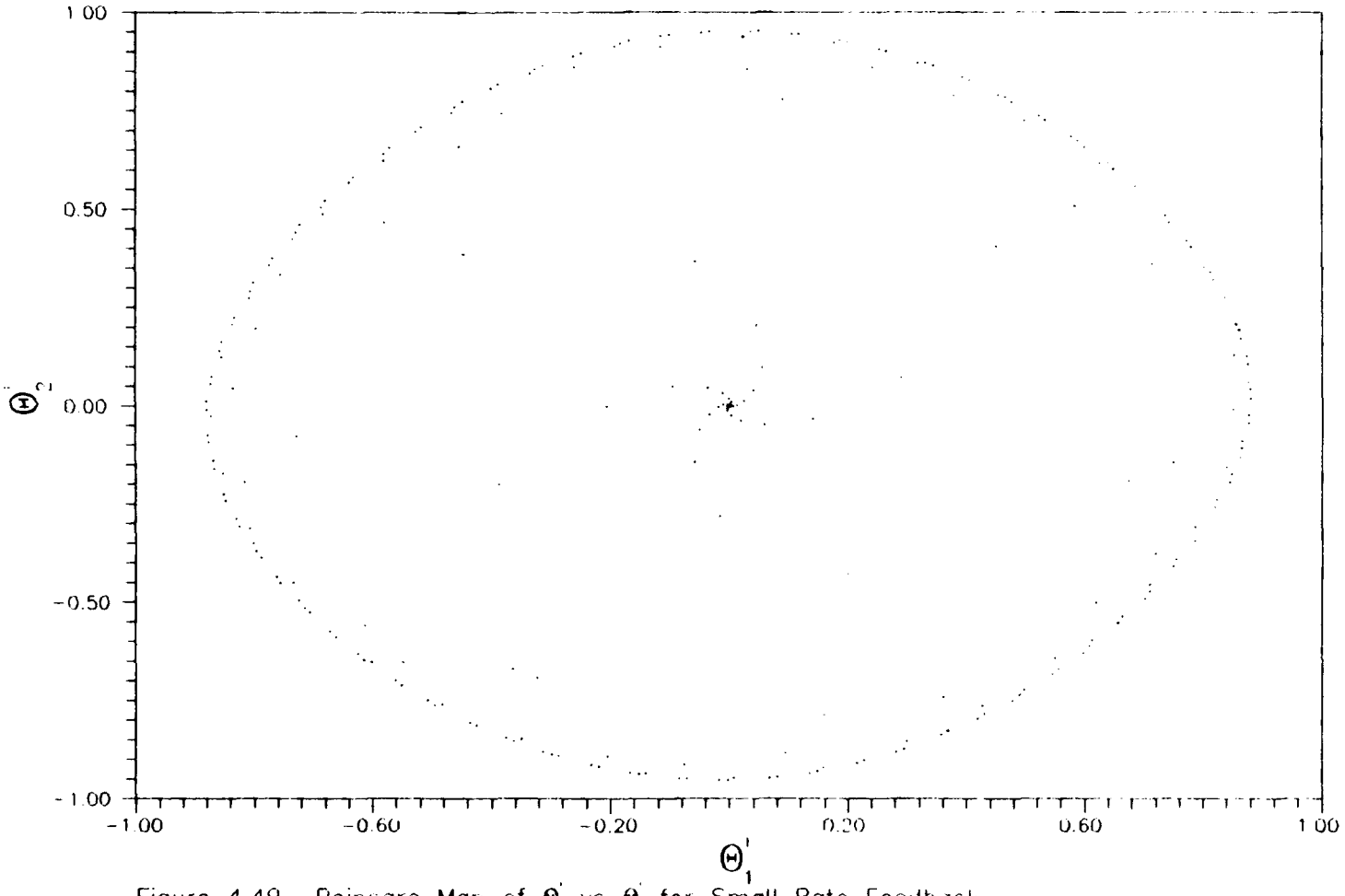

Figure 4.49 Poincare Map of $\dot{\Theta}_1$ vs $\dot{\Theta}_2$ for Small Rate Feedback Gain (500 Orbits Sampled at 4π, e=0.5, s=1.0, K=0.7, G_1=0.01)

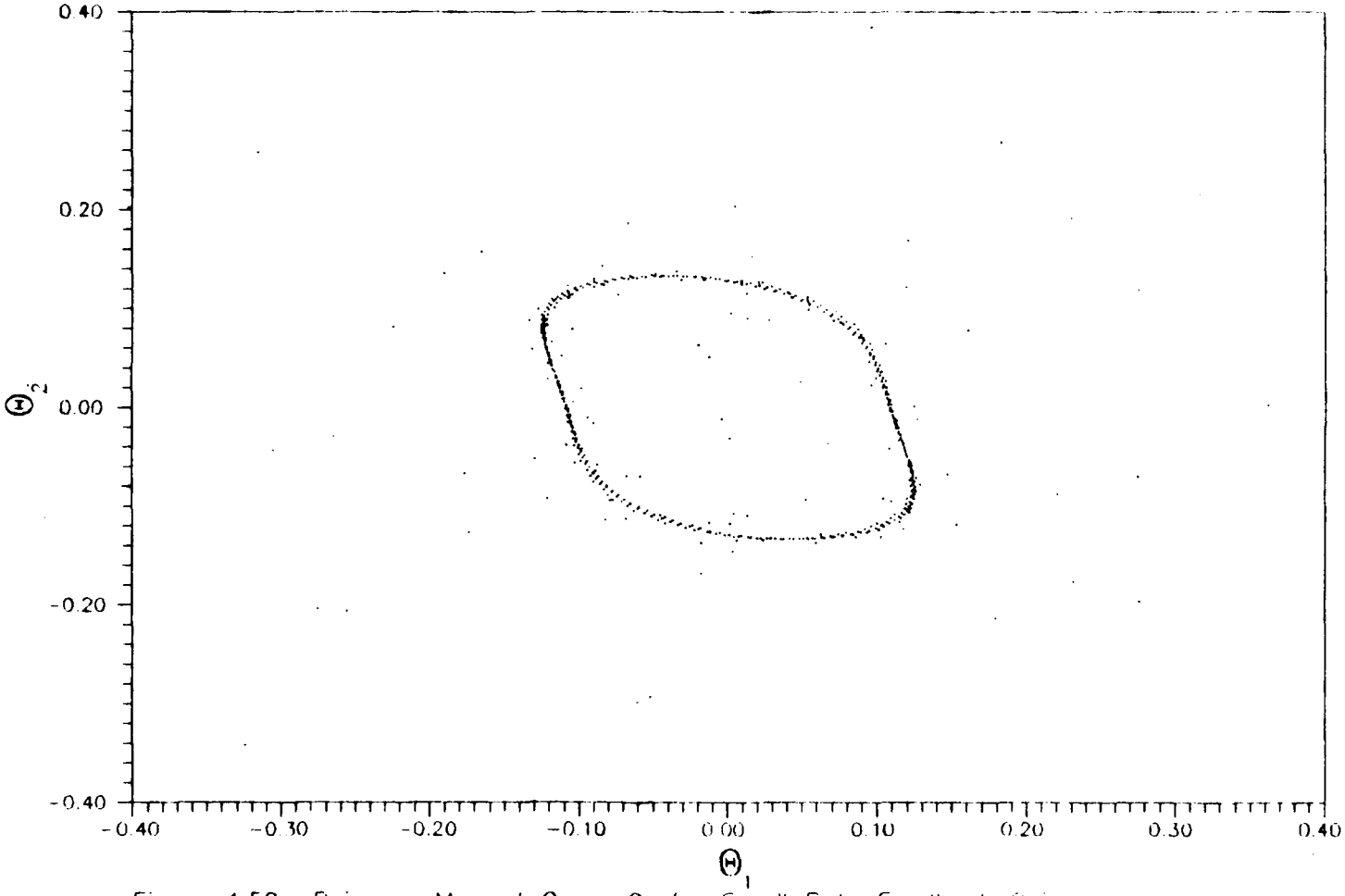

Figure 4.50 Poincare Map of Θ_1 vs Θ_2 for Small Rate Feedback Gain (500 Orbits Sampled at 2π,e=0.5,s=1.0,K=0.7,G_3=0.01)

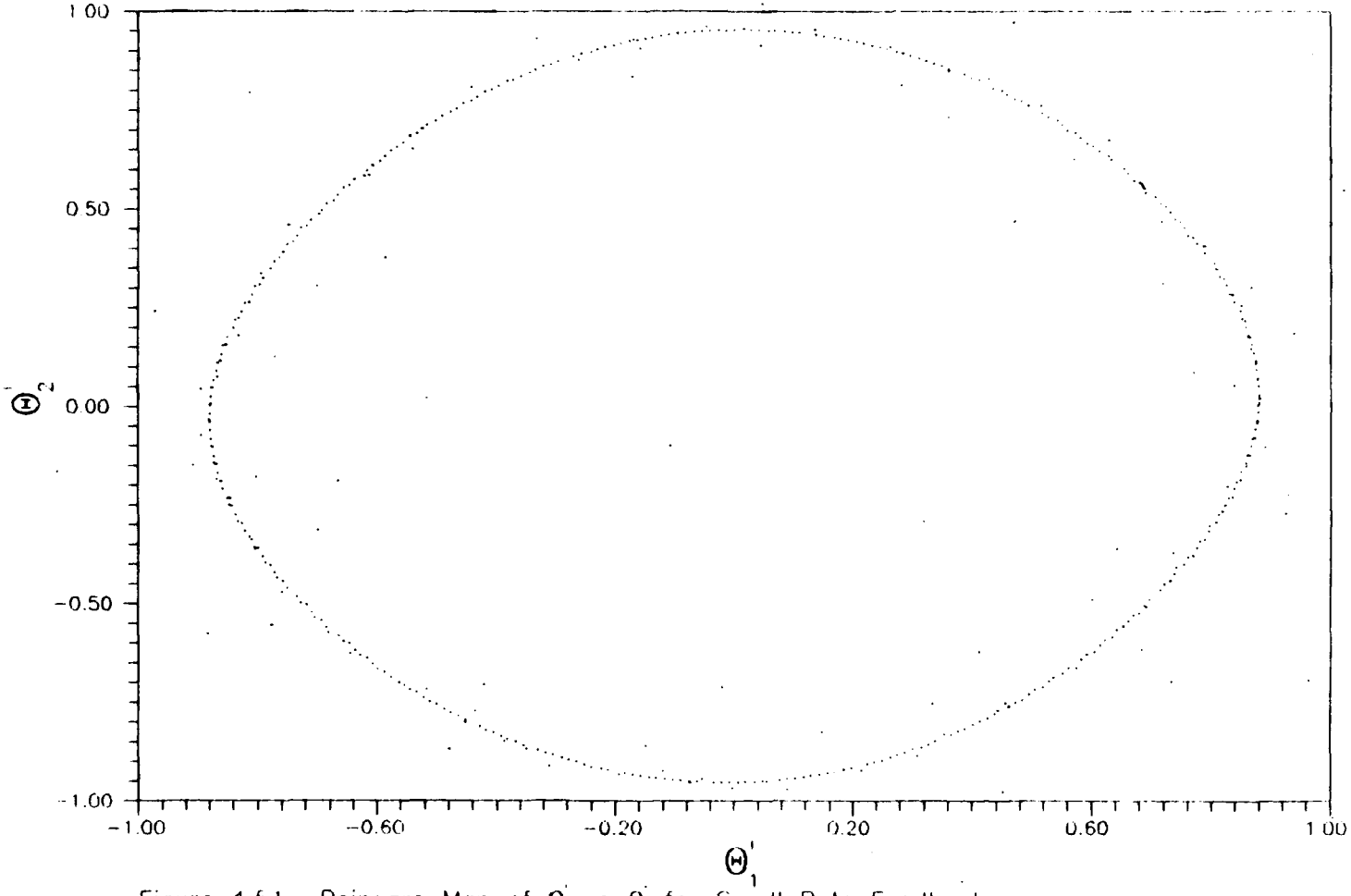

Figure 4.51 Poincare Map of Θ'_1 vs Θ'_2 for Small Rate Feedback Gain (500 Orbits Sampled at 2π, e=0.5, s=1.0, k=0.7, G_1=0.01)

attractor appeared for two disturbances differing by two orders of magnitude and two sampling intervals of 2π and 4π respectively.

When 10000 orbits were mapped using the smaller of the two disturbances, an interesting structure appeared in the phase space. Figures 4.52 and 4.53 depict the original attractor embedded in some intricate structure. An explanation for this is that the added dissipation was so small that the phase space still "wants to" resemble that of the original Hamiltonian system. But, some form of structure is present.

As G_j was increased, the intricate structure present began to shrink in size on the maps. When G_j=0.05, an attractor appeared at the origin which was without structure. This limit cycle attractor is exhibited by figures 4.54 and 4.55 by the fixed point at the origin of each map. This result was what we expected the rate feedback to accomplish. The larger of the two disturbances was used here. So, the rate feedback term did not preserve to the global attractor present for the Floquét controlled system. This is a more attractive approach to obtain the desired control since the global structure is not present for larger disturbances away from the equilibrium condition.

4.3 Continuation

Continuation was used in a limited fashion in this thesis because of the conservative nature of the symmetric spinning satellite problem. The continuation software, AUTO, primarily handles dissipative systems of equations. This is because conservative systems have multiple multipliers at unity which causes a non-uniqueness of closed orbits. The software was

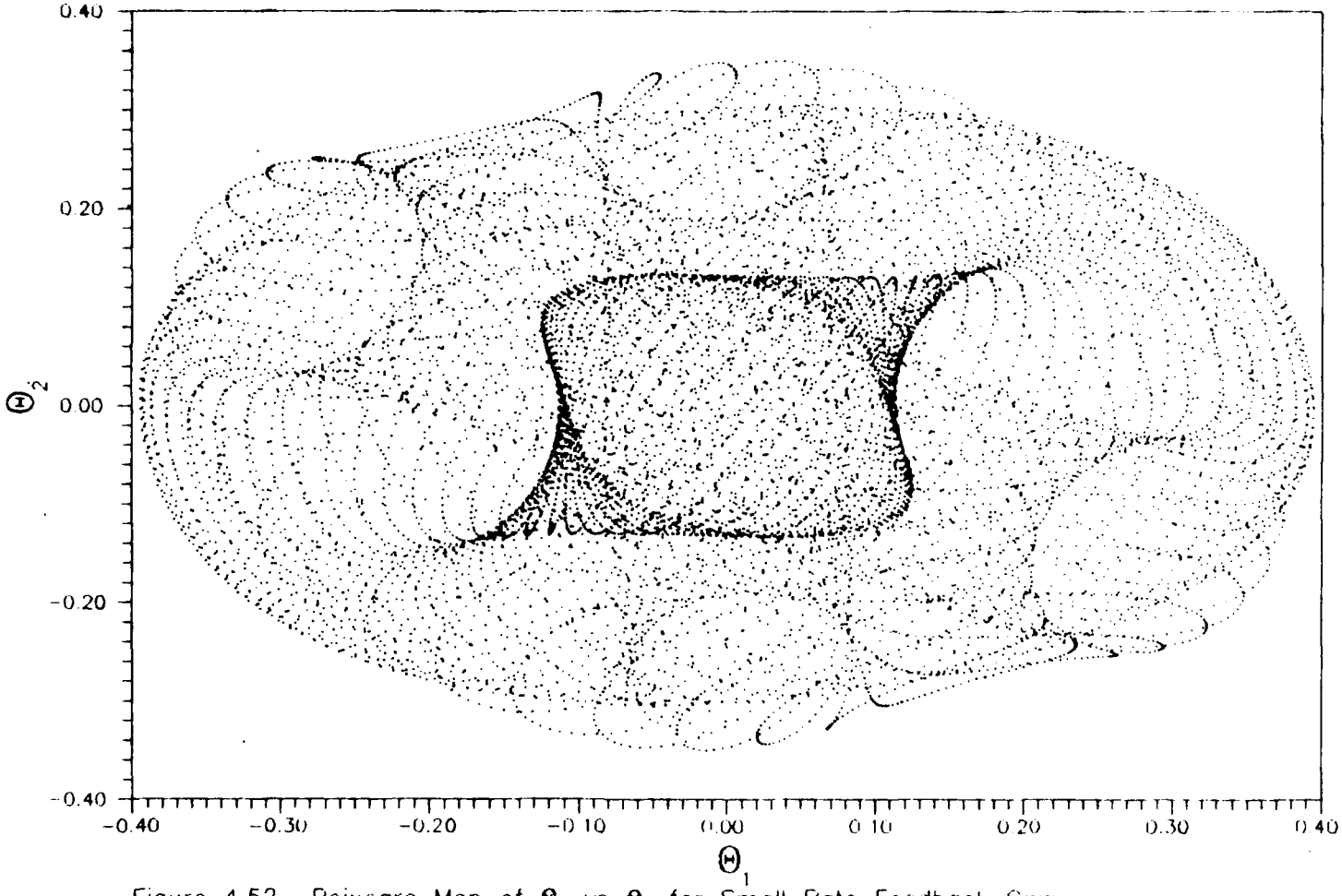

Figure 4.52 Poincare Map of Θ_1 vs Θ_2 for Small Rate Feedback Gain (10000 Orbits Sampled at 2π,e=0.5,s=1.0,k=0.7,G_3=0.01)

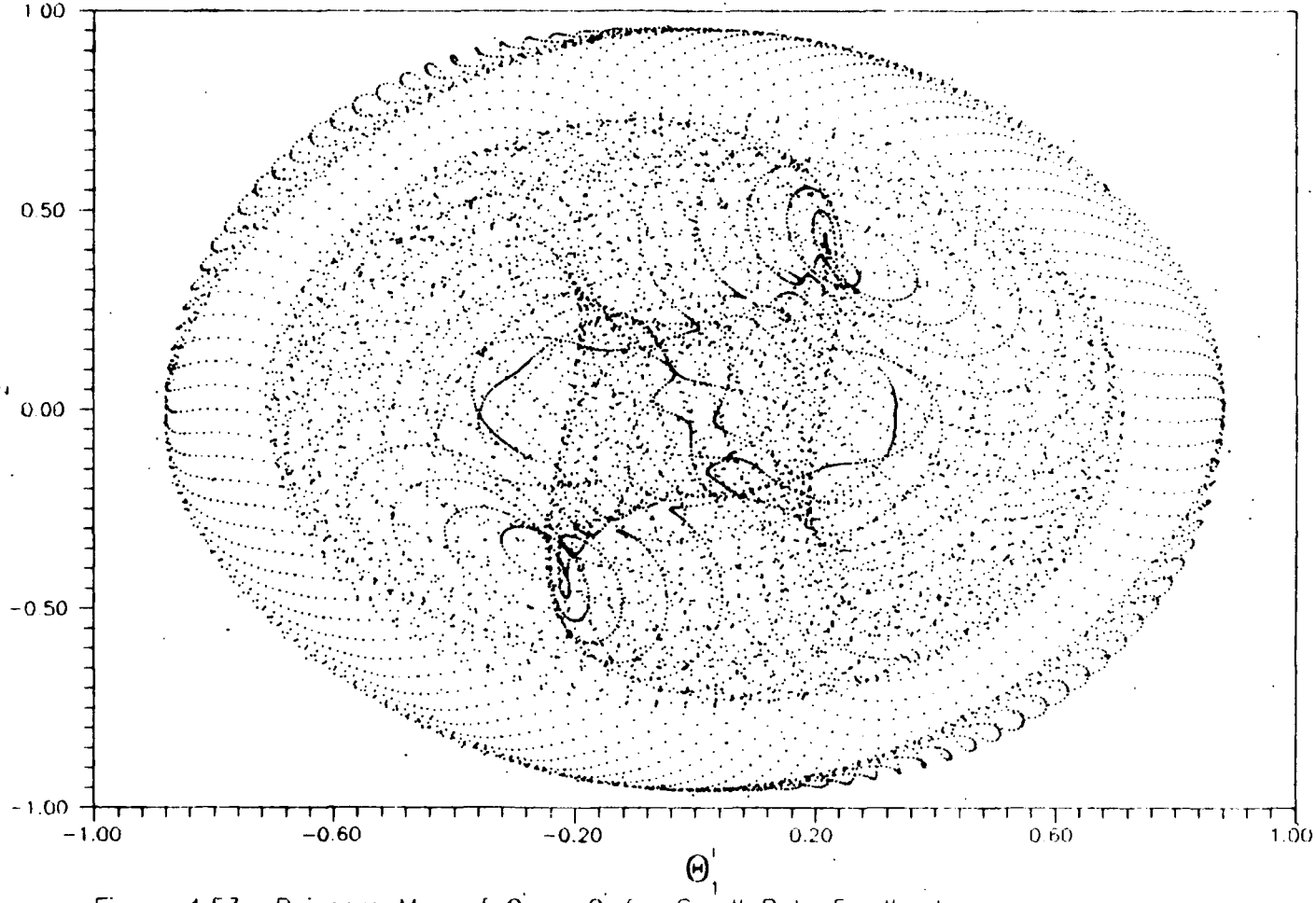

Figure 4.53 Poincare Map of θ_1 vs θ_2 for Small Rate Feedback Gain (10000 Orbits Sampled at 2π, e=0.5, s=1.0, K=0.7, G_3=0.01)

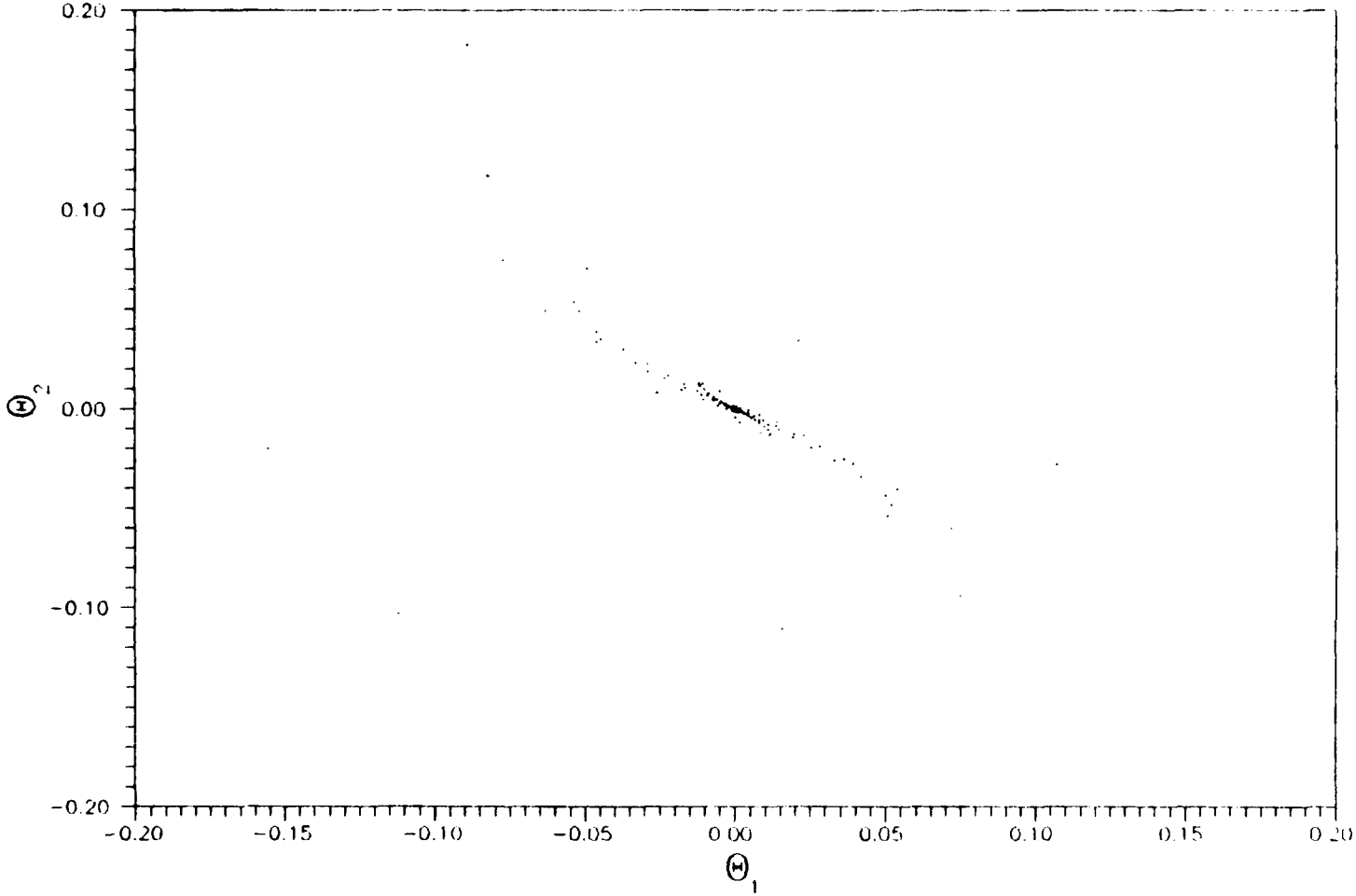

Figure 4.54 Poincare Map of Θ_1 vs Θ_2 for Small Rate Feedback Gain (500 Orbits Sampled at 2π, e=0.5, s=1.0, K=0.7, G_3=0.05)

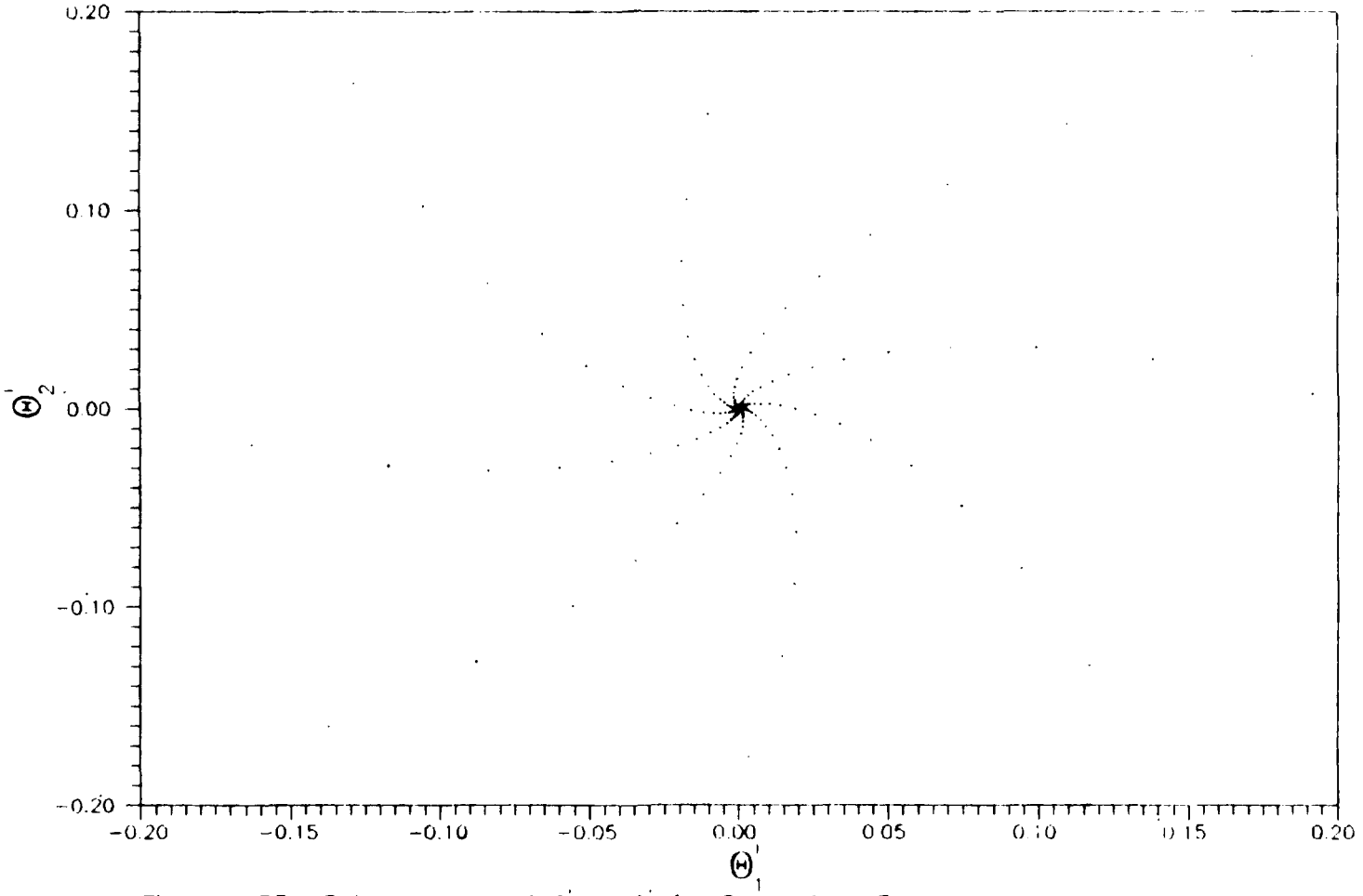

Figure 4.55 Poincare Map of $\dot{\Theta}_1$ vs $\dot{\Theta}_2$ for Small Rate Feedback Gain (500 Orbits Sampled at 2π, e=0.5, s=1.0, k=0.7, G_3=0.05)

tricked into working for the uncontrolled equations of motion by modifying the orbit equations of motion. The software never worked for the Floquét controlled equations of motion because of the abundance of multipliers at unity. However, the software did work for the rate and position feedback equations of motion. For these equations, more than one branch of solutions were calculated from an initial bifurcation point found during the Floquét analyses presented earlier.

4.3.1 Modified Orbit Equations of Motion for AUTO. The orbit equation given by equation (2.1) has an infinite family of closed-orbit solutions. This non-uniqueness was the crux of the problem for AUTO. Figure 4.56 shows a family of solutions for various initial conditions on a phase portrait for e=0.5. A program created by Dr. Wiesel was used to create this and other phase portraits presented here.

The problem (i.e. trick) here was to create a stable limit cycle at a desired orbit of interest. All other closed curves in the conservative phase portrait of (2.1) must be made to disappear to resolve the non-uniqueness problem. One of the desired orbits is shown in figure 4.57 for e=0.5. This orbit has a perigee of ζ=0.5 and an apogee of ζ=1.5. To achieve this desired orbit from any initial condition, a dissipation term must be added to the equation of motion for the orbit. This was described in chapter III, section 3.5. The dissipation term is shown in equation (3.8). Its main feature is that it is zero on the orbit of interest and not equal to zero elsewhere.

A phase portrait of the modified equation of motion for the orbit exhibited a limit cycle at the chosen orbit from the original conservative

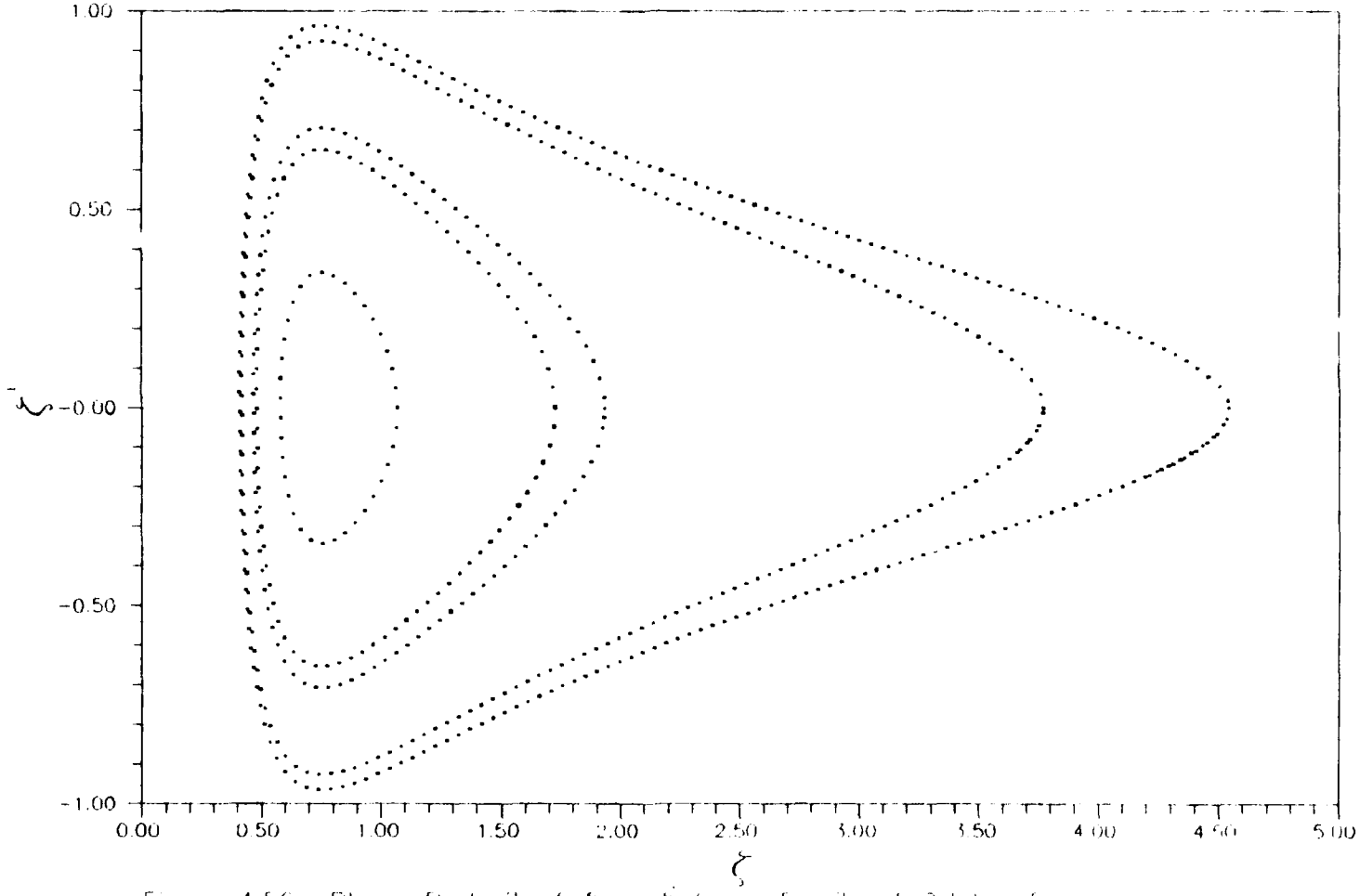

Figure 4.56 Phase Portrait of ζ vs ζ' for a Family of Orbits of Fixed Eccentricity (e=0.5)

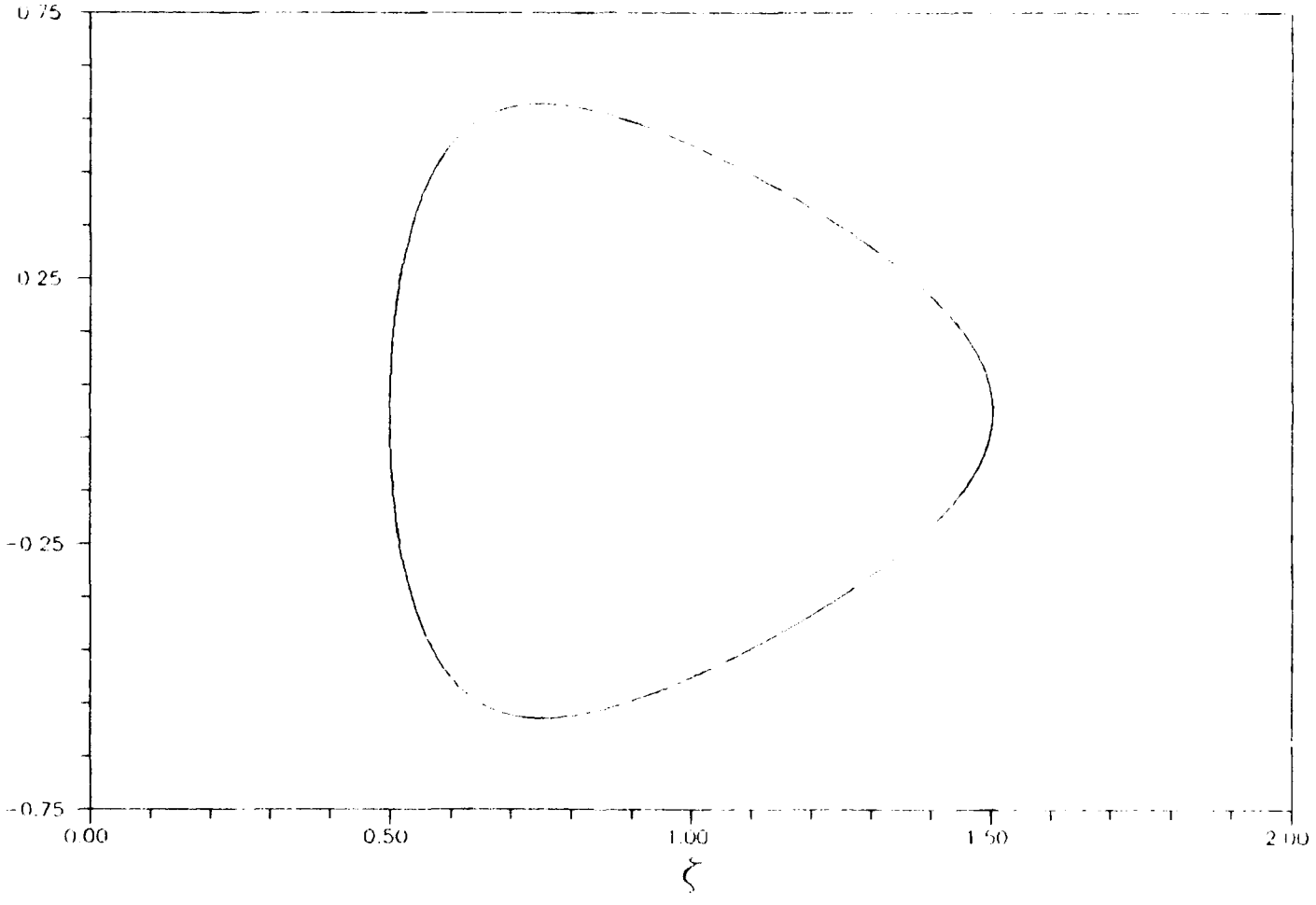

Figure 4.57 Desired Orbit Phase Portrait of ζ vs ζ' (μ=0.5)

system. Figure 4.58 shows how trajectories starting inside and outside the desired orbit converge on the created limit cycle. This addition of dissipation allowed AUTO to work for the uncontrolled and rate feedback equations.

4.3.2 Uncontrolled Equations of Motion. Using the modified dissipative orbit equations, the continuation software was run in an attempt to locate bifurcation points as parameters were varied. Yet, since the attitude equations were still conservative, no bifurcation points were detected because crossings occurred in multiple pairs while AUTO was looking for a single pair to cross. However, the software did compute the characteristic multipliers correctly. Figure 4.59 shows a plot of characteristic multipliers with the parameter values used to generate figure 4.1. Both plots contain the same information. Note that AUTO also included the orbit equation characteristic multipliers. One multiplier is a +1 while the other moves on the real axis inside the unit circle. This shows that the dissipation term has indeed created a limit cycle. This method of obtaining the characteristic multipliers was not efficient. So, few runs were made for this purpose.

4.3.3 Floquét Controlled Equations of Motion. Nonautonomous systems are not well suited for analysis using AUTO. Usually, auxiliary differential equations must be added to the original system of equations to make the total system autonomous. These auxiliary differential equations should have solutions that allow for the calculation of the nonautonomous variable. This method of tricking the software seemed attractive but was very difficult to implement without causing other

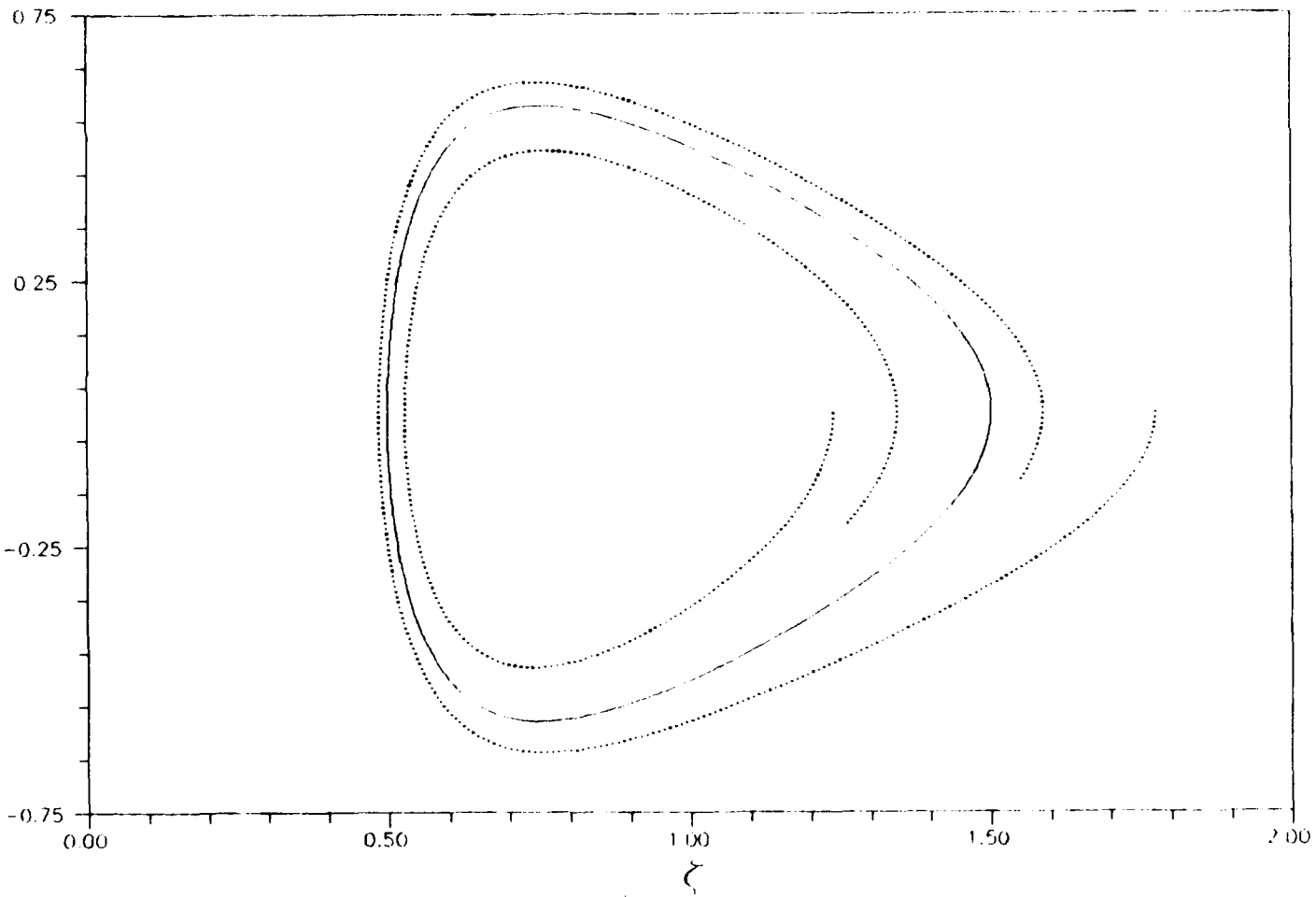

Figure 4.58 Phase Portrait of ζ vs ζ' for Orbit Equations with Dissipation Term ($\delta = 1.0$)

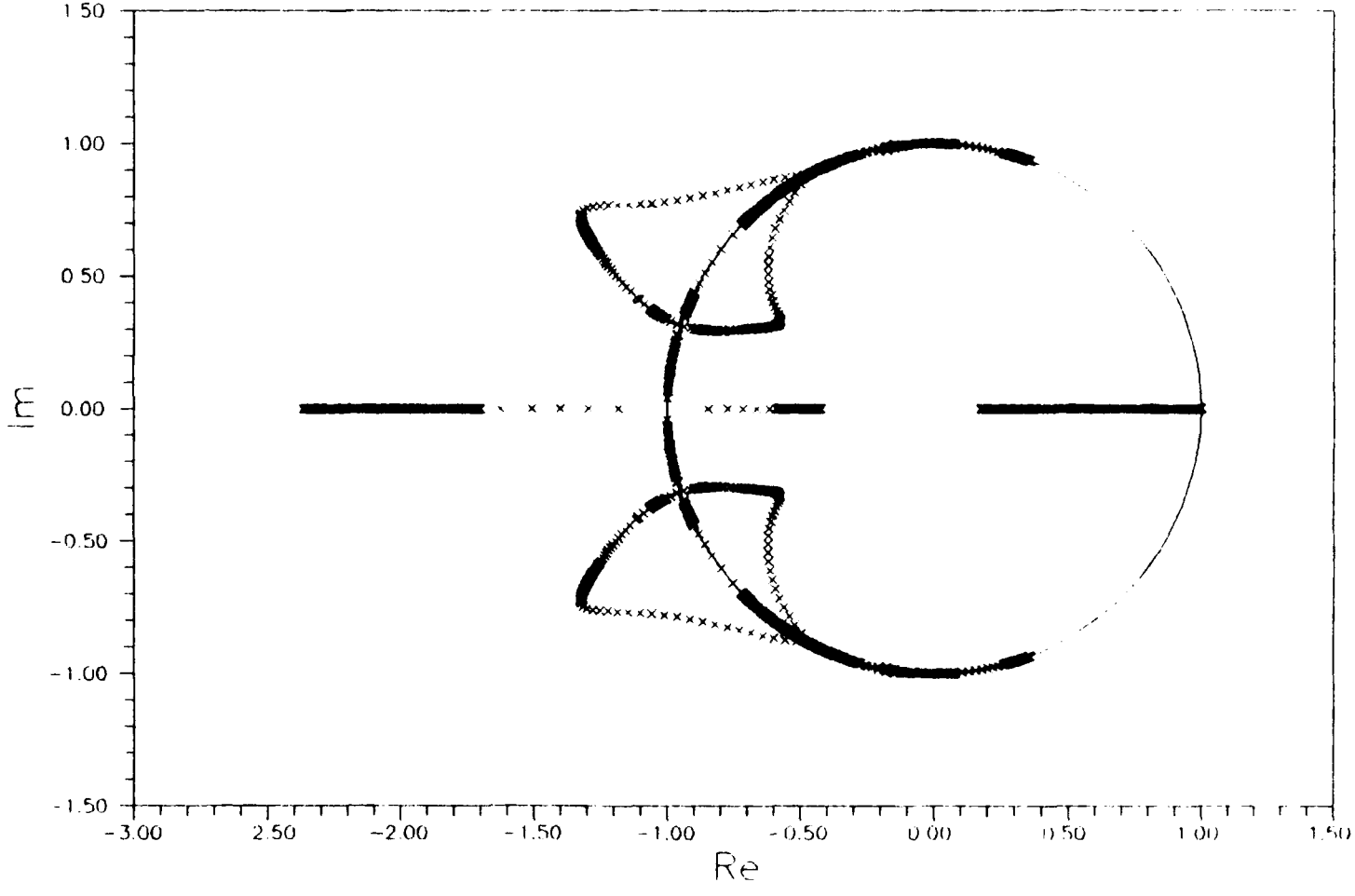

Figure 4.59 Uncontrolled System Multipliers from AUTO ($0.0 \le \epsilon \le 0.7, s = 1.0, k = 0.7$)

problems. The original Floquét controlled equations of motion fit into this category of problems since the approximation of the periodic feedback was given by a time dependent fourier series. No simple way was found to make the Floquét equations of motion autonomous.

First, the linear, time-periodic matrix set of differential equations defining the periodic control was appended to the system of equations to provide the controller feedback, thus eliminating the need for the fourier series. This matrix set of equations, given by equation (2.33), added sixteen auxiliary differential equations to the original set of six which described the Floquét controlled system. The continuation software never converged for this approach. This set of equations was then numerically integrated using Hamming to look for possible errors. It was found that the controller performed as expected over a short time scale. But, over the long time scale, the states of the auxiliary differential equations diverged. Since the controller equations were derived basically from the equations of variation, there was no guarantee that they would be stable. So, a Floquét analysis was performed on the controller differential equations. This generated a 16x16 monodromy matrix resulting in sixteen characteristic multipliers. Table 4.1 lists these characteristic multipliers and their moduli. There are four pairs on the unit circle, two pairs outside the unit circle, and two pairs inside the unit circle. This verifies that these equations are locally unstable. It can be concluded that the four pairs of multipliers at unity will lead to the non-uniqueness problem for AUTO discussed earlier. No other valid conclusions were reached on why AUTO did not converge.

Table 4.1 Characteristic Multipliers for Control Generation Equations

MULTIPLIER	|MULTIPLIER|
-0.129753±1.242112	1.248881
1.248881	1.248881
1.248881	1.248881
-0.103895±0.994588	1.000000
-0.103895±0.994588	1.000000
1.000000	1.000000
1.000000	1.000000
1.000000	1.000000
1.000000	1.000000
-0.008319±0.796383	0.800717
0.800717	0.800717
0.800717	0.800717

Finally, sixteen auxiliary differential equations were added to the original system of differential equations whose solutions provided the first eight trigonometric terms of the fourier series used to approximate the control. In other words, these auxiliary differential equations had solutions of sin(t), cos(t) and the higher order harmonics which made the system of equations autonomous. But, the convergence problem still existed. It was hypothesized that the harmonics of the auxiliary equations caused the problem for AUTO. So, in the end, the continuation

software could not be used to evaluate the Floquét controlled equations of motion.

4.3.4 Rate and Position Feedback Equations of Motion. There were two plots, figures 4.24 and 4.25, of characteristic multipliers for the rate feedback controller that exhibited bifurcation points that crossed the unit circle at +1. The bifurcation point found in figure 4.24 was analyzed using the continuation software. The results that generated figure 4.24 located a bifurcation point between $-0.29 \leq K \leq -0.28$. AUTO was initialized to compute branch 1 which is the parameter dependent branch of trivial solutions that contains this bifurcation point. AUTO located a pitchfork type bifurcation point at K=-0.2837217. The results from AUTO agreed with the Floquét analysis in that the solution became stable at this bifurcation point as the multiplier crossed into the unit circle.

AUTO was then used to continue from this bifurcation point to generate branch 2 of the solution. Since branch 2 was continued from a pitchfork bifurcation, two symmetric branches exist that are non-trivial. This branch exhibited a typical period doubling bifurcation. That is that the solution became unstable after the bifurcation at the critical parameter value with the birth of a stable orbit with twice the period. Successive branches up to branch 5 were computed with the continuation software to reveal a sequence of period doublings. Figures 4.60, 4.61, 4.62, and 4.63 plot the bifurcation diagrams using θ_1 and θ_2 maximum as measure of the solution response for these results. Table 4.2 then summarizes the bifurcation points found by AUTO.

A sequence of period doublings, if it continues ad infinitum,

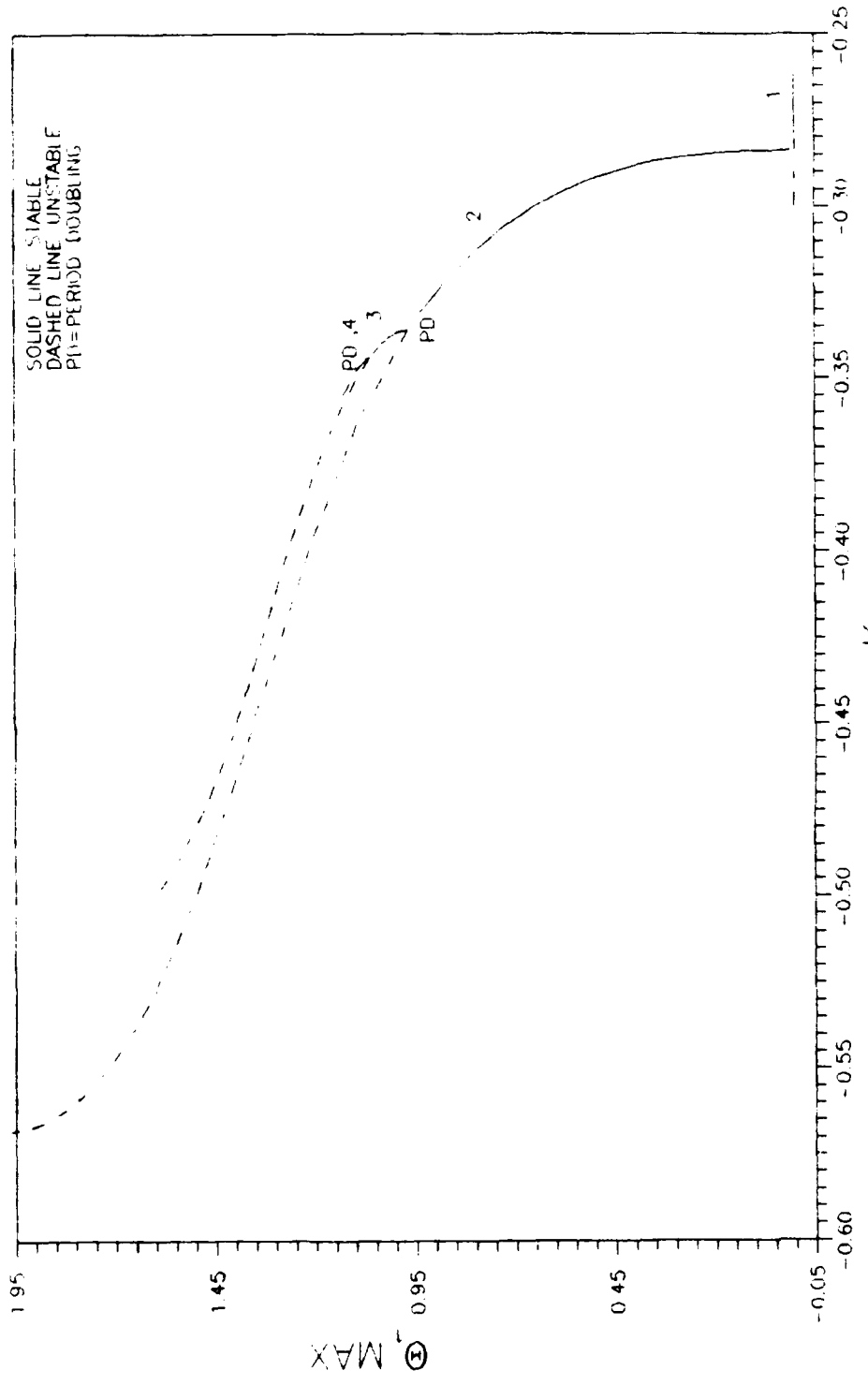

Figure 4.60 Bifurcation Diagram of K vs θ_1 MAX for Rate Feedback System ($e=0.5, s=1.0, G_3=0.85$)

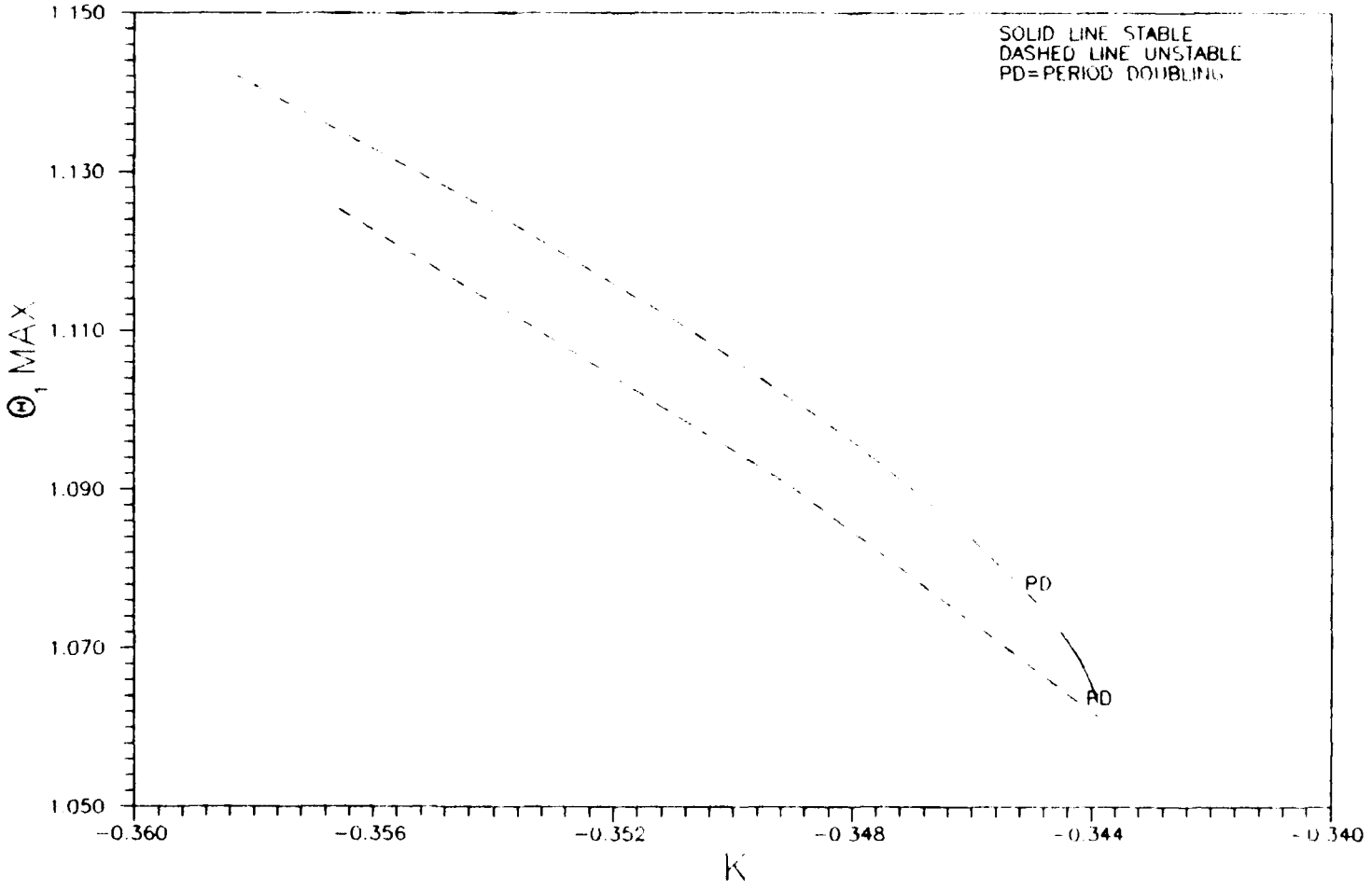

Figure 4.61 Branches 3 and 4 of Bifurcation Diagram of k vs Θ_1 MAX for Rate Feedback System ($e=0.5, s=1.0, G_1=0.85$)

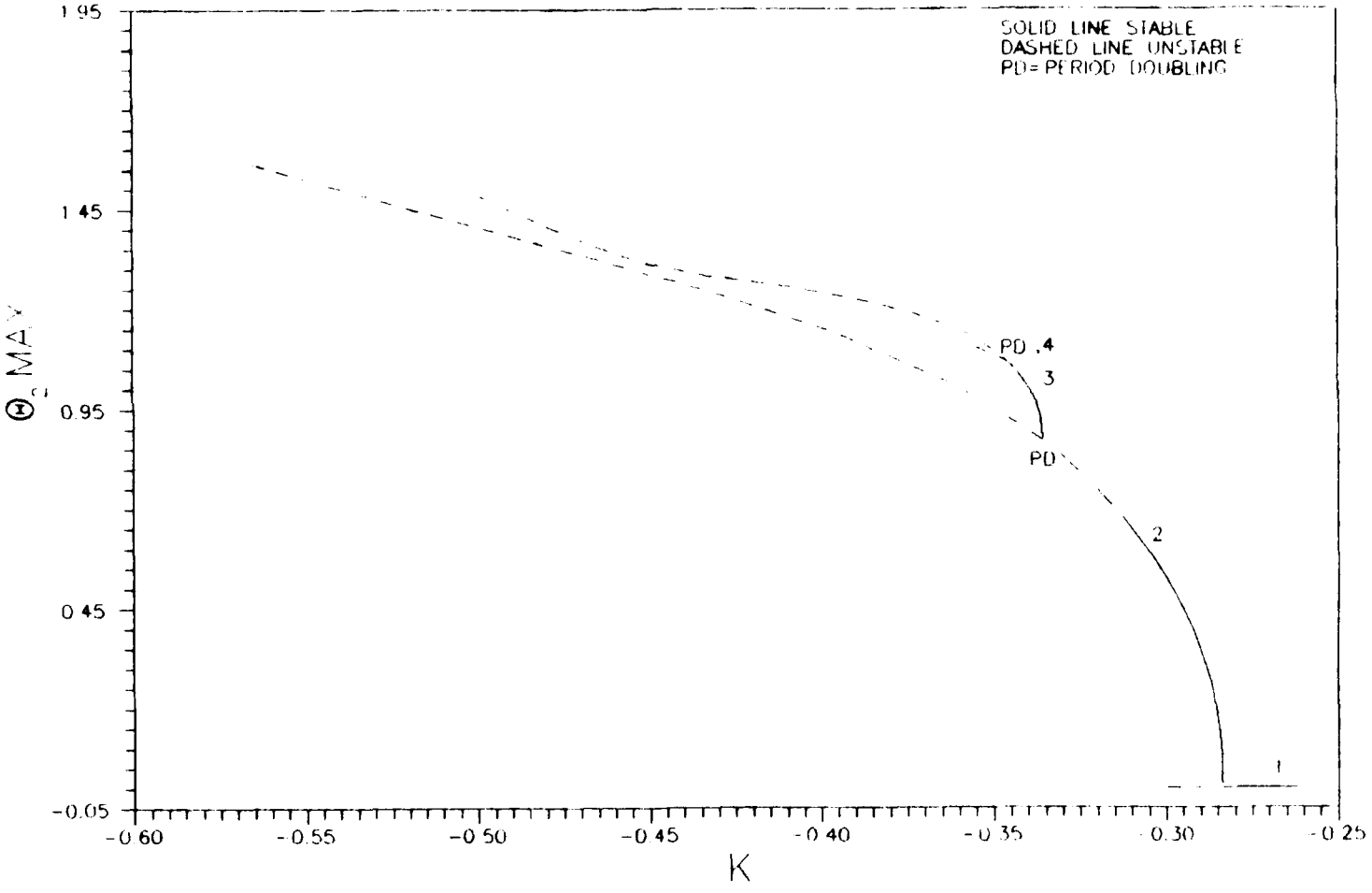

Figure 4.62 Bifurcation Diagram of K vs θ_2 MAX for Rate Feedback System ($e=0.5, s=1.0, G_3=0.85$)

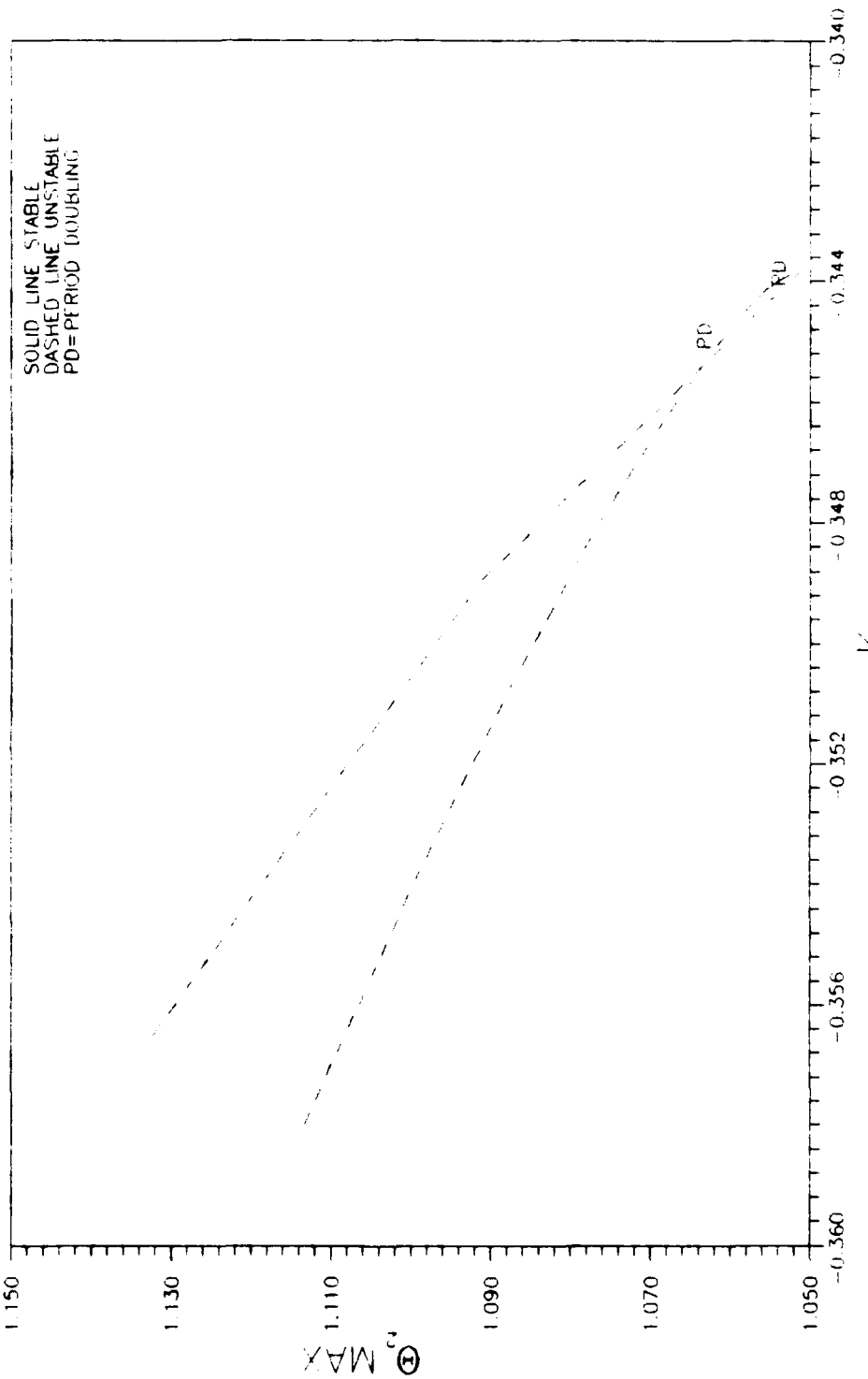

Figure 4.6.3 Branches 3 and 4 of Bifurcation Diagram of K vs Θ_2 MAX for Rate Feedback System ($e=0.5, s=1.0, G_3=0.85$)

Table 4.2 Summary of Bifurcation Points

BRANCH	TYPE	$K_{CRITICAL}$	MAXIMUM θ_1	MAXIMUM θ_2
1	Pitchfork	-0.2837217	0.000000	0.000000
2	Period Double	-0.3358687	0.967213	0.871232
3	Period Double	-0.3438680	1.061325	1.051574
4	Period Double	-0.3440923	1.075763	1.060851
5	Period Double	-0.3451118	1.077220	1.065944

satisfies the relationship discovered by Fiegenbaum which is

$$\delta_i=\lim_{i\to\infty}\frac{\lambda_i-\lambda_{i+1}}{\lambda_{i+1}-\lambda_{i+2}}=4.6692\cdots \qquad (4.1)$$

The λ's in this equation are the critical parameter values at which the bifurcation takes place. The Fiegenbaum sequence for the critical bifurcation parameters of this case is

$$\delta_i=7.734023,4.936993,\cdots \quad (i=1,\infty) \qquad (4.2)$$

It appears that this sequence of period doubling numbers is approaching the Fiegenbaum constant.

The time histories of θ_1 and θ_2 at different values of K depicted the effect of the period doubling on the attitude motion. Figures 4.64 and 4.65 are the time histories provided by AUTO for K=-0.339954. This point occurs on branch 3 of the solutions. Figures 4.66 and 4.67 are the time histories obtained by numerical integration between orbit 499 and

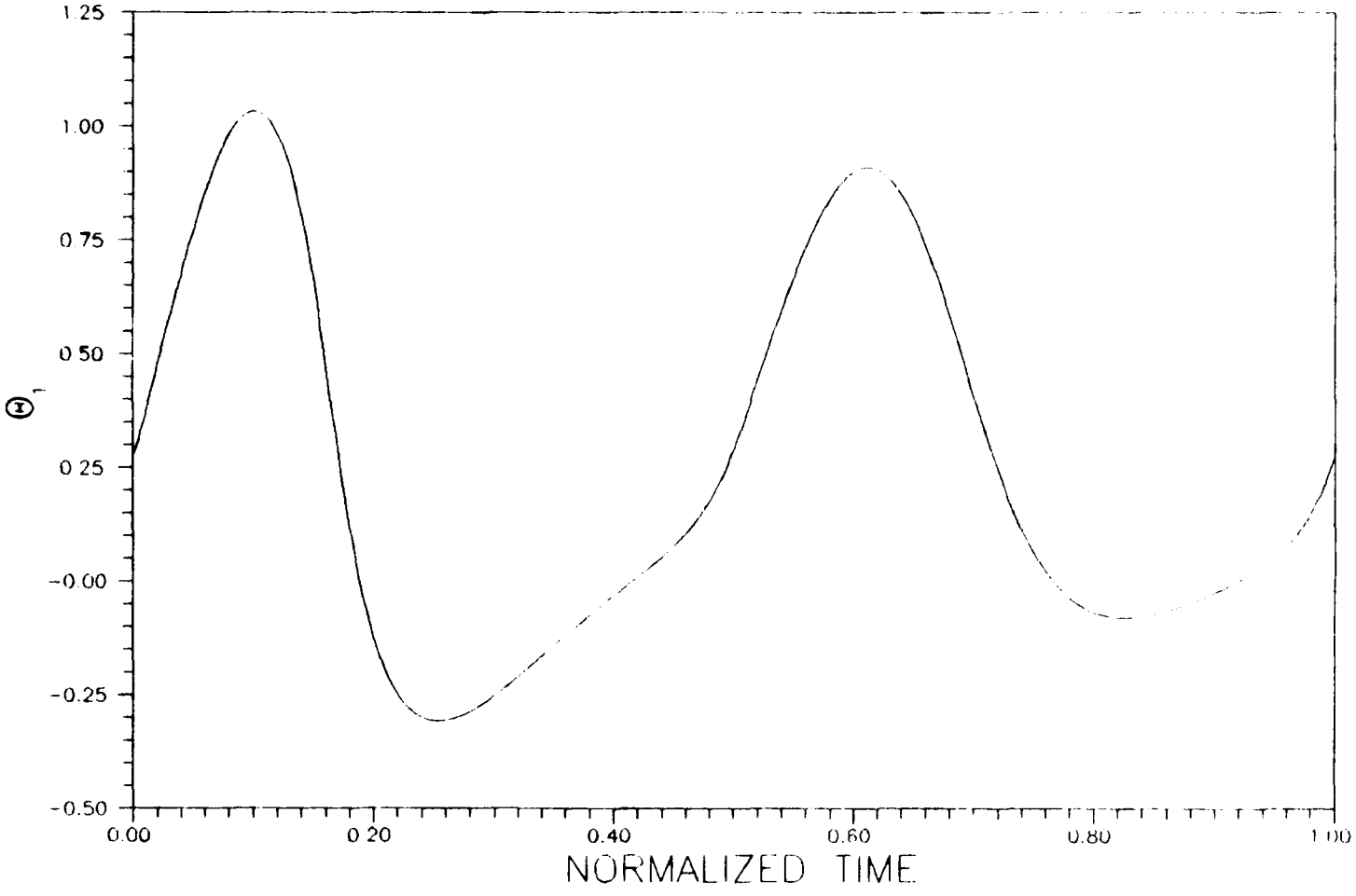

Figure 4.64 Period Doubled Orbit of θ_1 from Branch 3 of AUTO ($e=0.5, s=1.0, k=-0.339954, G_3=0.85$)

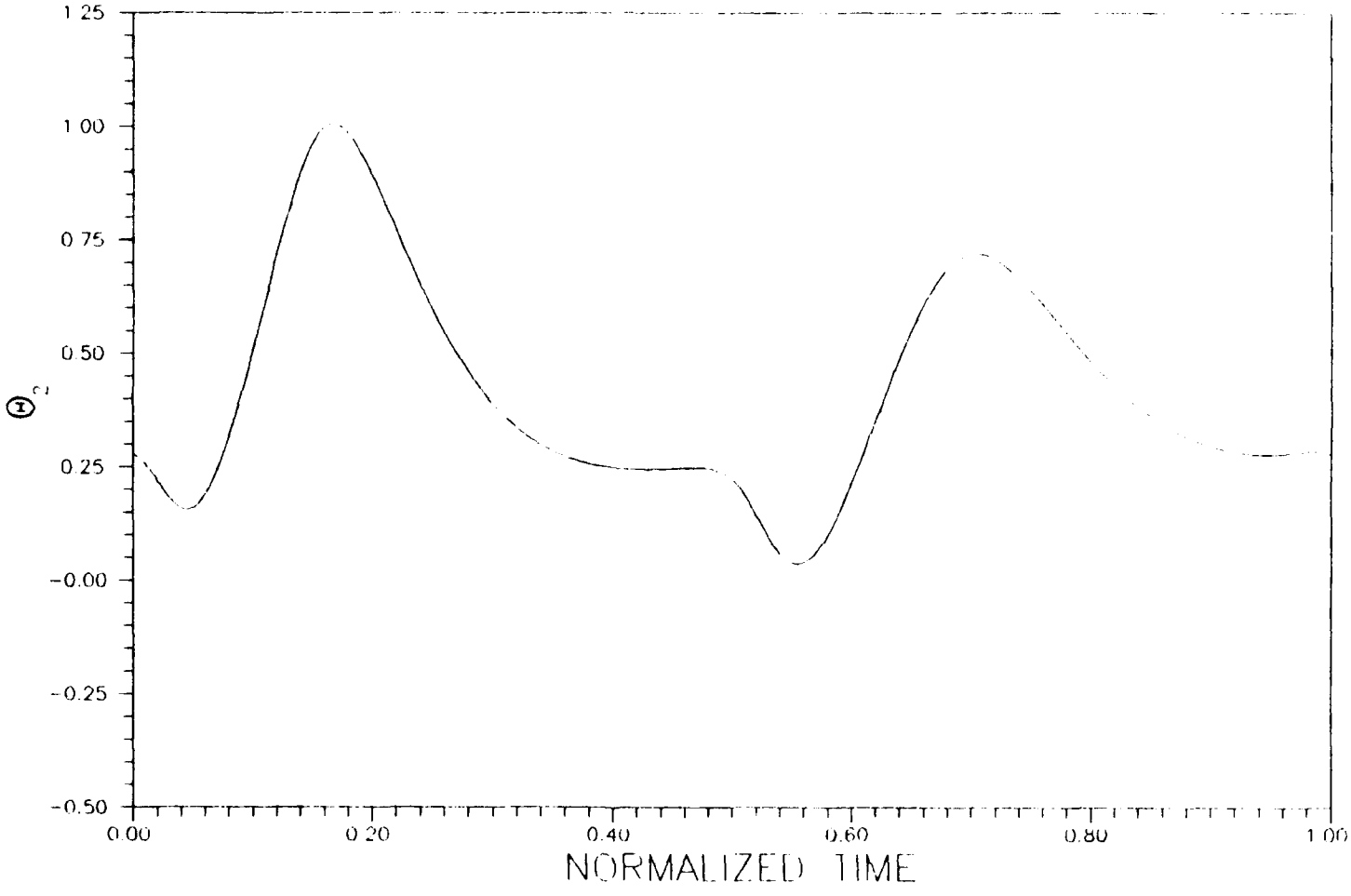

Figure 4.65 Period Doubled Orbit of Θ_2 from Branch 3 of AUTO
($e=0.5, s=1.0, k=-0.339954, G_3=0.85$)

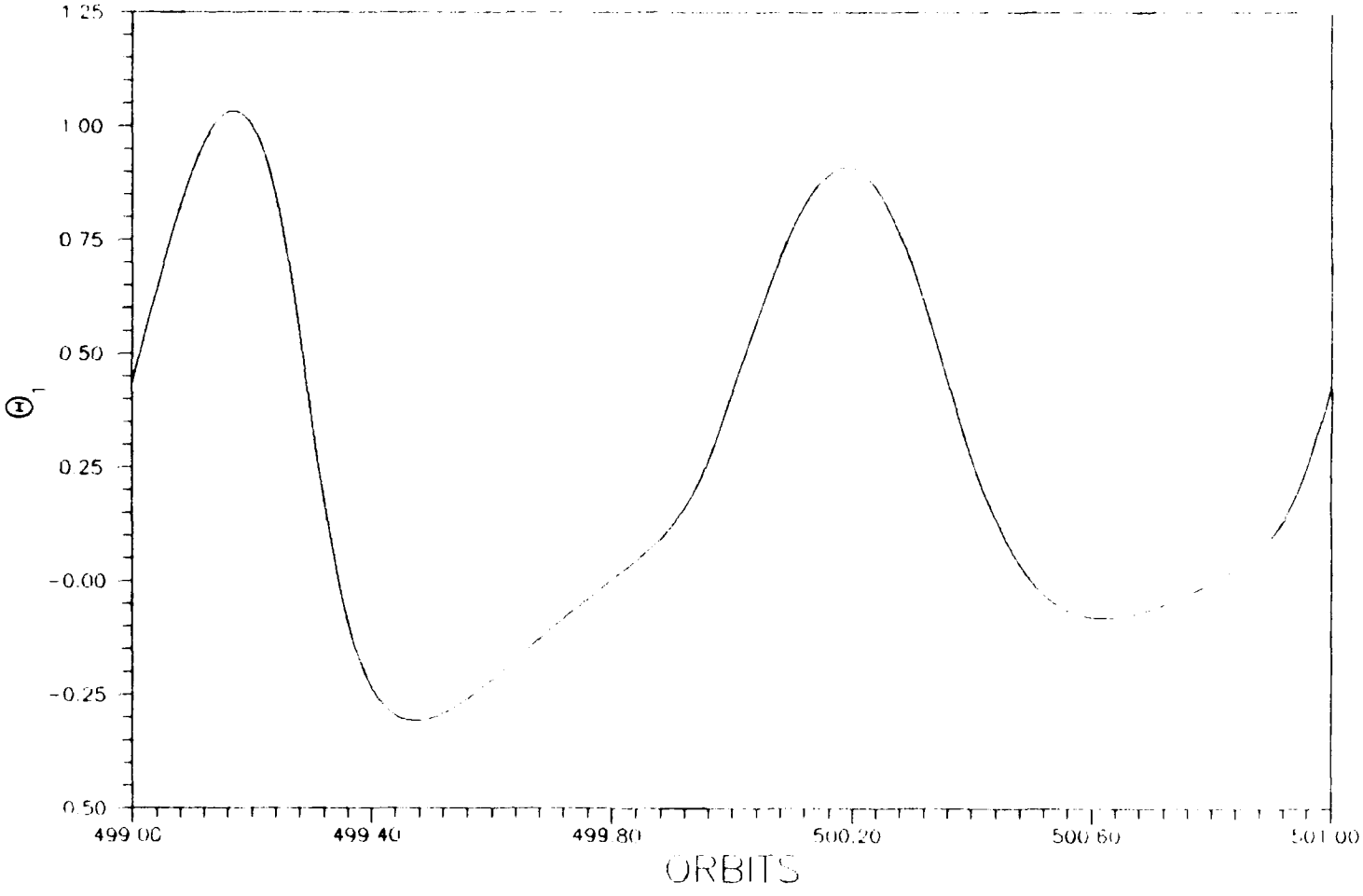

Figure 4.66 Numerically Integrated Period Doubled Orbit of Θ_1 ($e=0.5, s=1.0, K=-0.339954, G_3=0.85$)

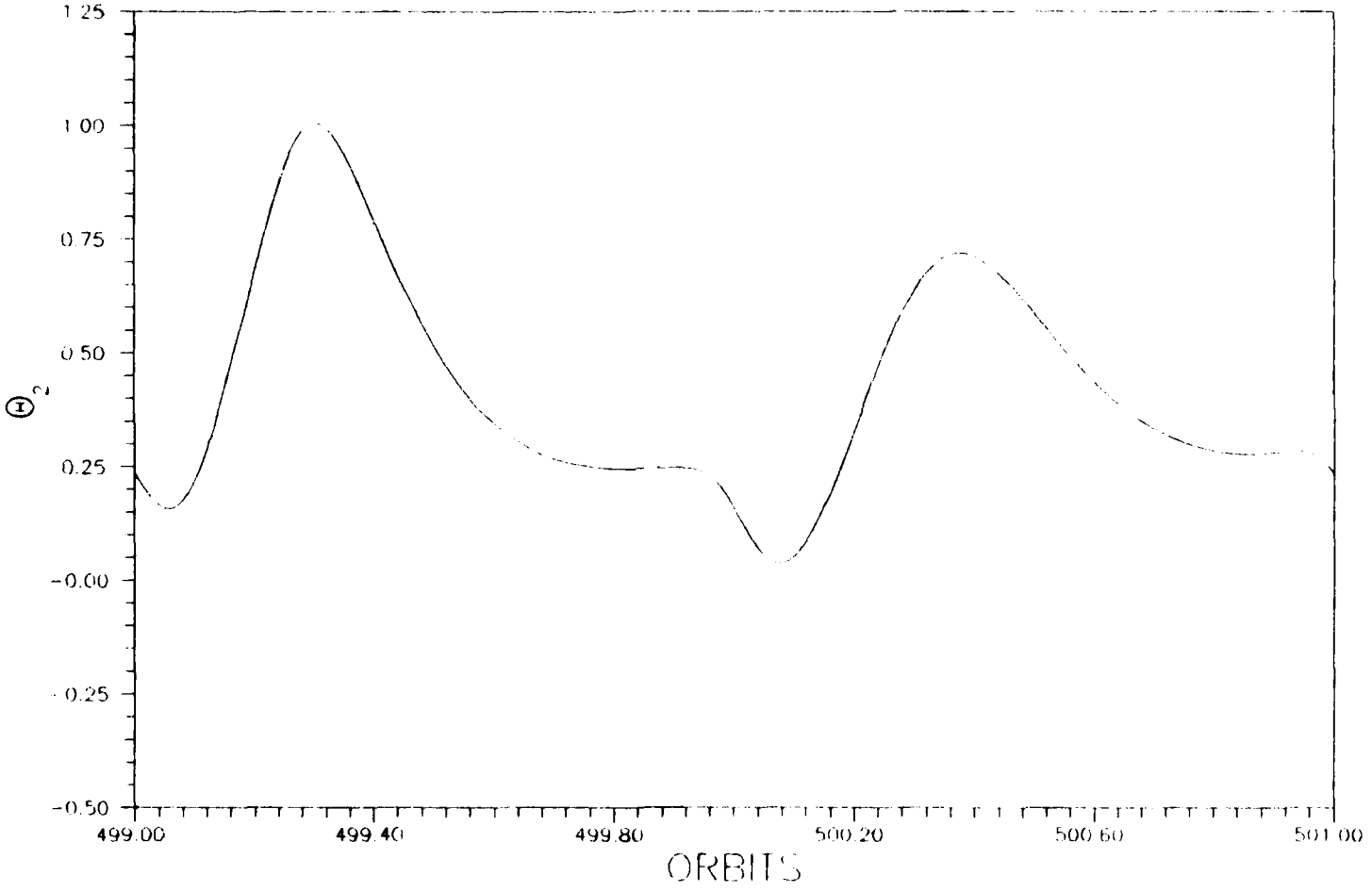

Figure 4.67 Numerically Integrated Period Doubled Orbit of Θ_2 ($e=0.5, s=1.0, K=-0.339954, G_3=0.85$)

501. The time histories for both AUTO and numerical integration are identical except for a small phase shift. The time histories show smooth, continuous motion with a 4π period. A Poincaré map was also plotted for this case. The map, shown in figure 4.68, contains two fixed points which is expected for a period doubled orbit. So, the three nonlinear analysis tools used in this thesis all reached the same conclusion here.

As an aside, the phase shift difference between the data from AUTO and numerical integration was looked into. A Poincaré map for 2500 orbits was generated with points being plotted at 4π intervals. One would expect a single point on the map. However, figure 4.69 shows a line instead. So, a time history was plotted for data between orbits 2001 and 2003 in an attempted to find the problem. This plot is shown in figure 4.70. When compared to figure 4.66, we see a very small phase shift between the two. Evidently, there must be some error in the numerical integration that slowly causes the two Poincaré map fixed points to shift over the long time scale. This explains the line on the Poincaré map.

In theory, a sequence of period doublings usually results in onset of chaotic motion. So, the parameter value was set to K=-0.3485 (well beyond the last doubling in the sequence) to see if this was the case here. The time histories between orbit 200 and 300 are shown in figures 4.71 and 4.72. The motion now looks less regular with no periodicity detectable. A Poincaré map was plotted for this case also to see if any identifiable structure appears in the phase space. Figure 4.73 shows the map for 1000 orbits sampled at a 2π interval. It does not show any well defined structure. So, it appears that this sequence of period doublings

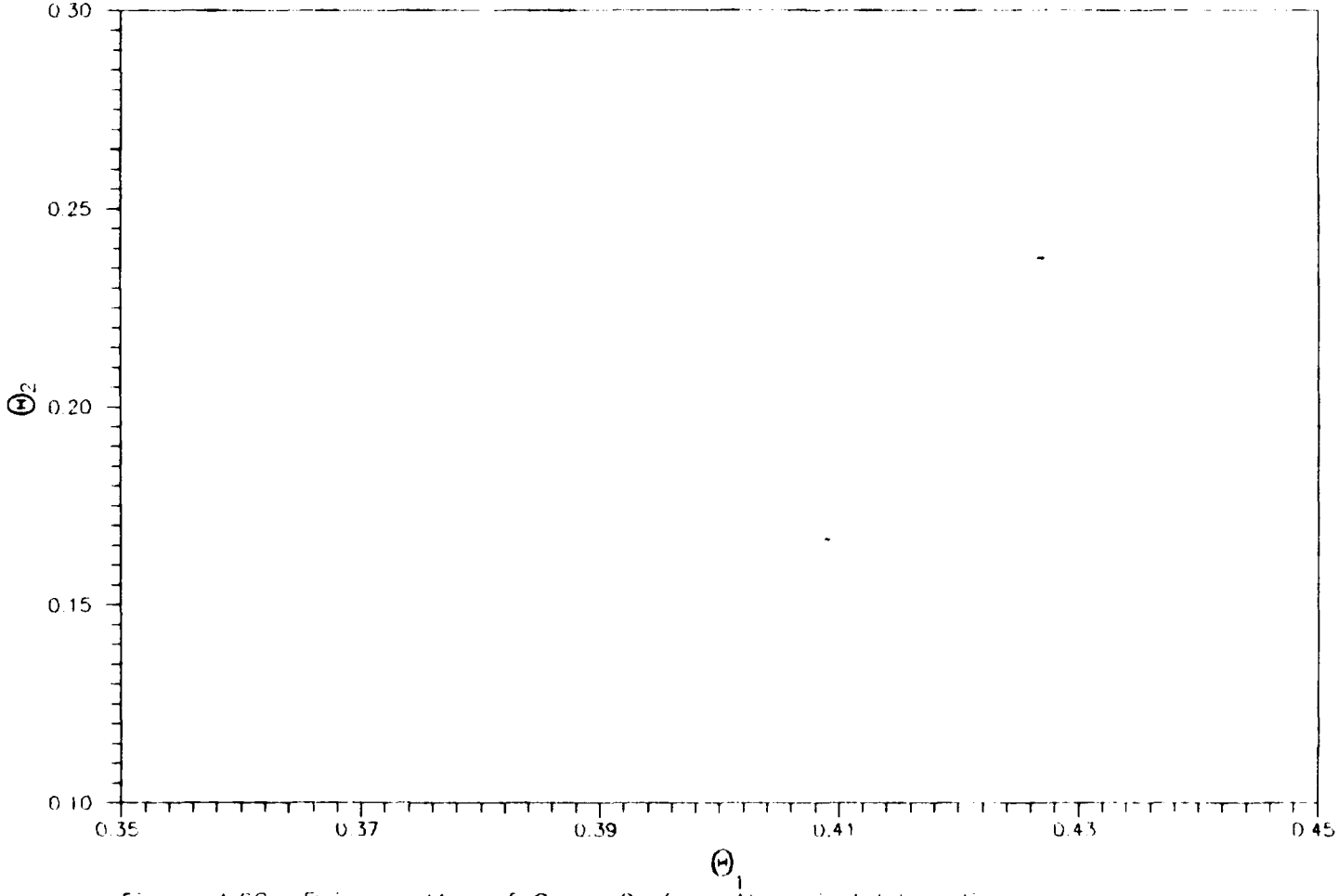

Figure 4.68 Poincare Map of Θ_1 vs Θ_2 from Numerical Integration
(50 Orbits Sampled at 2π,e=0.5,s=1.0,K=-0.339954,G_1=0.85)

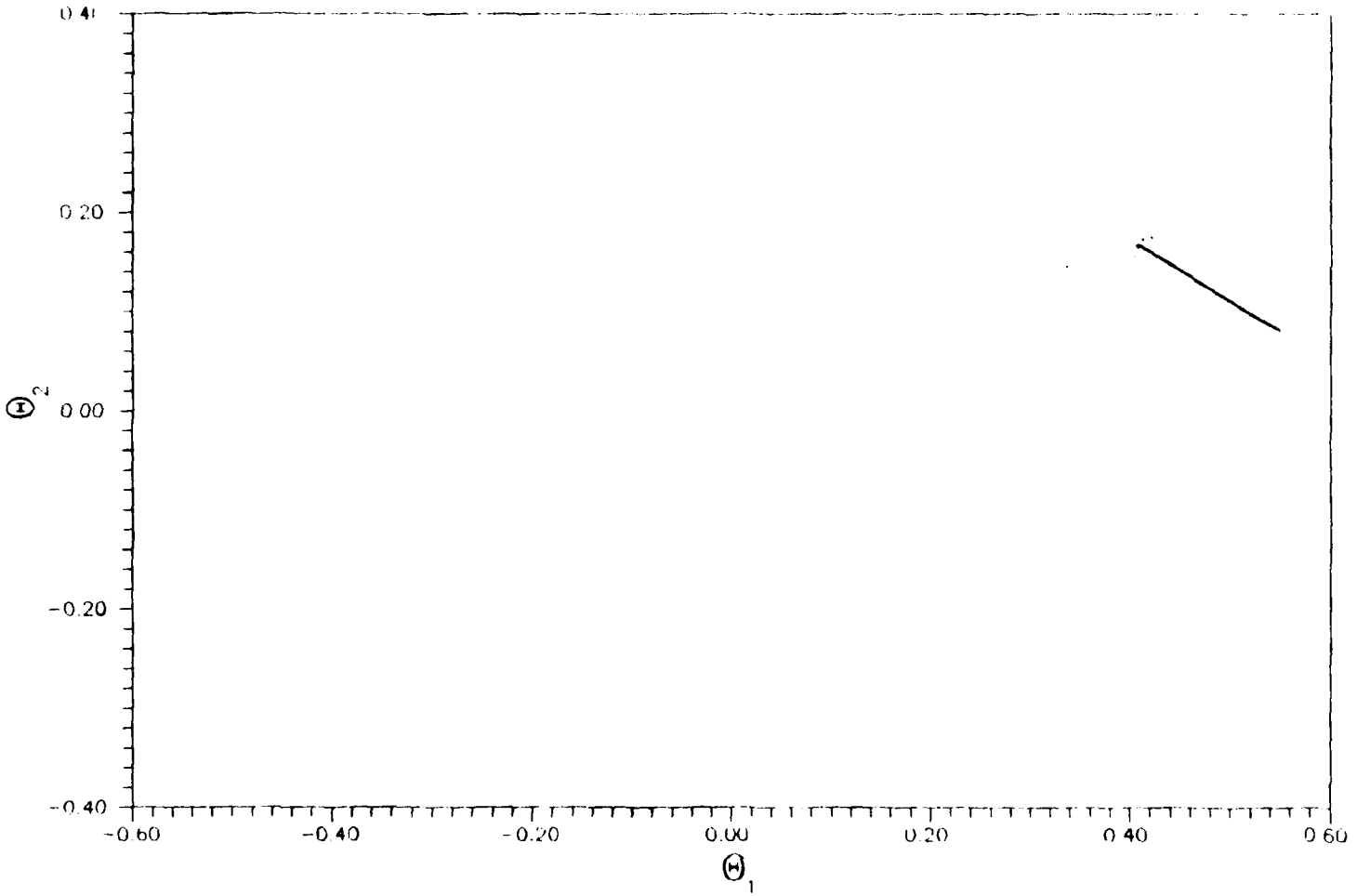

Figure 4.69 Poincare Map of Θ_1 vs Θ_2 from Numerical Integration
(2500 Orbits Sampled at 4π, e=0.5, s=1.0, k=-0.339954, C_3=0.85)

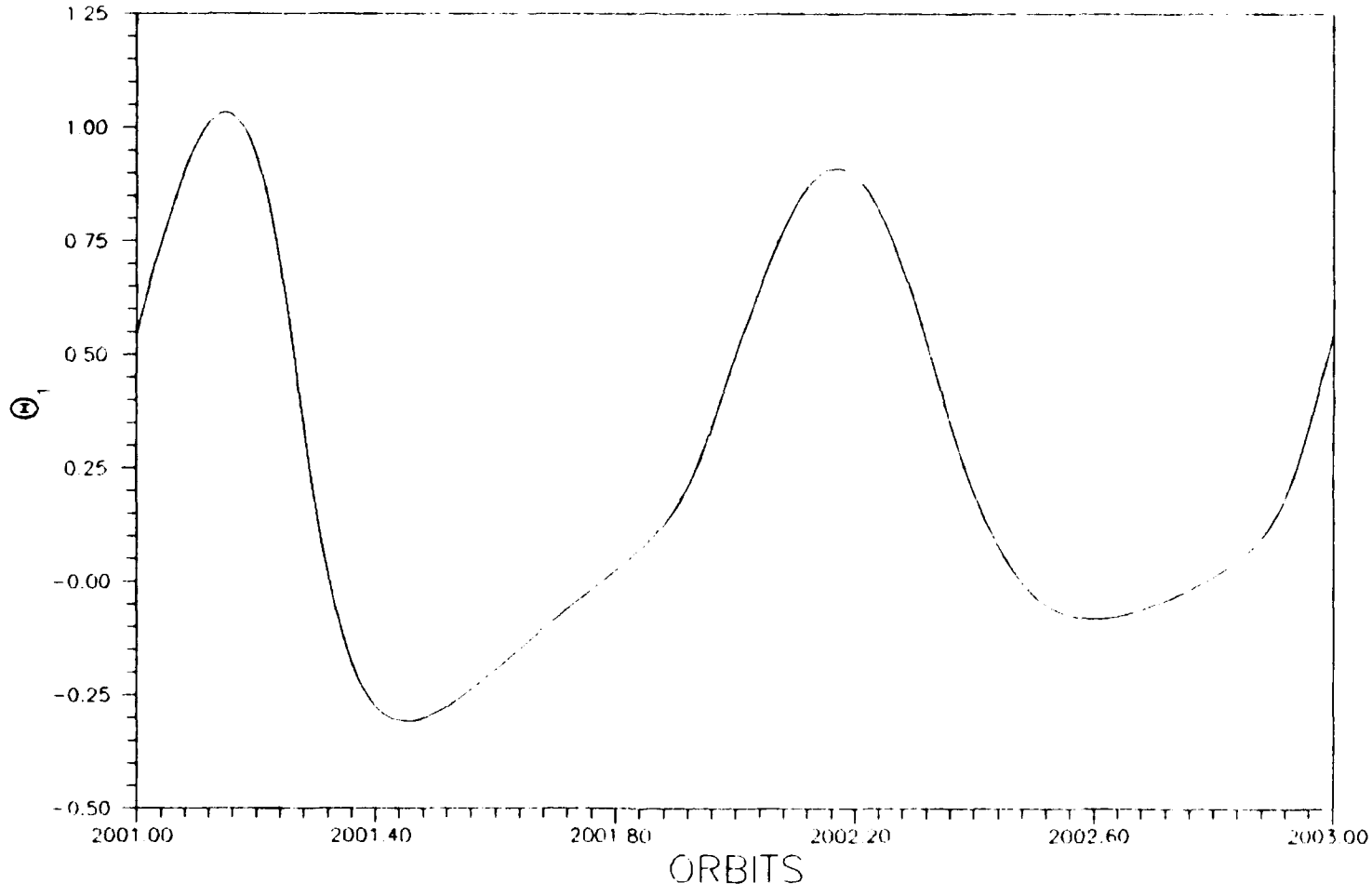

Figure 4.70 Numerically Integrated Period Doubled Orbit of θ_1 with Phase Shift ($e=0.5, s=1.0, k=-0.339954, G_3=0.85$)

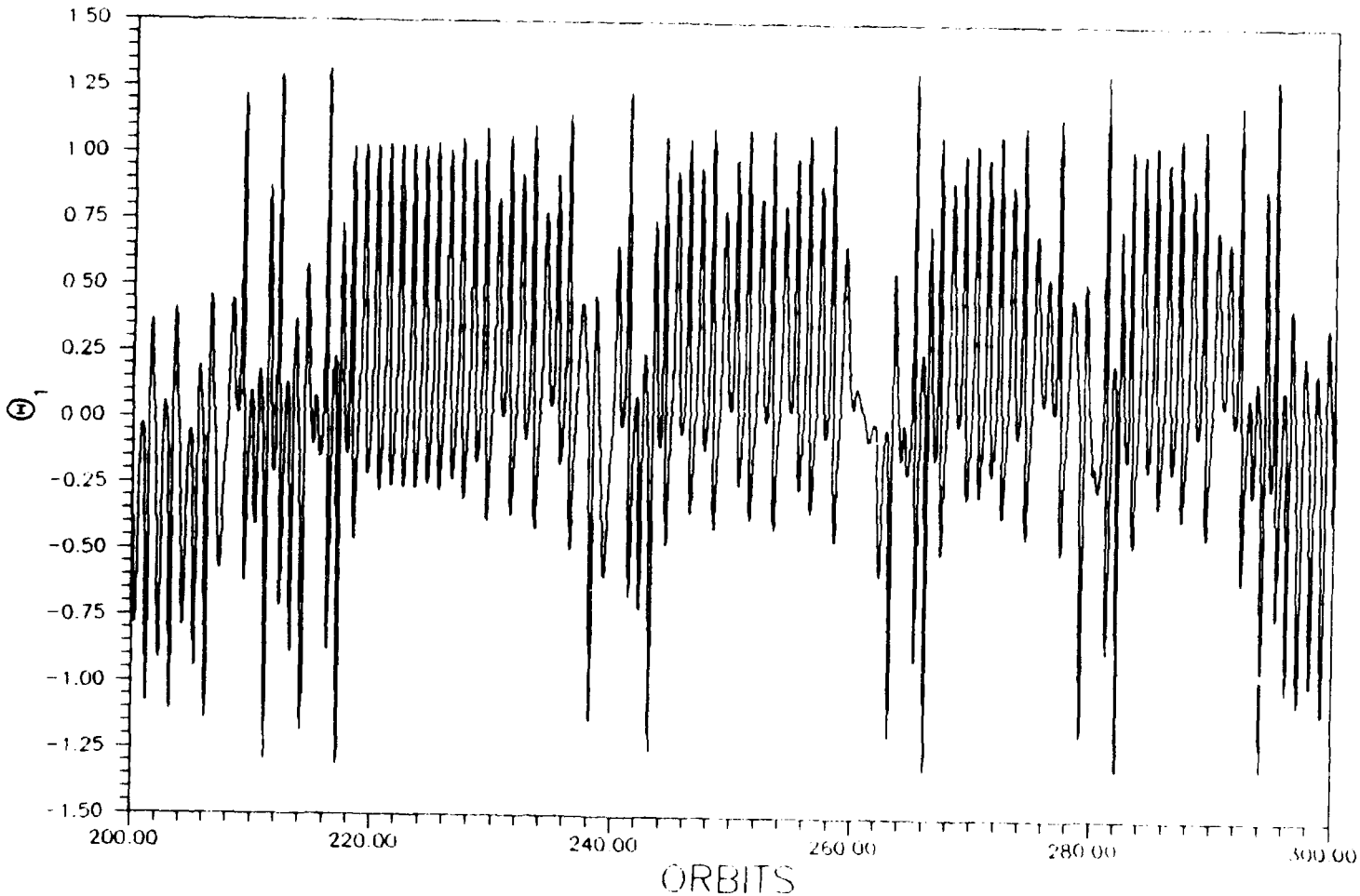

Figure 4.71 Numerically Integrated Orbits of θ_1 at Onset of Chaotic Motion ($e=0.5, s=1.0, k=-0.3485, G_3=0.85$)

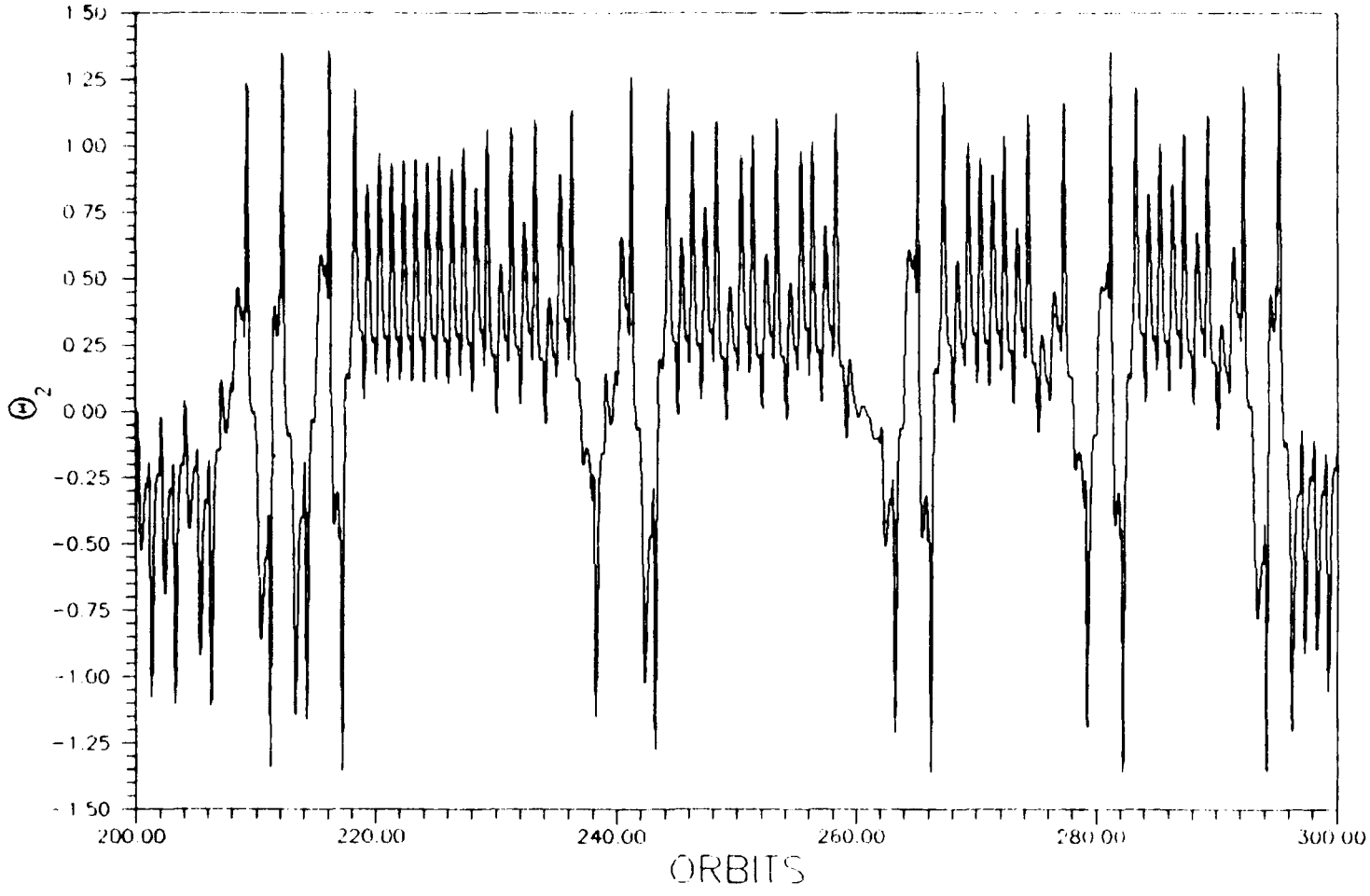

Figure 4.72 Numerically Integrated Orbits of Θ_2 at Onset of Chaotic Motion ($e=0.5, s=1.0, K=-0.3485, G_3=0.85$)

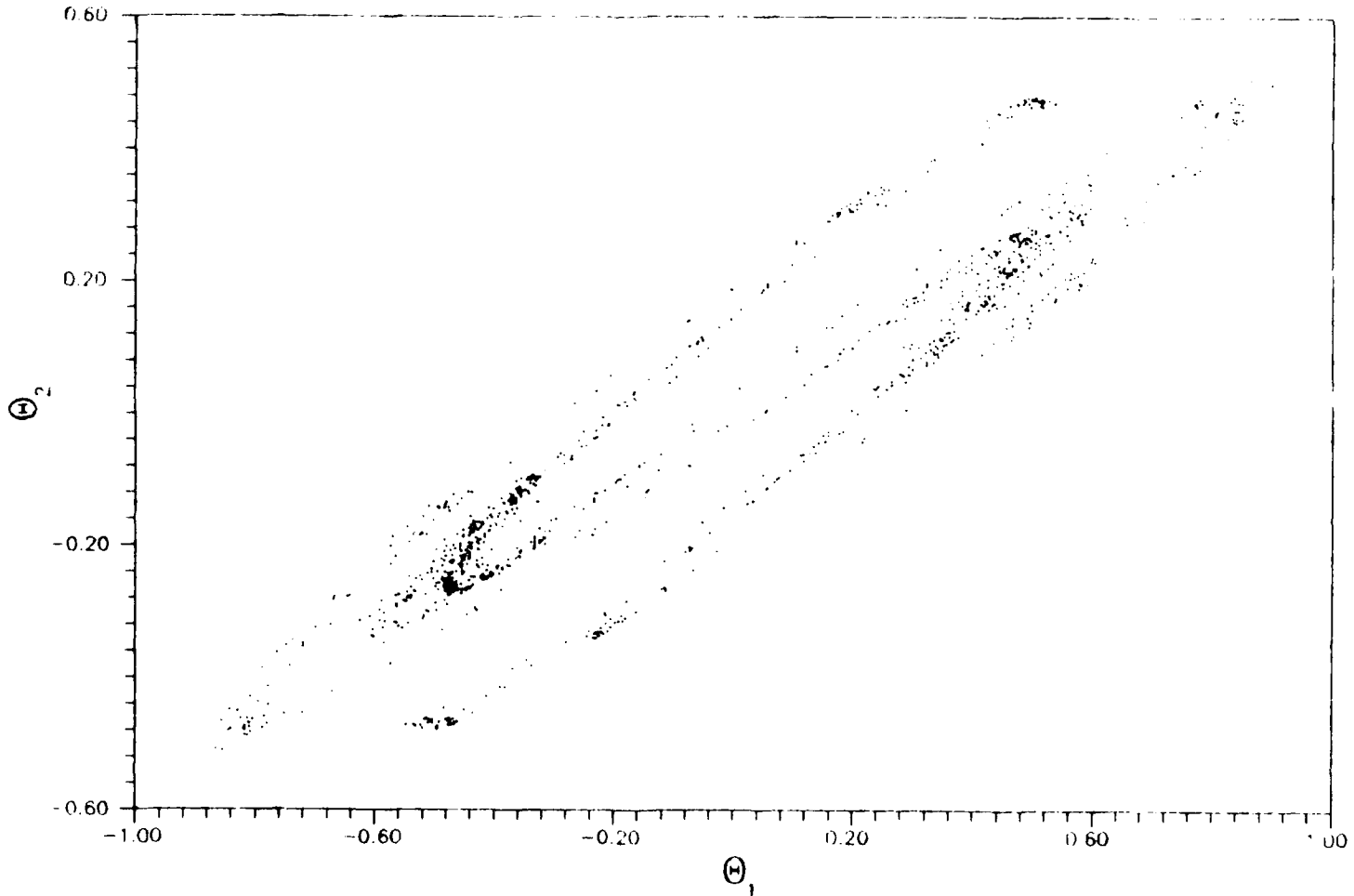

Figure 4.73 Poincare Map of θ_1 vs θ_2 from Numerical Integration (1000 Orbits Sampled at 2π,e=0.5,s=1.0,k=-0.3485,G_3=0.85)

leads to chaotic motion.

In summary, the uncoupled rate feedback control with a gain of G_j=0.85 was relatively robust in that it did not exhibit a global attractor for larger disturbances. This simple approach seemed to work well for a variety of conditions. However, extreme cases led to a sequence of period doublings.

V. Conclusions and Recommendations

The local stability analysis provides a finer detailed picture of the linear stability characteristics for the uncontrolled and controlled equations of motion than was known previously. The effect of the parameters varied show the many possible solutions for the attitude motion of the systems considered here. The existence of conservative period doubling, pitchfork or limit point, and torus bifurcations show the importance of analyzing the uncontrolled system in detail first. The same type of analyses for the controlled equations yields the same type of critical control design information. Basically, local stability is characterized for nominal and less than nominal conditions. These results establish a range of operating conditions near the equilibrium solution. A rate feedback gain of 0.85 is recommended over a wide range of conditions.

The global stability analysis indicates both expected and unexpected structure in the phase space. For example, the collapse of a region of phase space into an attractor with addition of damping through a range of feedback gain is expected. But, a torus-like attractor for the Floquét controller is not easy to explain. The nonlinear analyses do bound the limits of operation for the systems studied. However, each case studied is particular to the parameters and the initial conditions selected. Broad statements of global stability characteristics should be made with extreme caution. The characterization of nonlinear effects is indeed a difficult task to accomplish. Evidently though, simple rate feedback

might introduce less global behavior than Floquét control.

The continuation analysis shows some of the hidden phenomena of this system. The presence of a period doubling may be of interest if such motion is detected in an operational design. This type of analyses gives the control designer a valuable tool to characterize stability. However, the continuation software used here does not work well for conservative systems such as the one studied here without some careful modification.

The global stability analysis for this problem was too time consuming and computer intensive. Thus, further analyses in this area of study are not recommended unless a very specific set of parameter conditions needs to be investigated. However, efforts to adapt continuation software to study the uncontrolled equations of motion would be beneficial to the exploration of the many conservative bifurcation points found as parameters were varied.

Appendix A. Equations of Motion

In this appendix, the equations of motion of a spinning symmetric satellite in an elliptical orbit about a spherical attracting body are developed via Lagrange's method. The spin axis of the satellite is chosen to be in the plane of symmetry of the satellite and perpendicular to the orbital plane. The full nonlinear equations of motion are presented along with the development of the Lagrangian and the body angular velocities.

Kane and Barba studied the stability of the linearizred equations of motion developed herein [8:402-405]. An alternative development for the linearized equations of motion using Euler's moment equations is presented in their paper. Captain Dale Shell [13:2.23-2.25] and Captain Jim Cole [5:A-1-A-16] presented the same Newtonian development in their theses also.

A.1 Attitude Angular Velocities

The following develpoment for the angular velocites parallels that presented by Captain Jim Cole [5:A-4-A-9]. However, the resulting angular velocites here are used to form the kinetic energy of the satellite which I will call T. A 1-2-3 rotation through the angles θ_1, θ_2, and θ_3 measures the orientation of the satellite with respect to the orbital reference frame A. The resulting coordinate frame at the end of the three consecutive rotations is the body axis frame D. Figure A-1 shows this graphically.

Figure A-2 shows the orientation of the orbital reference frame A with repsect to an inertial reference frame I which has its origin at the

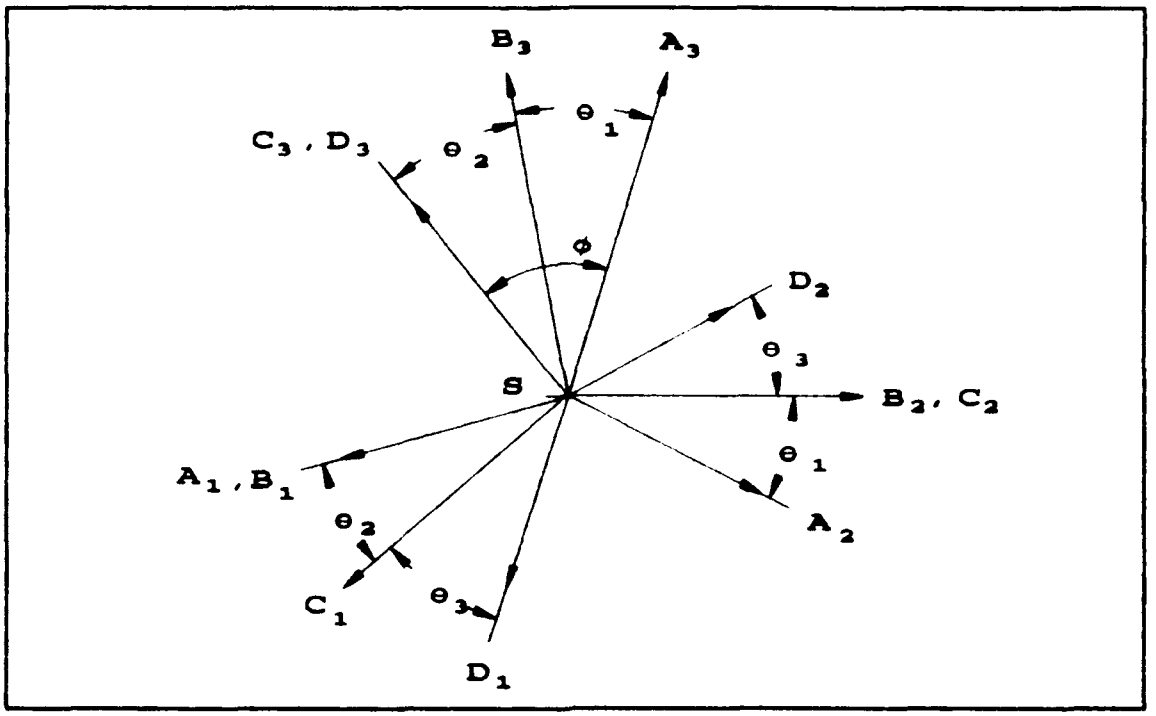

Figure A.1 Coordinate Reference Frames

center of the attracting body. Axis A_1 is in plane of the orbit and points along the radius vector to the satellite center of mass. Axis A_2 lies in the orbital plane in the direction of the motion of the satellite. And finally, A_3, which is perpendicular to the orbit plane, is simply $A_1 x A_2$ to form a dextral, orthogonal coordinate system.

Since the satellite is a symmetric body, we can simplify the development of the expressions for the angular velocities by using the nodal coordinate frame C. The nodal frame is achieved after the second rotation. Note that the final rotation is about an axis of symmetry. Thus, we need to express the angular velocity of the body frame D attached to the satellite with respect to the inertial coordinate frame I written

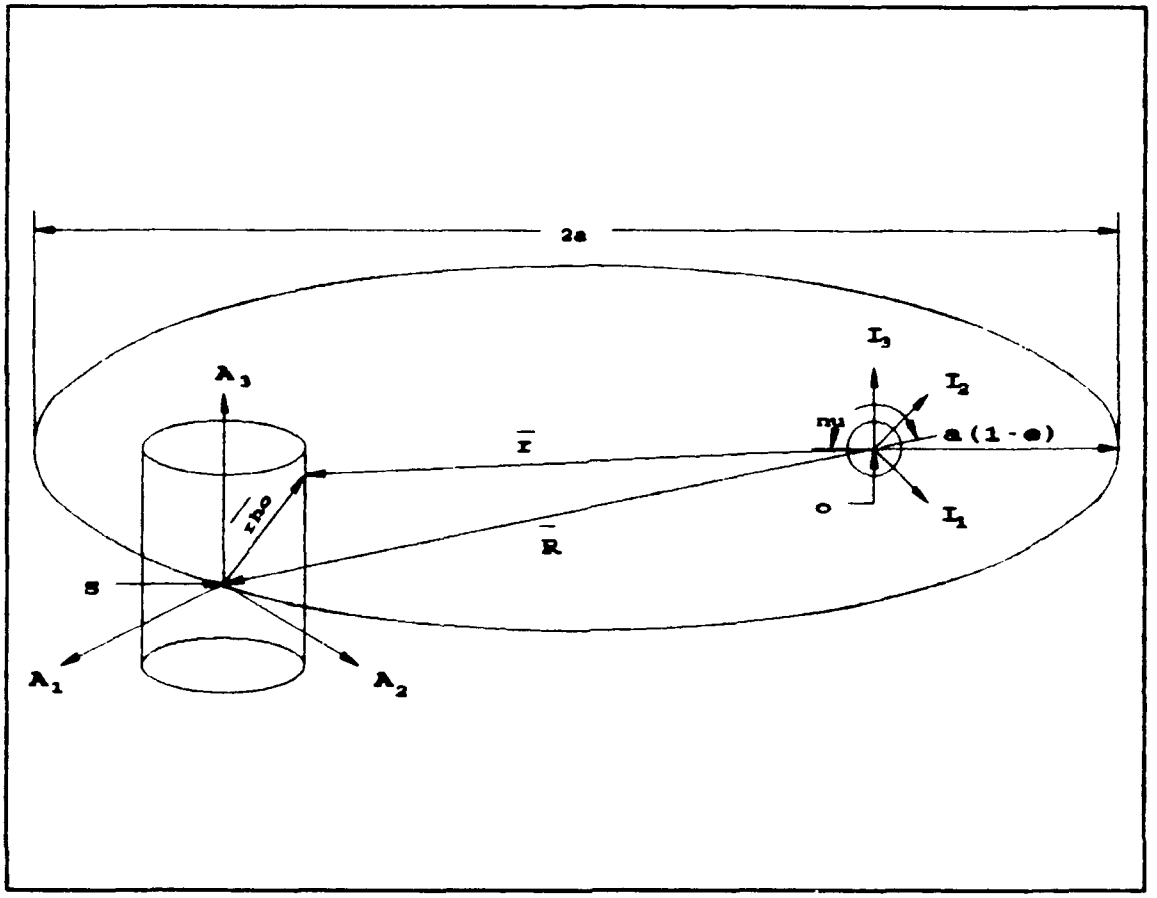

Figure A.2 Satellite Reference Frame and Orbit Description

in nodal coordinates C. This is simply the sum of the indivdual rotation rates to go from the A frame to the D frame.

$$\bar{\omega}^{D/I}\big|_C = \bar{\omega}^{A/I}\big|_C + \bar{\omega}^{B/A}\big|_C + \bar{\omega}^{C/B}\big|_C + \bar{\omega}^{D/C}\big|_C \qquad (A.1)$$

Now let us look at each individual rotation to describe its rotation rate and coodinate transforamtion. The angular velocity of the A frame with respect to the inertial frame is the rate of change of the true anomaly for the orbit.

$$\vec{\omega}^{A/I}=\begin{Bmatrix}0\\0\\\dot{\psi}\end{Bmatrix}_A \tag{A.2}$$

The transformation matrix for this rotation is not needed. The other relative rotation rates and their associated coodinate transformation matrices are

$$\vec{\omega}^{B/A}=\begin{Bmatrix}\dot{\theta}_1\\0\\0\end{Bmatrix}_B \tag{A.3}$$

$$L_{BA}=\begin{bmatrix}1 & 0 & 0\\0 & \cos\theta_1 & \sin\theta_1\\0 & -\sin\theta_1 & \cos\theta_1\end{bmatrix} \tag{A.4}$$

$$\vec{\omega}^{C/B}=\begin{Bmatrix}0\\\dot{\theta}_2\\0\end{Bmatrix}_C \tag{A.5}$$

$$L_{CB}=\begin{bmatrix}\cos\theta_2 & 0 & -\sin\theta_2\\0 & 1 & 0\\\sin\theta_2 & 0 & \cos\theta_2\end{bmatrix} \tag{A.6}$$

$$\vec{\omega}^{DC}=\begin{Bmatrix}0\\0\\\dot{\theta}_3\end{Bmatrix}_D \tag{A.7}$$

$$L_{DC}=\begin{bmatrix}\cos\theta_3 & \sin\theta_3 & 0\\-\sin\theta_3 & \cos\theta_3 & 0\\0 & 0 & 1\end{bmatrix} \tag{A.8}$$

In order to form the sum of these components of the angular velocity, they all must be expressed in the nodal coordinate frame C. To accomplish this, the required transformations must be formed such that

$$\vec{\omega}^{D/I}\big|_C = \begin{Bmatrix}\omega_1\\ \omega_2\\ \omega_3\end{Bmatrix}_C \tag{A.9}$$

In other words, we must rewrite equation (A.1) as

$$\vec{\omega}^{D/I}\big|_C = \vec{\omega}^{C/B}\big|_C + L_{CB}\vec{\omega}^{B/A}\big|_B + L_{CA}\vec{\omega}^{A/I}\big|_A + \vec{\omega}^{D/C}\big|_C \tag{A.10}$$

and perform the matrix multiplication to transform all the angular velocities to the C frame. The transformation matrices needed in equation (A.10) are

$$L_{CB} = \begin{bmatrix}\cos\theta_2 & 0 & -\sin\theta_2\\ 0 & 1 & 0\\ \sin\theta_2 & 0 & \cos\theta_2\end{bmatrix} \tag{A.11}$$

$$L_{CA} = L_{CB}L_{BA} = \begin{bmatrix}\cos\theta_2 & \sin\theta_1\sin\theta_2 & -\cos\theta_1\sin\theta_2\\ 0 & \cos\theta_1 & \sin\theta_1\\ \sin\theta_2 & -\sin\theta_1\cos\theta_2 & \cos\theta_1\cos_2\end{bmatrix} \tag{A.12}$$

L_{DA} is not needed to form the angular velocity, but it will be needed later for the derivation of the potential energy. So, it is given as

$$L_{DA} = L_{DC}L_{CA} = \begin{bmatrix}l_1 & l_2 & l_3\\ m_1 & m_2 & m_3\\ n_1 & n_2 & n_3\end{bmatrix} \tag{A.13}$$

where

$$l_1 = \cos\theta_2\cos\theta_3 \tag{A.14}$$

$$l_2 = \sin\theta_1\sin\theta_2\cos\theta_3 + \cos\theta_1\sin\theta_3 \tag{A.15}$$

$$l_3 = -\cos\theta_1\sin\theta_2\cos\theta_3 + \sin\theta_1\sin\theta_3 \tag{A.16}$$

$$m_1 = -\cos\theta_2 \sin\theta_3 \tag{A.17}$$

$$m_2 = -\sin\theta_1 \sin\theta_2 \sin\theta_3 + \cos\theta_1 \cos\theta_3 \tag{A.18}$$

$$m_3 = \cos\theta_1 \sin\theta_2 \sin\theta_3 + \sin\theta_1 \cos\theta_3 \tag{A.19}$$

$$n_1 = \sin\theta_2 \tag{A.20}$$

$$n_2 = -\sin\theta_1 \cos\theta_2 \tag{A.21}$$

$$n_3 = \cos\theta_1 \cos\theta_2 \tag{A.22}$$

Substituting the transforamtions into equation (A.10) and performing the matrix algebra results in the expessions for the angular velocity of the satellite expessed in nodal coordinates.

$$\vec{\omega}^{B/I}\Big|_C = \begin{Bmatrix} \dot{\theta}_1 \cos\theta_2 - \dot{\nu}\cos\theta_1 \sin\theta_2 \\ \dot{\theta}_2 + \dot{\nu}\sin\theta_1 \\ \dot{\theta}_3 + \dot{\theta}_1 \sin\theta_2 + \dot{\nu}\cos\theta_1 \cos\theta_2 \end{Bmatrix}_C \tag{A.23}$$

A.2 Kinetic Energy of the Satellite

The expression for the kinetic enregy, T, is needed to form the Lagangian which is used to derive the equations of motion. A good presentation of this derivation is in Wiesel [17:103-104] and is presented here for completeness. The general expression for the T is

$$T = \int \frac{1}{2} \vec{v} \cdot \vec{v} \, dm \tag{A.24}$$

Figure A-2 shows the position vector R to the center of mass of the satellite and the vector ρ to a mass element dm in the body. The velocity of the mass element dm is

$$\vec{V}=\frac{d\vec{R}}{dt}+\frac{d\vec{\rho}}{dt} \tag{A.25}$$

where

$$\frac{d\vec{\rho}}{dt}=\vec{\omega}^{D/I}\times\{\vec{\rho}\}_D \tag{A.26}$$

Substituting these expessions into equation (A.24) results in the following integral over the body.

$$T=\frac{1}{2}\int\left(\frac{d\vec{R}}{dt}+(\vec{\omega}^{D/I}\times\{\vec{\rho}\}_D)\right)\cdot\left(\frac{d\vec{R}}{dt}+(\vec{\omega}^{D/I}\times\{\vec{\rho}\}_D)\right)dm \tag{A.27}$$

$$\begin{aligned}T=\frac{1}{2}\int\{\ &\frac{d\vec{R}}{dt}\cdot\frac{d\vec{R}}{dt}+\frac{d\vec{R}}{dt}\cdot(\vec{\omega}^{D/I}\times\{\vec{\rho}\}_D)\\&+(\vec{\omega}^{D/I}\times\{\vec{\rho}\}_D)\cdot\frac{d\vec{R}}{dt}\\&+(\vec{\omega}^{D/I}\times\{\vec{\rho}\}_D)\cdot(\vec{\omega}^{D/I}\times\{\vec{\rho}\}_D)\ \}\,dm\end{aligned} \tag{A.28}$$

But, since the mass element dm is measured from the center of mass,

$$\int\{\vec{\rho}\}_D\,dm=0 \tag{A.29}$$

So, equation (A.28) reduces to

$$T=\frac{1}{2}m\frac{d\vec{R}}{dt}\cdot\frac{d\vec{R}}{dt}+\frac{1}{2}\int(\vec{\omega}^{D/I}\times\{\vec{\rho}\}_D)\cdot(\vec{\omega}^{D/I}\times\{\vec{\rho}\}_D)\,dm \tag{A.30}$$

where

$$\{\vec{\omega}^{D/I}\}_D\times\{\vec{\rho}\}_D=\begin{Bmatrix}\omega_2x_3-\omega_3x_2\\\omega_3x_1-\omega_1x_3\\\omega_1x_2-\omega_2x_1\end{Bmatrix}_D \tag{A.31}$$

Substituting equation (A.31) into equation (A.30), we get

$$T=\frac{1}{2}m\frac{d\vec{R}}{dt}\cdot\frac{d\vec{R}}{dt}+\frac{1}{2}\int\{\omega_2^2(x_3^2+x_1^2)+\omega_3^2(x_2^2+x_1^2)+\omega_1^2(x_2^2+x_3^2)-2\omega_2\omega_3x_2x_3-2\omega_1\omega_3x_1x_3-2\omega_1\omega_2x_1x_2\}\,dm \tag{A.32}$$

From rigid body dynamics, the moment of inertia matrix can be written as

$$I=\begin{bmatrix}\int(x_2^2+x_3^2)dm & -\int x_1x_2\,dm & -\int x_1x_3\,dm\\ -\int x_1x_2\,dm & \int(x_1^2+x_3^2)dm & -\int x_2x_3\,dm\\ -\int x_1x_3\,dm & -\int x_2x_3\,dm & \int(x_1^2+x_2^2)dm\end{bmatrix} \tag{A.33}$$

Let us use a principal body axes frame to simplify the moment of inertia matrix and let the principal moments of inertia be A, B , and C. For further reading on this subject see reference [17:102]. For a symmetric body, B=A, thus the moment of inertia matrix becomes

$$I=\begin{bmatrix}A&0&0\\0&B&0\\0&0&C\end{bmatrix}=\begin{bmatrix}A&0&0\\0&A&0\\0&0&C\end{bmatrix} \tag{A.34}$$

Substituting the moment of inertia terms into equation (A.32) reduces the expression for the kinetic energy for the satellite to

$$T=\frac{1}{2}m\frac{d\vec{R}}{dt}\cdot\frac{d\vec{R}}{dt}+\frac{1}{2}A(\omega_1^2+\omega_2^2)+\frac{1}{2}C\omega_3^2 \tag{A.35}$$

This is simply the kinetic energy of the translational motion of the center of mass plus the kinetic energy of the rotational motion about the center of mass. The velocity of the center of mass is

$$\frac{d\vec{R}}{dt}=\frac{d}{dt}\begin{Bmatrix}R\\0\\0\end{Bmatrix}_A+\vec{\omega}^{A/I}\times\begin{Bmatrix}R\\0\\0\end{Bmatrix}_A \tag{A.36}$$

After performing the cross product, we get

$$\frac{d\vec{R}}{dt}=\begin{Bmatrix}\dot{R}\\ R\dot{\psi}\\ 0\end{Bmatrix}_A \tag{A.37}$$

Since the satellite is a symmetric body, we can use the angular velocity written in the nodal coordinates to simplify the calculation of the kinetic energy. Substituting the angular velocity components of equation (A.23) and the velocity of the center of mass above, we get an expression for the kinetic energy that looks like

$$\begin{aligned}T=&\frac{1}{2}m(\dot{R}^2+R^2\dot{\psi}^2)+\frac{1}{2}A(\dot{\theta}_1\cos\theta_2-\dot{\psi}\cos\theta_1\sin\theta_2)^2\\&+\frac{1}{2}A(\dot{\theta}_2+\dot{\psi}\sin\theta_1)^2+\frac{1}{2}C(\dot{\theta}_3+\dot{\theta}_1\sin\theta_2+\dot{\psi}\cos\theta_1\cos\theta_2)^2\end{aligned} \tag{A.38}$$

A.3 Potential Energy of the Satellite

The potential energy of the satellite, V, is the gravitational potential. This is derived in Meirovitch [9:430:438] and presented here in further detail. In order to derive the potential, we must locate a mass element dm in the satellite body with respect to the inertial frame at the origin of the attracting body. Figure A-2 shows the vector R from the center of the attracting body to the center of mass of the satellite, the vector ρ from the satellite center of mass to the mass element dm, and the vector r such that

$$\vec{r}=\vec{R}+\vec{\rho} \tag{A.39}$$

The potential can be written as

$$V=\int_B -\frac{GM}{r}\,dm \tag{A.40}$$

where G is the universal gravitational constant and M is the mass of the

attracting body. We can write the magnitude of the vector r as

$$r=\sqrt{\vec{r}\cdot\vec{r}}=\sqrt{(\vec{R}+\vec{\rho})\cdot(\vec{R}+\vec{\rho})}=\sqrt{R^2+2\vec{R}\cdot\vec{\rho}+\rho^2} \tag{A.41}$$

We can factor out an R so that

$$r=R\sqrt{1+2\hat{e}_R\cdot\left(\frac{\vec{\rho}}{R}\right)+\left(\frac{\rho}{R}\right)^2} \tag{A.42}$$

where $\hat{e}_R$ is the unit vector in the direction of the R vector. Taking the inverse of this expession results in

$$\frac{1}{r}=\frac{1}{R}\left(1+2\hat{e}_R\cdot\left(\frac{\vec{\rho}}{R}\right)+\left(\frac{\rho}{R}\right)^2\right)^{-\frac{1}{2}} \tag{A.43}$$

which allows us to readily expand it via the binomial expansion keeping only second order terms.

$$(1+\varepsilon)^m=1+m\varepsilon+m(m-1)\frac{\varepsilon^2}{2!}+\cdots \tag{A.44}$$

The result after the expansion is

$$\frac{1}{r}=\frac{1}{R}\left\{1-\frac{1}{2}\left[2\hat{e}_R\cdot\left(\frac{\vec{\rho}}{R}\right)+\left(\frac{\rho}{R}\right)^2\right]+\left(-\frac{1}{2}\right)\left(-\frac{3}{2}\right)\left(\frac{4}{2!}\right)\left(\hat{e}_R\cdot\frac{\vec{\rho}}{R}\right)^2\right\}+\cdots \tag{A.45}$$

Substituting the expansion into equation (A.40) for the potential calculation, we get

$$V=-\frac{GM}{R}\int_B\left\{1-\hat{e}_R\cdot\left(\frac{\vec{\rho}}{R}\right)-\frac{1}{2}\left(\frac{\rho}{R}\right)^2+\frac{3}{2}\left(\hat{e}_R\cdot\frac{\vec{\rho}}{R}\right)^2\right\}dm \tag{A.46}$$

Again, since ρ is measured from the mass center,

$$\frac{\hat{e}_R}{R}\cdot\int_B\vec{\rho}\,dm=0 \tag{A.47}$$

and equation (A.46) reduces to

$$V=-\frac{GMm}{R}-\frac{3}{2}\frac{GM}{R^3}\int_B\left\{(\hat{e}_R\cdot\vec{\rho})^2-\frac{\rho^2}{3}\right\}dm \tag{A.48}$$

The unit vector in the radial direction can be expressed in the body frame by the following:

$$\hat{e}_R=(\hat{e}_R\cdot\hat{i})\hat{i}+(\hat{e}_R\cdot\hat{j})\hat{j}+(\hat{e}_R\cdot\hat{k})\hat{k}=l_1\hat{i}+m_1\hat{j}+n_1\hat{k} \tag{A.49}$$

Let us define the vector ρ in the body frame D to be

$$\vec{\rho}=x_1\hat{i}+x_2\hat{j}+x_3\hat{k} \tag{A.50}$$

Substituting equations (A.49) and (A.50) into the remaining integral of equaution (A.48) leaves the potential as

$$\begin{aligned}V=-\frac{GMm}{R}-\frac{GM}{2R^3}\int_B\{&(3l_1^2-1)x_1^2+(3m_1^2-1)x_2^2\\&+(3n_1^2-1)x_3^2+6l_1m_1x_1x_2+6m_1n_1x_2x_3+6l_1n_1x_1x_3\}\,dm\end{aligned} \tag{A.51}$$

With some manipulation of the integrals in the moment of inertia matrix of equation (A.33), the following integrals can be shown to be

$$\int_B x_1^2\,dm=\frac{1}{2}(A+B+C) \tag{A.52}$$

$$\int_B x_2^2\,dm=\frac{1}{2}(A+C-B) \tag{A.53}$$

$$\int_B x_3^2\,dm=\frac{1}{2}(A+B-C) \tag{A.54}$$

We again assume a set of principal axes to null the integrals of the product terms. Making the appropriate substitutions into equation (A.51) and performing the algebra, the potential reduces to

$$V=-\frac{GMm}{R}-\frac{3GM}{4R^3}\left\{l_1^2(B+C-A)+m_1^2(A+C-B)+n_1^2(A+B-C)-\frac{1}{3}(A+B+C)\right\} \quad (A.55)$$

Substituting in for l_1, m_1, and n_1 and making B=A in the moment of inertia matrix, the potential becomes

$$V=-\frac{GMm}{R}-\frac{3}{4}\frac{GM}{R^3}\left[C\cos^2\theta_2+2A\sin^2\theta_2-C\sin^2\theta_2-\frac{1}{3}(2A+C)\right] \quad (A.56)$$

But, using the trigonometric identity

$$C\sin^2\theta_2+C\cos^2\theta_2=C \quad (A.57)$$

we can show that the potential simply becomes

$$V=-\frac{GMm}{R}-\frac{3}{2}\frac{GM}{R^3}\left[(A-C)\sin^2\theta_2-\frac{1}{3}(A-C)\right] \quad (A.58)$$

A.4 Lagranges Equations of Motion

Lagrange's equations of motion for holonomic, conservative, dynamical systems are formed by using the equation

$$\frac{d}{dt}\frac{\partial L}{\partial \dot{q}_k}-\frac{\partial L}{\partial q_k}=0 \qquad k=1,2,\cdots,n \quad (A.59)$$

An excellent reference on this material is Meirovitch's text on analytical dynamics. [9] The q_k's are the generalized coordinates for the system and L is termed the Lagrangian which is simply

$$L=T-V \quad (A.60)$$

where T is the kinetic energy and V is the potential energy. These are given respectively by equations (A.38) and (A.58) from the previous derivations. So, substituting T and V gives the Lagrangian

$$L=\frac{1}{2}m(\dot{R}^2+R^2\dot{\nu}^2)+\frac{1}{2}A(\dot{\theta}_1\cos\theta_2-\dot{\nu}\cos\theta_1\sin\theta_2)^2+\frac{1}{2}A(\dot{\theta}_2+\dot{\nu}\sin\theta_1)^2 \quad (A.61)$$
$$+\frac{1}{2}C(\dot{\theta}_3+\dot{\theta}_1\sin\theta_2+\dot{\nu}\cos\theta_1\cos\theta_2)^2+\frac{GMm}{R}+\frac{3}{2}\frac{GM}{R^3}\left[(A-C)\left(\sin^2\theta_2-\frac{1}{3}\right)\right]$$

The nice thing about analytical dynamics is that constants of the motion are identified rather easily. In this case, one of the constants of motion is identified by the coordinate θ_j not appearing in the Lagrangian, thus making it an ignorable coordinate. Further, since

$$\frac{\partial L}{\partial\theta_3}=0 \quad (A.62)$$

then it follows that the conjugate generalized angular momentum,

$$P_{\theta_3}=\frac{\partial L}{\partial\dot{\theta}_3} \quad (A.63)$$

is constant by rearrangement of equation (A.59) to show that

$$\frac{d}{dt}\frac{\partial L}{\partial\dot{\theta}_3}=\frac{\partial L}{\partial\theta_3}=0 \quad (A.64)$$

Note that the coordinate ν does not appear in the Lagrangian either. However, we will uses this constant of the motion later to get one of the equations of motion. Also, I would like to mention that the Lagrangian does not contain time explicitly which leads to a constant of the motion known as Jacobi's integral. However, we will not need Jacobi's integral to form our equations of motion so it will not be presented here. On the other hand, it is worthwhile to mention that the Jacobi's integral is a statement of the law of conservation of energy.

Since the Lagrangian for the satellite dynamics has two ignorable coordinates and does not contain time explicitly, we can use Routh's method for the ignoration of coordinates. However, we will only use this

technique to remove the constant of motion for the coordinate θ_3. For a detailed explanation of this method, you are again referred to Meirovitch's text. [9:85-88] The Routhian function is

$$R=L-P_{\theta_3}\dot{\theta}_3 \tag{A.65}$$

where

$$P_{\theta_3}=C(\dot{\theta}_3+\dot{\theta}_1\sin\theta_2+\dot{\psi}\cos\theta_1\cos\theta_2) \tag{A.66}$$

After making the appropriate substitutions for L and some work, the Routhian function becomes

$$\begin{aligned} R=&\frac{1}{2}m(\dot{R}^2+R^2\dot{\psi}^2)+\frac{1}{2}A(\dot{\theta}_1\cos\theta_2-\dot{\psi}\cos\theta_1\sin\theta_2)^2 \\ &+\frac{1}{2}A(\dot{\theta}_2+\dot{\psi}\sin\theta_1)^2+P_{\theta_3}(\dot{\theta}_1\sin\theta_2+\dot{\psi}\cos\theta_1\cos\theta_2) \\ &-\frac{1}{2C}P_{\theta_3}^2+\frac{GMm}{R}+\frac{3}{2}\frac{GM}{R^3}\left[(A-C)\left(\sin^2\theta_2-\frac{1}{3}\right)\right] \end{aligned} \tag{A.67}$$

It can be shown that the equations of motion for the remaining coordinates are formed by using equation (A.59) and replacing L with R. The solutions to these equations allow us to solve for the ignorable coordinate, θ_3, using the constant of motion given by equation (A.63).

We are now ready to form the equations of motion using ψ, R, θ_1, and θ_2 as our generalized coordinates. Let's start by deriving the equation for the coordinate ψ. The partial derivatives and the derivative with respect to time are

$$P_\psi=\frac{\partial R}{\partial\dot{\psi}}=mR^2\dot{\psi} \tag{A.68}$$

$$\frac{d}{dt}P_\psi=mR^2\ddot{\psi}+2mR\dot{R}\dot{\psi} \tag{A.69}$$

$$\frac{\partial R}{\partial v}=0 \tag{A.70}$$

Note that we assumed that the attitude motion of the satellite does not effect the orbital motion, thus the approximation for P_v given by equation (A.68). The coordinate v does not appear in the Lagrangian, so P_v is a constant of motion also which merely states that the angular momentum of the orbit is conserved. We now write the specific angular momentum, H, as a function of the two body orbital elements

$$H=R^2\dot{v}=\sqrt{a}\sqrt{\mu}\sqrt{1-e^2}=\frac{\sqrt{\mu}}{\sqrt{a^3}}a^2\sqrt{1-e^2} \tag{A.71}$$

where the mean motion of the satellite is

$$n=\frac{2\pi}{T}=\sqrt{\frac{\mu}{a^3}} \tag{A.72}$$

and the gravitational parameter is approximated by

$$\mu=GM=n^2a^3 \tag{A.73}$$

Any fundamental text in astrodynamics such as Bate, Mueller, and White shows this in further detail [2]. So, our equation for the coordinate v is

$$R^2\dot{v}=na^2\sqrt{1-e^2} \tag{A.74}$$

The derivatives needed to for the equation of motion for the coordinate R are

$$P_R=\frac{\partial R}{\partial \dot{R}}=m\dot{R} \tag{A.75}$$

$$\frac{d}{dt}P_R = m\ddot{R} \tag{A.76}$$

$$\frac{\partial R}{\partial R} = -\frac{GMm}{R^2} \tag{A.77}$$

Again, we assume that the attitude motion of the satellite does not effect the orbit by the approximation in equation (A.77). So, dividing by m and using the relation in equation (A.73), we get

$$\ddot{R} + \frac{\mu}{R^2} - R\dot{\psi}^2 = 0 \tag{A.78}$$

or

$$\ddot{R} - R\dot{\psi}^2 + \frac{n^2a^3}{R^2} = 0 \tag{A.79}$$

Now we substitute equation (A.74) into the above to get the equation for R in terms of the orbital elements.

$$\ddot{R} - \frac{a^4n^2(1-e^2)}{R^3} + \frac{n^2a^3}{R^2} = 0 \tag{A.80}$$

It is to our advantage to nondimensionalize by introducing the new variables

$$\tau = nt \tag{A.81}$$

$$\zeta = \frac{R}{a} \tag{A.82}$$

with

$$\frac{d\tau}{dt} = n \tag{A.83}$$

In order to nondimensionalize equations (A.74) and (A.79), we need to find all derivatives with respect to τ, which will be represented by primes.

So, applying the chain rule, we get

$$\dot{R}=\frac{dR}{dt}=\frac{d}{d\tau}\left(\frac{d\tau}{dt}R\right)=\frac{d}{d\tau}(n\zeta a)=\zeta' na \qquad (A.84)$$

and

$$\ddot{R}=\frac{d}{dt}\left(\frac{dR}{dt}\right)=\frac{d}{d\tau}\left(\frac{d\tau}{dt}\left(\frac{dR}{dt}\right)\right)=\zeta'' n^2 a \qquad (A.85)$$

using our new variable definitions. If we divide equation (A.80) by n^2a, we get

$$\frac{\ddot{R}}{n^2a}+\frac{(e^2-1)a^3}{R^3}+\frac{a^2}{R^2}=0 \qquad (A.86)$$

Then by using equations (A.84) and (A.85), we get the transformed equation for the R coordinate to be

$$\zeta''+\frac{1}{\zeta^2}+\frac{e^2-1}{\zeta^3}=0 \qquad (A.87)$$

To nondimensionalize equation (A.74), we use the chain rule again to get

$$\frac{dv}{d\tau}=\frac{dv}{dt}\frac{dt}{d\tau}=\frac{a^2n(1-e^2)^{\frac{1}{2}}}{R^2}\frac{1}{n} \qquad (A.88)$$

which becomes

$$v'=\frac{(1-e^2)^{\frac{1}{2}}}{\zeta^2} \qquad (A.89)$$

We now take the derivative with respect to τ to get

$$v''=\frac{-2(1-e^2)^{\frac{1}{2}}}{\zeta^3}\zeta' \qquad (A.90)$$

which we will need later.

Now that we have the nondimensionalized orbital equations, we must

make the appropriate coordinate transformation on the initial conditions. We arbitrarily select the satellite to be at perigee at $t=\tau=0$. So, in the old coordinates,

$$R(0)=a(1-e) \tag{A.91}$$

and

$$\dot{R}(0)=0 \tag{A.92}$$

are the initial conditions. In the new nondimensional coordinates, we get

$$\zeta(0)=1-e \tag{A.93}$$

and

$$\zeta'(0)=0 \tag{A.94}$$

for our initial conditions.

Next, we turn our attention to the attitude equations of motion. The required partial and time derivatives for the θ_1 coordinate are

$$P_{\theta_1}=\frac{\partial R}{\partial \theta_1}=A(\dot{\theta}_1\cos\theta_2-\dot{\psi}\cos\theta_1\sin\theta_2)\cos\theta_2+P_{\theta_3}\sin\theta_2 \tag{A.95}$$

$$\begin{aligned}\frac{d}{dt}P_{\theta_1}=&A\ddot{\theta}_1\cos^2\theta_2-2A\dot{\theta}_1\dot{\theta}_2\cos\theta_1\cos\theta_2\sin\theta_2\\&-A\dot{\psi}\dot{\theta}_2\cos\theta_1(\cos^2\theta_2-\sin^2\theta_2)+A\dot{\psi}\dot{\theta}_1\sin\theta_1\sin\theta_2\cos\theta_2\\&-A\ddot{\psi}\cos\theta_1\cos\theta_2\sin\theta_2+P_{\theta_3}\dot{\theta}_2\cos\theta_2\end{aligned} \tag{A.96}$$

$$\begin{aligned}\frac{\partial R}{\partial \theta_1}=&-A(\dot{\theta}_1\cos\theta_2-\dot{\psi}\cos\theta_1\sin\theta_2)(\dot{\psi}\sin\theta_2\sin\theta_1)\\&+A(\dot{\theta}_2+\dot{\psi}\sin\theta_1)(\dot{\psi}\cos\theta_1)-P_{\theta_3}\dot{\psi}\sin\theta_1\cos\theta_2\end{aligned} \tag{A.97}$$

After substituting the derivatives into equation (A.59), Lagrange's equation, we get

$$0=\ddot{\theta}_1-2\dot{\theta}_1\dot{\theta}_2\tan\theta_2-\dot{\psi}\dot{\theta}_2\cos\theta_1(1-\tan^2\theta_2)+\dot{\psi}\dot{\theta}_1\sin\theta_1\tan\theta_2$$
$$-\dot{\psi}\cos\theta_1\tan\theta_2+\frac{P_{\theta_2}}{A}\dot{\theta}_2\sec\theta_2-\dot{\psi}\dot{\theta}_1\sin\theta_1\tan\theta_2$$
$$+\dot{\psi}^2\cos\theta_1\sin\theta_1\tan^2\theta_2-\dot{\theta}_2\dot{\psi}\cos\theta_1(1+\tan^2\theta_2) \qquad (A.98)$$
$$-\dot{\psi}^2\cos\theta_1\sin\theta_1(1+\tan^2\theta_2)+\frac{P_{\theta_2}}{A}\dot{\psi}\sin\theta_1\sec\theta_2$$

We see that six terms conveniently cancel out and two terms combine to simplify to

$$0=\ddot{\theta}_1-2\dot{\theta}_1\dot{\theta}_2\tan\theta_2-2\dot{\psi}\dot{\theta}_2\cos\theta_1-\dot{\psi}\cos\theta_1\tan\theta_2$$
$$-\dot{\psi}^2\cos\theta_1\sin\theta_1+\frac{P_{\theta_2}}{A}\sec\theta_2(\dot{\theta}_2+\dot{\psi}\sin\theta_1) \qquad (A.99)$$

Finally,

$$\ddot{\theta}_1=2\dot{\theta}_1\dot{\theta}_2\tan\theta_2+2\dot{\psi}\dot{\theta}_2\cos\theta_1+\dot{\psi}\cos\theta_1\tan\theta_2$$
$$+\dot{\psi}^2\cos\theta_1\sin\theta_1-(K+1)\frac{P_{\theta_2}}{C}\sec\theta_2(\dot{\theta}_2+\dot{\psi}\sin\theta_1) \qquad (A.100)$$

is the equation of motion for the θ_1 coordinate where

$$K=\frac{C-A}{A} \qquad (A.101)$$

and

$$s+1=\frac{P_{\theta_2}}{C} \qquad (A.102)$$

is the constant of motion which is the spin rate about the symmetry axis.

The required derivatives for the θ_1 coordinate are

$$P_{\theta_2}=\frac{\partial R}{\partial\dot{\theta}_2}=A(\dot{\theta}_2+\dot{\psi}\sin\theta_1) \qquad (A.103)$$

$$\frac{d}{dt}P_{\theta_2}=A\ddot{\theta}_2+A\dot{\psi}\dot{\theta}_1\cos\theta_1+A\ddot{\psi}\sin\theta_1 \qquad (A.104)$$

$$\frac{\partial R}{\partial \theta_2} = A(\dot{\theta}_1\cos\theta_2 - \dot{\psi}\cos\theta_1\sin\theta_2)(-\dot{\theta}_1\sin\theta_2 - \dot{\psi}\cos\theta_1\cos\theta_2) + P_{\theta_2}(\dot{\theta}_1\cos\theta_2 - \dot{\psi}\cos\theta_1\sin\theta_2) + \frac{3\mu}{R^3}(A-C)\sin\theta_2\cos\theta_2 \tag{A.105}$$

Multiplying out the terms reduces equation (A.105) to

$$\frac{\partial R}{\partial \theta_2} = -A\dot{\theta}_1^2\sin\theta_2\cos\theta_2 - A\dot{\theta}_1\dot{\psi}\cos\theta_1\cos^2\theta_2 + A\dot{\psi}\dot{\theta}_1\cos\theta_1\sin^2\theta_2 + A\dot{\psi}^2\cos^2\theta_1\sin\theta_2\cos\theta_2 + P_{\theta_2}(\dot{\theta}_1\cos\theta_2 - \dot{\psi}\cos\theta_1\sin\theta_2) + \frac{3\mu}{R^3}(A-C)\sin\theta_2\cos\theta_2 \tag{A.106}$$

Substituting the derivatives into Lagrange's equation one last time results in

$$0 = \ddot{\theta}_2 + \dot{\psi}\dot{\theta}_1\cos\theta_1 + \ddot{\psi}\sin\theta_1 + \dot{\theta}_1^2\sin\theta_2\cos\theta_2 + \dot{\theta}_1\dot{\psi}\cos\theta_1\cos^2\theta_2 - \dot{\theta}_1\dot{\psi}\cos\theta_1\sin^2\theta_2 - \dot{\psi}^2\cos^2\theta_1\sin\theta_2\cos\theta_2 - \frac{P_{\theta_2}}{A}(\dot{\theta}_1\cos\theta_2 - \dot{\psi}\cos\theta_1\sin\theta_2) + \frac{3\mu}{R^3}\left(\frac{C-A}{A}\right)\sin\theta_2\cos\theta_2 \tag{A.107}$$

for the θ_2 coordinate. Rearranging the above equation and substituting in for K reduces the equation of motion to

$$\ddot{\theta}_2 = (K+1)\frac{P_{\theta_2}}{C}(\dot{\theta}_1\cos\theta_2 - \dot{\psi}\cos\theta_1\sin\theta_2) - 3\frac{\mu}{R^3}K\sin\theta_2\cos\theta_2 - \ddot{\psi}\sin\theta_1 - \dot{\theta}_1^2\sin\theta_2\cos\theta_2 + \dot{\psi}^2\cos^2\theta_1\sin\theta_2\cos\theta_2 - \dot{\psi}\dot{\theta}_1\cos\theta_1 + \dot{\psi}\dot{\theta}_1\cos\theta_1(\sin^2\theta_2 - \cos^2\theta_2) \tag{A.108}$$

And finally, using the trigonometric identity

$$\sin^2\theta_2 - \cos^2\theta_2 = 1 - 2\cos^2\theta_2 \tag{A.109}$$

the equation of motion for the θ_2 coordinate simplifies to

$$\ddot{\theta}_2=(K+1)\frac{P_{\theta_3}}{C}\left(\dot{\theta}_1\cos\theta_2-\dot{v}\cos\theta_1\sin\theta_2\right)-\dot{v}\sin\theta_1 \\ -2\dot{v}\dot{\theta}_1\cos\theta_1\cos^2\theta_2-\left(\dot{\theta}_1^2-\dot{v}^2\cos^2\theta_1+\frac{3K\mu}{R^3}\right)\sin\theta_2\cos\theta_2 \tag{A.110}$$

Now we nondimensionalize equations (A.100) and (A.110) using the new nondimensional coordinates given by equations (A.81) and (A.82). Using the chain rule, it is easy to see that

$$\frac{d\theta_1}{dt}=\frac{d\theta_1}{d\tau}\frac{d\tau}{dt}=n\frac{d\theta_1}{d\tau}=n\theta_1' \tag{A.111}$$

and

$$\frac{d}{dt}\left(\frac{d\theta_1}{dt}\right)=\frac{d}{d\tau}\left(\frac{d\theta_1}{d\tau}\right)\frac{d\tau}{dt}n=n^2\frac{d^2\theta_1}{d\tau^2}=n^2\theta_1'' \tag{A.112}$$

are obvious. Using these results with equation (A.100) makes the θ_1 coordinate equation of motion transform to

$$\theta_1''n^2=2n^2\theta_1'\theta_2'\tan\theta_2+2n^2v'\theta_2'\cos\theta_1+n^2v''\cos\theta_1\tan\theta_2 \\ +n^2v'^2\cos\theta_1\sin\theta_1-(K+1)n^2\frac{P_{\theta_3}}{C}\left(\theta_2'+v'\sin\theta_1\right)\sec\theta_2 \tag{A.113}$$

where

$$P_{\theta_3}=C\left(\theta_3'+\theta_1'\sin\theta_2+v'\cos\theta_1\cos\theta_2\right)=C(s+1) \tag{A.114}$$

after the transformation. Now, dividing both sides by n^2 gives the transformed result for the θ_1 coordinate as

$$\theta_1''=2\theta_1'\theta_2'\tan\theta_2+2v'\theta_2'\cos\theta_1+v''\cos\theta_1\tan\theta_2+v'^2\cos\theta_1\sin\theta_1 \\ -(K+1)\frac{P_{\theta_3}}{C}\left(\theta_2'+v'\sin\theta_1\right)\sec\theta_2 \tag{A.115}$$

Next, using the relations

$$a^3 = \frac{\mu}{n^2} \tag{A.116}$$

and

$$\frac{1}{\zeta^3} = \frac{a^3}{R^3} \tag{A.117}$$

we remove the R from the θ_2 equation of motion. Then, in order to transform the θ_2 equation of motion to the nondimensional coordinates, we follow the exact steps as we did for the θ_1 equation of motion. The final result for the θ_2 coordinate is

$$\theta_2'' = (K+1)\frac{P_{\theta_2}}{C}\left(\theta_1'\cos\theta_2 - v'\cos\theta_1\sin\theta_2\right) \tag{A.118}$$
$$-\left(\theta_1'^2 - v'^2\cos^2\theta_1 + \frac{3K}{\zeta^3}\right)\sin\theta_2\cos\theta_2 - v''\sin\theta_1 - 2v'\theta_1'\cos\theta_1\cos^2\theta_2$$

Equilibrium conditions of the attitude equations can now be determined. The equilibrium condition arises when

$$\theta_1' = \theta_2' = \theta_1'' = \theta_2'' = 0 \tag{A.119}$$

The values of

$$\theta_1 = \theta_2 = 0 \tag{A.120}$$

make these conditions true. In this case,

$$\theta_3 = (s+1)\tau - v = (s+1)nt - v \tag{A.121}$$

This equilibrium condition makes the satellite spin axis perpendicular to the orbit plane. In this thesis, this is the equilibrium the satellite control system is designed about.

Bibliography

1. Andronov, A. and others. *Theory of Bifurcations of Dynamic Systems on a Plane.* New York, NY: Halsted Press, John Wiley and Sons, Inc., 1973.

2. Bate, Roger R. and others. *Fundamentals of Astrodynamics.* New York, NY: Dover Publications, Inc., 1971.

3. Calico, R.A. and W.E. Wiesel. "Control of Time-Periodic Systems," *Journal of Guidance and Control, and Dynamics, 7*(6):671-676 (November-December 1984).

4. Calico, R.A. and G.S. Yeakel. "Active Attitude Control of a Spinning Symmetrical Satellite in an Elliptic Orbit," *Journal of Guidance and Control, and Dynamics, 6*(4):315-318 (July-August 1983).

5. Cole, James W. *Control and Stability of a Spinning Symmetric Satellite in an Elliptical Orbit.* MS thesis, AFIT/GAE/ENY/89D-05, 1989.

6. Doedel, Eusebius. *AUTO: Software for Continuation and Bifurcation Problems in Ordinary Differential Equations.* (May 1986).

7. Jordan, D. W. and P. Smith. *Nonlinear Differential Equations* (Second Edition). New York, NY: Oxford University Press, 1987.

8. Kane T. R. and P. M. Barba. "Attitude Stability of a Spinning Satellite in an Elliptic Orbit," *Journal of Applied Mechanics, 33*:402-405 (June 1966).

9. Kubíček, M. and M. Marek. *Computational Methods in Bifurcation Theory and Dissipative Structures.* New York, NY: Springer Verlag Inc., 1983.

10. Meirovitch, Leonard. *Methods of Analytical Dynamics.* New York, NY: McGraw-Hill Book Company, 1970.

11. Moon, Francis C. *Chaotic Vibrations.* New York, NY: John Wiley and Sons Ltd., 1987.

12. Myers, Gregory E. *Active Control of Linear Periodic System with Two Unstable Modes.* MS thesis, AFIT/GAE/AA/82D-21, 1982.

13. Seydel, Rüdiger. *From Equilibrium to Chaos.* New York, NY: Elsevier Science Publishing Company, Inc., 1988.

14. Shell, Dale E. *Stability Solution to Linearized Equations of Motion for a Symmetric Spinning Satellite in an Elliptical Orbit Applied to the Non-linear Equations.* MS thesis, AFIT/GA/AA/88D-09, 1988.

15. Thompson, J. M. T. and H. B. Stewart. *Nonlinear Dynamics and Chaos.* New York, NY: John Wiley and Sons Ltd., 1986.

16. Wallace, Frank B. and Leonard Meirovitch. "Attitude Instability Regions of a Spinning Symmetric Satellite in an Elliptic Orbit," *AIAA Journal*, *5*(9):1642-1650 (September 1967).

17. Wiesel, William E. *Spaceflight Dynamics.* New York, NY: McGraw-Hill Book Company, 1989.

Vita

Michael Ulisse was born in Trenton, New Jersey on 24 August 1963. He was the second son of five of Carmela Ulisse and the late Ferdinando Ulisse. He graduated from Trenton Central High School in 1981 and attended the United States Air Force Academy where he graduated in 1985 as a distinguished graduate with a Bachelor of Science in Astronautical Engineering. He was then given a regular commission as a 2nd Lieutenant in the USAF and assigned to the Air Force Armament Laboratory, Eglin AFB, Florida. During that assignment, he contributed as an Astronautical engineer specializing in guidance and control to the research and development of space-based interceptors for the Strategic Defense Initiative. In 1989, he was selected to enter the Air Force Institute of Technology. After graduation, he will be assigned Space Systems Division, Los Angeles AFB, California.

He married Patricia Joanne Erjavec on 26 April 1986 and they have two sons named Joseph Michael and Matthew.

Permanent Address: 341 William St.
Trenton, New Jersey
08610

REPORT DOCUMENTATION PAGE

Form Approved
OMB No. 0704-0188

Public reporting burden for this collection of information is estimated to average 1 hour per response, including the time for reviewing instructions, searching existing data sources, gathering and maintaining the data needed, and completing and reviewing the collection of information. Send comments regarding this burden estimate or any other aspect of this collection of information, including suggestions for reducing this burden, to Washington Headquarters Services, Directorate for information Operations and Reports, 1215 Jefferson Davis Highway, Suite 1204, Arlington, VA 22202-4302, and to the Office of Management and Budget, Paperwork Reduction Project (0704-0188), Washington, DC 20503.

1. AGENCY USE ONLY (Leave blank)	2. REPORT DATE	3. REPORT TYPE AND DATES COVERED
	December 1990	Master's Thesis

4. TITLE AND SUBTITLE
NONLINEAR ANALYSIS OF A SPINNING SYMMETRIC SATELLITE IN AN ELLIPTICAL ORBIT

5. FUNDING NUMBERS

6. AUTHOR(S)
Michael Ulisse, Captain, USAF

7. PERFORMING ORGANIZATION NAME(S) AND ADDRESS(ES)
Air Force Institute of Technology, WPAFB OH 45433-6583

8. PERFORMING ORGANIZATION REPORT NUMBER
AFIT/GA/ENY/90D-13

9. SPONSORING/MONITORING AGENCY NAME(S) AND ADDRESS(ES)

10. SPONSORING/MONITORING AGENCY REPORT NUMBER

11. SUPPLEMENTARY NOTES

12a. DISTRIBUTION/AVAILABILITY STATEMENT
Approved for public release; distribution unlimited

12b. DISTRIBUTION CODE

13. ABSTRACT *(Maximum 200 words)*

Controlled and uncontrolled equations of motion for a spinning symmetric satellite in an elliptical orbit are analyzed using Floquét theory, Poincaré maps, and continuation. The equations of motion for the uncontrolled system are derived via energy methods. A simple feedback controller design and one based on Floquét theory are presented. Parameters varied in the equations of motion include the spin about the symmetry axis of the satellite, the inertia ratio of the satellite, the eccentricity of the orbit, and the controller gains. Floquét analyses determine local stability and bifurcation points. Poincaré maps exhibit some interesting and complex structure in the global phase space. Continuation using a bifurcation analysis computer code (AUTO) reveals a sequence of period doublings, which is verified via numerical integration, for the simple rate feedback controller. The onset of chaotic motion is detected for this sequence of period doublings.

14. SUBJECT TERMS	15. NUMBER OF PAGES
Satellite Attitude, Floquét Theory, Poincaré Maps Continuation, Nonlinear Analysis, Feedback Control	157
	16. PRICE CODE

17. SECURITY CLASSIFICATION OF REPORT	18. SECURITY CLASSIFICATION OF THIS PAGE	19. SECURITY CLASSIFICATION OF ABSTRACT	20. LIMITATION OF ABSTRACT
Unclassified	Unclassified	Unclassified	UL